UNIVERSIDAD AUTONOMA DE MADRID

Departamento de Bioquímica

Utilización del contenido de vesículas extracelulares circulantes en sangre periférica para el manejo clínico de pacientes con gliomas

TESIS DOCTORAL

Noemí García Romero

Madrid, 2017

Departamento de Bioquímica

Facultad de Medicina

Universidad Autónoma de Madrid

Utilización del contenido de vesículas extracelulares circulantes en sangre periférica para el manejo clínico de pacientes con gliomas

Memoria que presenta

Noemí García Romero

Licenciada en Biotecnología

Directores de tesis

Dr. Ángel Ayuso Sacido y Dr. Cristóbal Belda Iniesta.

Fundación de Investigación HM-Hospitales - IMDEA Nanociencia

Un científico en su laboratorio no es sólo un técnico, es también un niño colocado ante fenómenos naturales que le impresionan como un cuento de hadas."

Marie Curie

AGRADECIMIENTOS

En primer lugar, me gustaría agradecer a mis directores de tesis por haber hecho realidad este proyecto. Al Dr. Cristóbal Belda, gracias por confiar en mí, abrirme las puertas del laboratorio y darme esta magnífica oportunidad. Al Dr. Ayuso por ser mi guía académico en estos años, a Ángel por serlo en lo personal. Gracias por contagiarme tu ilusión, por obligarme a echar volar la imaginación, por darme palabras de aliento en momentos difíciles, en definitiva, porque ¡Con gente como tú la ciencia merece la pena!

¡Qué haría yo sin mis "Ayusas"! Pepa, agradecerte todo lo que has hecho por mí desde el primer día que vine a este laboratorio, empezamos de cero, incluso descubriendo como se quitaban las puntas de las pipetas…jaja. Gracias por ser mi GPS, por enseñarme tantos truquillos, y por tener esa gran paciencia. Susi, la pelirroja sin alma, gracias por las risas, por las conversaciones tanto de ciencia como de temas inverosímiles en el despacho, por compartir conciertos y preocupaciones. A las dos, muchísimas gracias también por echarme una mano en el temido animalario y estar siempre disponibles, sobre todo en este último periodo de locura.

Gorjana, gracias por abrirnos la mente a esas cosas que llamas "proteínas", gracias por tu dulzura, creo que se equilibra con mi brusquedad, por lo que estoy segura que formaremos un buen equipo ;)

A Carmen, qué pena no habernos conocido más, confío en que te va a ir fenomenal en tu nueva andadura, ¡disfruta el momento!

A toda la gran familia que forma el IMMA. Gracias a los técnicos, Ricardo, creo que después de todo hemos sabido aguantarnos el uno al otro. A Javi, porque, aunque estemos todo el día como el perro y el gato, has estado ahí en todo momento, siempre sacándome una gran carcajada. A Virginia, ¡por fin alguien que pueda formalizar el laboratorio de histología! Gracias por preocuparte siempre. Y gracias a los tres por echarme una mano siempre que he necesitado de vosotros. A Paloma, por preocuparse de que las cosas vayan bien, por esos ánimos en todos estos últimos años.

A las Irenes, por siempre estar dispuestas a ayudar con una sonrisa, por la serenidad que me transmitís cuando estáis cerca de mi WB.

Dani, qué sería de nosotros sin esos "spring waters", por esas charlas y discusiones sobre estadística, por esas cervezas y confesiones fuera del laboratorio, has sido uno de mis grandes apoyos y por ello te estoy muy agradecida.

A Cira, gracias por ser como eres, por compartir tantas risas y preocupaciones. Y por tus palabras de aliento en situaciones de caos…en muchas ocasiones sólo nos hace falta una mirada para saber lo que va mal.

A Nico, gracias por ese apoyo que me has brindado, por dejarme desahogarme contigo, eres una gran persona.

A María, por su buen humor y por esas palabras de ánimo cuando ve que el agobio se apodera de mí.

Al Dr. Domingo Barber, por su profesionalidad y cercanía.

A las nuevas incorporaciones; Estanis, Sergio, Leti, Marisa, seguro que tenemos tiempo para conocernos mejor.

A toda la gente que ha pasado por el laboratorio durante estos años, en especial a Sonia, de todos ellos me llevo algo. Mención especial merece mi Gontxi, uno de los mejores vascos que he conocido nunca.

Gracias a la Dra. Pilar Sánchez y a todo su laboratorio, por tratarme como una más de su grupo, y por su gran disposición a ayudar, colaborar y tender una mano siempre que lo he necesitado.

A la Dra. Rosario Perona y al Dr. Leandro Sastre, gracias por abrirnos las puertas del IIB y estar siempre accesibles para lo que hemos necesitado.

A Ana Ortiz, muchas gracias por tu ayuda con las Resonancias y por tu disponibilidad, debiese de haber más gente como tú, con esas ganas e ilusión que transmites.

A los pacientes y a toda la gente de los Hospitales HM, Gregorio Marañón y La Fe de Valencia que han contribuido en hacer realidad este proyecto ¡la unión hace la fuerza!

Al Dr. Barreiro por enseñarme su disciplina en el laboratorio cuando aún no sabía nada de este mundillo. Te agradezco haberme contagiado muchas de tus manías.

A Cristina, porque pasaste de ser una desconocida a ser una gran amiga en muy poco tiempo.

A mis amig@s de la Uni, Irene, Chemi, Nati, Olatz, Ander, Pibe, Japo, Antón, Guille y Bombero, por todos los momentos vividos en León y esos reencuentros que saben a gloria. Y gracias también a Maitane, Albert y las dos Marías por el año que compartimos en Vitoria y por todo lo que nos apoyamos mutuamente.

A mis amigas de toda la vida, Mónica, Lucías, Mara, Vane, María, Aixa, Larita, Tania e Isabel. Porque son la familia que se elige, sobre todo a Mónica, por esas inyecciones de moral cuando más lo he necesitado, por apoyarme siempre, porque desde que subiste a aquel autobús no nos hemos separado nunca. Y a Lucía, por estar ahí en los buenos y los malos momentos desde la guardería. A todo ese grupo de chicos, que siempre han estado ahí. Mención especial se merecen también mi Gregoria, Pin y Víctor Mantilla por ese apoyo desde la distancia. A Dudin, porque en estos últimos años he descubierto un gran dibujante y mejor persona…gracias por la magnífica portada.

A mis abuelos, y mi tío Eduardo, debieseis de ser eternos… sé que estaréis muy orgullosos de mí. A mi abuela Carmen, que siempre me dice "¿pero vas a parar de estudiar algún día?". A mis tíos y primos, que siempre han estado ahí, en los buenos y los malos momentos, juntos como una piña. En especial a mi primo Héctor, que siempre ha sido como mi hermano mayor.

A la familia Castañeda-Revuelta, incluido Kike, por el cariño que me dais y por tratarme como una más desde el principio.

A Álvaro, porque has vivido esta tesis desde el principio, porque "nunca es demasiado", por quererme, por saberme serenar en momentos difíciles, por todos esos viajes que hemos hecho y todo lo que hemos aprendido y reído juntos. Gracias por tu apoyo y paciencia infinita, sobre todo en estos últimos meses. Por escuchar todas mis historias sobre ciencia y animarme a seguir. ¡Por llenar mi vida de música!

A mis padres, por brindármelo todo sin pedir nada a cambio, sin vosotros nada de esto hubiera sido posible, gracias por confiar en mí desde el primer momento y darme la oportunidad de llegar hasta aquí. Por dejarme elegir y seguir mi camino, por vuestro esfuerzo, por perdonar mis ausencias y mis malos días, por siempre ayudarme a continuar, por hacer de mí una mejor persona. ¡Esto lo hemos construido juntos!

"El mundo está en las manos de aquellos que tienen el coraje de soñar y correr el riesgo de vivir sus sueños"

Paulo Coelho

A mis padres

RESUMEN

Los gliomas son los tumores primarios más comunes en el Sistema Nervioso Central. El Glioblastoma (GBM) es el tumor primario de origen glial más frecuente y agresivo, con una supervivencia media que rara vez supera los 15 meses. El fracaso terapéutico se debe en parte a la existencia de una población celular denominada células iniciadoras de tumor (CIT) a las que se les atribuye la responsabilidad del inicio del tumor, de la invasividad y la resistencia a los tratamientos actuales. Por lo que las CIT se han propuesto como el mejor modelo pre-clínico para el estudio de los gliomas. En este trabajo nos planteamos el estudio de la evolución *in vitro* de cultivos primarios aislados de muestras quirúrgicas de pacientes diagnosticados con GBM, así como analizamos su patrón de diseminación en ratones inmunodeprimidos. Nuestros resultados muestran que las CIT son susceptibles de evolucionar a lo largo de los pases en cultivo, presentando eventos de inestabilidad cromosómica, un aumento en la expresión de marcadores específicos de CIT y de troncalidad, además de fluctuaciones importantes en su perfil de viabilidad y en el patrón de respuesta a fármacos.

El hecho de que las CIT secreten vesículas extracelulares (VEs) al espacio extracelular y que estas VEs transporten material genético de las células productoras, ha hecho que se postulen como uno de los mejores tipos de biopsia líquida disponibles en la actualidad. Sin embargo, en la mayoría de los gliomas de bajo grado la barrera hematoencefálica (BHE) mantiene su estructura, por lo que su liberación al torrente sanguíneo puede estar limitada. Para ello creamos un modelo animal xenotrasplantado con CIT que presentaba la BHE intacta, de esta manera hemos creado una metodología indirecta que nos permite separar las VEs procedentes del tumor de las del propio ratón. En dicho modelo demostramos por primera vez que los tres tipos de VEs: cuerpos apoptóticos, vesículas de shedding, y exosomas, son capaces de atravesar la BHE y aparecer en el torrente sanguíneo llevando en su interior secuencias de ADNg secretadas por el tumor. Finalmente, demostramos la presencia de *IDH1*^{G395A} en las VEs aisladas de sangre periférica procedente de una cohorte de pacientes diagnosticados con gliomas de bajo y alto grado, lo que supone un método minimamente invasivo para la detección de este marcador esencial para el diagnóstico, pronóstico y seguimiento de los pacientes.

ABSTRACT

Gliomas are the most common primary tumors in the central nervous system. Glioblastoma (GBM) is the most frequent and aggressive glial primary tumor, with an average survival of 15 months. The therapeutic failure is in part due to the existence of a cell population call cancer initiating cells (CIT), which are considered to be responsible for tumor initiation, invasiveness and resistance to current therapy. For this reason, CIT have been proposed as the best pre-clinical model for glioma studies. In this work we investigated the *in vitro* evolution of primary cell cultures isolated from GBM patients's surgical samples, as well as their dissemination pattern in immunocompromised mice. Our results demonstrated that CIT evolve along the passages in culture, showing chromosomic instability events, increased stemness marker expression, as well as significant variation in viability rates and response to drug treatment.

CIT secrete extracellular vesicles (EVs), which carry genetic cargo of originating cells and have been proposed as one of the best type of liquid biopsy available nowadays. However, most low-grade gliomas maintain intact blood-brain barrier (BBB), which might limit EV release into the bloodstream. We used orthotopic xenotransplant mouse model of GBM-CIT featuring an intact BBB. We demonstrated for the first time, that all EV types — apoptotic bodies, shedding microvesicles and exosomes — cross the BBB and can be detected in peripheral blood carrying gDNA secreted by tumor cells.

Finally, we demonstrated the presence of *IDH1*^{G395A} mutation inside EVs isolated from from a cohort of low and high grade glioma patients' peripheral blood, which provides a minimally invasive method to detect this marker essential for diagnosis, prognosis and patient follow-up.

ÍNDICE

ABREVIATURAS

ADN: Ácido Desoxirribonucleico

gADN: ADN genómico

GBM: Glioblastoma

SNC: Sistema Nervioso Central

TMZ: Temozolomida

BHE: Barrera Hematoencefálica

RT: Radioterapia

PcP: Profilaxis para la neumonía por Pneumocystis

MGMT: Metilguanidina-ADN Metiltransferasa

TCGA: del inglés *The Cancer Genome Atlas*

RB: Retinoblastoma

RTK: Receptor Tirosina quinasa

PI3K: Fosfoinositol 3-quinasa

PTEN: Fosfatidilinositol-3,4,5-trisfosfato 3-fosfatasa

ALDH: Aldehído Deshidrogenasa

CIT: Células Iniciadoras de Tumor

G-CIMP: del inglés *GBM-CpG island methylation phenotype*

RMN: Resonancia Magnética Nuclear

VEs: Vesículas Extracelulares

ABs: Cuerpos Apoptóticos

SMVs: Ectosomas o del inglés *Sheding Microvesicles*

EXOs: Exosomas

ABC: del inglés *ATP Binding Cassette*

ESCRT: complejo de clasificación endosomal para el tranporte

PS: Fosfatidilserina

ARN: Ácido Ribonucléico

OMS: Organización Mundial de la Salud

MVS: Cuerpos Multivesiculares

FACS: del inglés *Fluorescence-activated cell sorting*

HSP: del inglés *Heat Shock Protein*

MMP: Metaloproteasas

NK: del inglés *Natural killer*

NSC: Células Neuronales Adultas

CGH: Hibridación Genómica Comparativa

LOH: Pérdida de Heterocigosidad

CCT: Células Circulantes de Tumor

ADNct: ADN circulante

LCF: Líquido Cefalorraquídeo

PCR: Reacción en Cadena de la Polimerasa

NTA: del inglés *Nanopartilce Tracking Analysis*

UTR: del inglés *Untranslated Region*

ALA: Ácido aminolevulínico

1. TESIS COMO COMPENDIO DE TRABAJOS PREVIAMENTE PUBLICADOS

La presente Tesis doctoral, de acuerdo con el informe correspondiente, autorizado por los Directores de Tesis y el Órgano Responsable del Programa de Doctorado, se presenta como un compendio de tres trabajos previamente publicados. Las referencias completas de los artículos que constituyen el cuerpo de la tesis son los siguientes:

- **García-Romero N**, González-Tejedo C, Carrión-Navarro J, Esteban-Rubio S, Rackov G, Rodríguez-Fanjul V, Oliver-De La Cruz J, Prat-Acín R, Peris-Celda M, Blesa D, Ramírez-Jiménez L, Sánchez-Gómez P, Perona R, Escobedo-Lucea C, Belda-Iniesta C, Ayuso-Sacido A. Cancer stem cells from human glioblastoma resemble but do not mimic original tumors after in vitro passaging in serum-free media. *Oncotarget. 2016.*

- **García-Romero N**, Carrión-Navarro J, Esteban-Rubio S, Lázaro-Ibáñez E, Peris-Celda M, Alonso MM, Guzmán-De-Villoria J, Fernández-Carballal C, Ortiz de Mendivil A, García-Duque S, Escobedo-Lucea C, Prat-Acín R, Belda-Iniesta C, Ayuso-Sacido A. DNA sequences within glioma-derived extracellular vesicles can cross the intact Blood-Brain Barrier and be detected in peripheral blood of patients. *Oncotarget*. 2016.

- **García-Romero N**, Rackov G, Belda-Iniesta C, Ayuso-Sacido A. The use of peripheral extracelullar vesicles for identification of molecular biomarkers in a solid tumor mouse model. *Methods in Molecular Biology. Springer. 2016.*

Así mismo, se considera oportuno incluir en los anexos I, II y III de la Tesis los siguientes artículos que han constituido parte de la base formativa del doctorando y en los cuales participa como coautor:

- Núñez C, Baeta M, Cardoso S, Palencia-Madrid L, **García-Romero N**, Llanos A, M de Pancorbo M. Mitochondrial DNA Reveals the Trace of the Ancient Settlers of a Violently Devastated Late Bronze and Iron Ages Village. *Plos One. 2016.*

- Ocampo SM, Rodriguez V, de la Cueva L, Salas G, Carrascosa JL, Rodríguez MJ, **García-Romero N**, Cuñado JL, Camarero J, Miranda R, Belda-Iniesta C, Ayuso-Sacido A. g-force induced giant efficiency of nanoparticles internalization into living cells. *Scientific Reports. 2015.*

- Oliver-de la Cruz Jorge, Carrión Navarro Josefa, **García-Romero Noemí,** Gutiérrez-Martín Antonio, Lázaro-Ibañez Elisa, Escobedo-Lucea Carmen, Perona Rosario, Belda-Iniesta Cristóbal, Ayuso-Sacido Angel. SOX2+ cell population from normal human brain white matter is able to generate mature oligodendrocytes. *Plos One. 2014.*


2
Introducción

2.1 TUMORES GLIALES

El cáncer es una de las principales causas de mortalidad a nivel mundial. Este término, engloba multitud de distintas enfermedades que se caracterizan por el desarrollo y crecimiento de células anormales de una manera no controlada. Se estima que en el año 2030 serán diagnosticadas por un proceso neoplásico 22 millones de personas (Bray *et al.,* 2012). Dentro de esta devastadora enfermedad, encontramos los cánceres que afectan al Sistema Nervioso Central (SNC), con una incidencia de 6,4 casos por cada 100.000 habitantes. En este subgrupo, los gliomas son los tumores primarios más comunes, ya que constituyen el 81% de los tumores malignos que afectan al cerebro (Ostrom *et al.,* 2014). Aunque se pueden encontrar en cualquier parte del SNC, mayoritariamente se desarrollan en el tejido glial (Ostrom *et al.,* 2013).

Los gliomas derivan de tres tipos celulares distintos: de los astrocitos (astrocitomas), de los oligodendrocitos (oligodendrogliomas) y de células ependimarias (ependimomas) (Martín-Villalba *et al.,* 2008).

Históricamente los métodos de clasificación de la Organización Mundial de la Salud (OMS) se han basado en criterios histopatológicos, siendo los más comunes: el estudio de la actividad mitótica, la atipia nuclear, la proliferación del endotelio vascular y la presencia o ausencia de necrosis (Gudinaviciene *et al.,* 2004). A medida que estos signos se hacen más evidentes, se aumenta el grado de malignidad del tumor, variando de bajo grado (I-II) a alto grado (III-IV). En los últimos años, con el fin de poder explicar las distintas evoluciones observadas entre tumores con el mismo grado y diagnóstico histopatológico, se ha ido profundizando en el estudio de los distintos perfiles moleculares presentes en estas neoplasias, facilitado en parte por el desarrollo de las plataformas ómicas. Concretamente, en este último año, se ha publicado una actualización de la cuarta revisión de la Clasificación de la OMS de los tumores del SNC. Y, por primera vez, en esta clasificación se añade el análisis de parámetros moleculares junto a los histológicos, lo que supone un importante avance en el subtipado de los gliomas, permitiendo mejorar la precisión diagnóstica y pronóstica de los pacientes. La clasificación de los gliomas difusos se basa

principalmente en el análisis del estado del gen *IDH*, del que se hablará detalladamente más adelante. Además, se incluyen otros estudios como el examen del gen *ATRX* (que codifica para un complejo remodelador de la cromatina) y su frecuente pérdida en los astrocitomas difusos, la mutación en *TP53* y la deleción conjunta del brazo corto del cromosoma 1 y del largo del cromosoma 19 (1p/19q) presente en los oligodendrogliomas (Louis *et al.,* 2016) (**Figura 1**). Por tanto, esta nueva clasificación permitirá la estratificación de los pacientes en función de su perfil molecular. En este sentido, dentro del subtipo de tumores astrocíticos, los que tienen pérdida en la expresión de *ATRX* pueden definir un subgrupo con un pronóstico más favorable (Wiestler *et al.,* 2013). Del mismo modo, la pérdida de los cromosomas 1p/19q está asociada con una morfología oligodendroglial, con mayor número de mutaciones en el gen *IDH1* y una mayor supervivencia (Smith J *et al.,* 2000; Yan *et al.,* 2009).

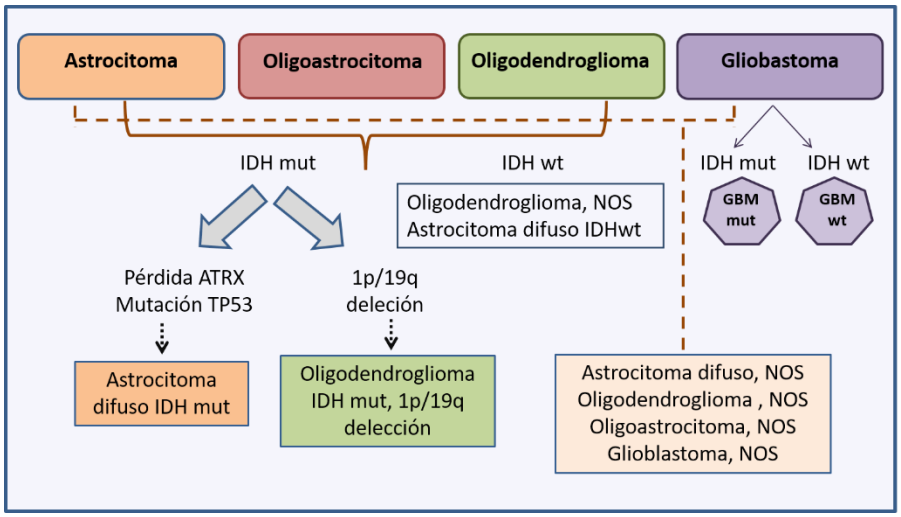

Figura 1. Actualización de la 4ª revisión de la OMS de la Clasificación de los tumores del SNC. NOS: casos en los que no se ha realizado el análisis genético o el resultado no ha sido concluyente. (Adaptada de Louis *et al.,* 2016).

2.1.1 El gen *IDH*

La familia de genes *IDH* está compuesta por cinco genes: *IDH1*, *IDH2*, *IDH3A*, *IDH3B* e *IDH3G* que codifican para las enzimas IDH1, IDH2 e IDH3, respectivamente (Stancheva *et al.,* 2014). Las dos enzimas principales, IDH1 e IDH2, en su estado

salvaje catalizan la conversión del isocitrato a 2-oxaglutarato, por lo que la presencia de formas mutantes de ambas enzimas implica una alteración en el metabolismo (**Figura 2**). Existen varias hipótesis acerca del mecanismo por el cual estos genes mutados promueven la tumorogénesis, las dos más importantes difieren sobre su mecanismo de acción, una de ellas propone que el R-2-hidroxiglutarato actúa como un onco-metabolito y promueve la transformación celular, alterando el estado redox de las células (Reitman *et al.,* 2010). Por el contrario, la otra sugiere que, al alterar la función normal de la mitocondria, se promueve la activación de las células cancerosas hacia la glucolisis (Leonardi *et al.,* 2012).

El gen *IDH1,* localizado en el brazo largo del cromosoma 2 (2q33), presenta mutaciones heterocigotas que afectan al codón 132 de la proteína, situado en el centro activo de esta enzima citoplasmática, donde tiene lugar la conversión al sustrato. Las mutaciones que aparecen con mayor frecuencia en los gliomas de bajo grado tienen lugar en la base nitrogenada situada en la posición 395, donde se produce una transición entre bases púricas; se transforma una Guanina en Adenina (G395A). Esto produce un cambio en el codón proteico de arginina a histidina, conocida como R132H. Dicha mutación está presente en el 70-80% de todos los gliomas de bajo grado y en un 5-10% en los de alto grado (Yan *et al.,* 2009). Existen también otras mutaciones en el mismo codón, como R132G (C394G), R132S (C394A), R132C (C394T) y R132L (G395T), pero éstas aparecen con menor frecuencia. Así mismo, y aunque en una proporción menor al 3%, los tumores gliales también presentan mutaciones en el centro activo de la enzima mitocondrial IDH2, concretamente en el codón 172. Tanto las mutaciones de *IDH1* como de *IDH2* tienen lugar en un solo alelo y son mutuamente excluyentes (Cohen *et al.,* 2013).

En este sentido, hay varios estudios que reflejan que estas mutaciones confieren un aumento de supervivencia (Sanson *et al.,* 2009), e incluso afirman que la mutación es la causa de un fenotipo hipermetilado en gliomas denominado "GBM-CpG island methylation phenotype" (G-CIMP) (Turcan *et al.,* 2012), lo cual está centrando la búsqueda de agentes hipometilantes para su posible uso terapéutico (Christensen *et al.,* 2011).

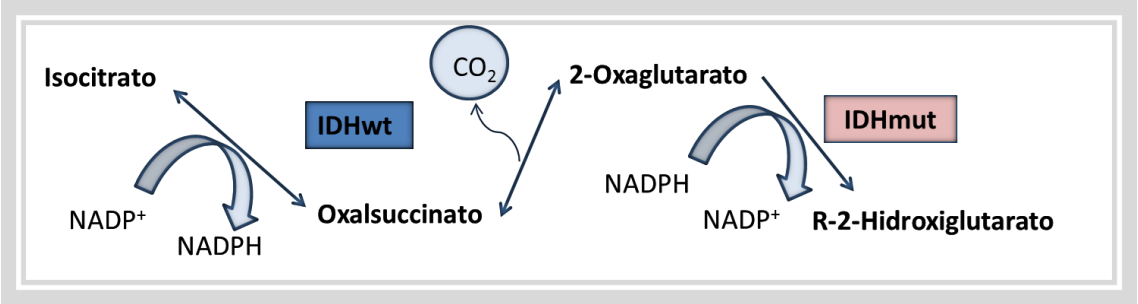

Figura 2. Reacciones catalizadas por las enzimas IDH1 y IDH2. El estado mutante es incapaz de catalizar la carboxilación de R-2-Hidroxiglutarato hasta 2-Oxaglutarato. (Adaptado de Losman *et al.,* 2013).

2.2 EL GLIOBLASTOMA

El glioblastoma (GBM) es el tumor glial más frecuente, con una incidencia de 3 casos al año por cada 100.000 habitantes, y supone aproximadamente el 1.4 % de todos los cánceres diagnosticados anualmente (Ostrom *et al.,* 2015). Los GBMs pueden originarse sin neoplasia astrocitaria preexistente (GBM primarios o *de novo*), constituyendo el 90 % de los casos, o bien desarrollarse a partir de un astrocitoma difuso o anaplásico previo (GBM secundario). Estos tumores se caracterizan por presentar un crecimiento rápido, dando lugar a focos de necrosis y de proliferación vascular en el tejido, además de signos marcados de anaplasia. Los GBMs únicamente tienden a invadir el tejido normal adyacente, y rara vez, del 0,4 al 2%, provocan metástasis fuera del SNC (Hamilton *et al.,* 2014), por lo que se caracterizan por una pronunciada invasividad (Patel *et al.,* 2014) así como una gran heterogeneidad, tanto intra como inter tumoral (Verhaak *et al.,* 2010). Todo ello, dificulta la clasificación, lo que conlleva a que se puedan obtener diferentes diagnósticos del mismo tumor dependiendo de la región que se adquiera para el análisis histopatológico (Sottoriva *et al.,* 2013).

2.2.1 CLASIFICACIÓN EN FUNCIÓN DE LOS PATRONES DE EXPRESIÓN GÉNICA

Con el fin de aumentar el conocimiento de la biología de este tumor, en 2008 el grupo denominado Atlas Genómico del Cancer o TCGA (del inglés *The Cancer Genome Atlas*) realizó un estudio en una gran cohorte, de más de 200 muestras de

pacientes diagnosticados con GBM. Dicho análisis reveló alteraciones en varias vías importantes de la biología de este tumor. Se observaron modificaciones en las vías de supresión tumoral del retinoblastoma (RB) y TP53, y en la más frecuente en estas neoplasias; la vía del Receptor Tirosina quinasa/ RAS/ Fosfoinositol 3-quinasa/(*RTK/RAS/PI3K*). Estudios posteriores realizados con plataformas de expresión génica subdividieron los GBMs en 4 grupos, basándose principalmente en la asociación de alteraciones moleculares de los genes *PDGFRA, IDH1, EGFR y NFI* (Verhaak *et al.,* 2010). El fenotipo clásico, se relaciona con la pérdida del cromosoma 10, la ganancia del cromosoma 7 y, por tanto, la amplificación del gen *EGFR,* así como la deleción homocigota de *CDKN2A*. El subtipo mesenquimal formado por tumores que presentan deleciones hemicigotas del gen *NF1* y sobreexpresión de marcadores de células mesenquimales como *CHI3L1 y MET*. El fenotipo proneural se caracteriza por tener amplificación y/o mutación de la secuencia codificante de *PDGFRA* y mutaciones puntuales en *IDH1/2*, así como G-CIMP^{+}. Por último, el fenotipo neural, que aunque es el menos estudiado y no posee una vía dominante, presenta sobre-expresión de marcadores característicos neuronales como *NEFL, GABRA1, SYT1 y SLC12A5*.

Además de estos subtipos, la actual clasificación divide al GBM en función de la secuencia génica de *IDH,* agrupándolos en: **GBM_*IDH* salvaje** (secuencia igual a la del genoma de referencia), **GBM_*IDH* mutante** (secuencia con alteraciones respecto a la secuencia de referencia) y, por último, **GBM_NOS** (del inglés, *Not Otherwise Specified*) en el que incluyen los tumores a los que no se les ha realizado el análisis genético o el resultado no ha sido concluyente. Dentro del grupo de los GBM_*IDH* salvaje, con una frecuencia observada del 90%, podemos encontrarnos otros tres tipos: Gliosarcoma, que se caracteriza por presentar una mezcla de células tumorales de origen glial, junto a células de origen mesenquimal. El GBM epitelioide, que como su nombre indica, dispone de grandes células epitelioides, cromatina vesicular y nucleolos prominentes (Louis *et al.,* 2016). Y, por último, el subtipo menos frecuente, con un porcentaje de aparición del 2 al 5%, el GBM de células gigantes en el que predominan células de gran tamaño, multinucleadas y con un citoplasma eosinófilo (Ohgaki *et al.,* 2000).

2.2.2 SÍNTOMAS Y DIAGNÓSTICO

Los síntomas del GBM suelen variar en función del tumor, y se subdividen en dos grupos: focales y no focales. Los síntomas no focales están relacionados con el cambio de la presión intracraneal producida por el tumor, la cual provoca frecuentemente cefaleas intensas, convulsiones, náuseas o vómitos en el paciente. Por otro lado, los síntomas focales corresponden a la zona concreta en la que se localiza el tumor. En el caso de que la lesión abarque los lóbulos frontal y temporal se pueden experimentar cambios en el humor y/o en la personalidad, así como, pueden ocurrir cambios en la visión o en la audición, pérdida de memoria, y en alguna ocasión se puede observar disfunción del lenguaje.

La primera aproximación para establecer un diagnóstico es el uso de técnicas de imagen, ya sea por Resonancia Magnética o Tomografía Computarizada, en las cuales, el GBM se caracteriza por presentar bordes irregulares, captación de contraste en función del estado de la barrera hematoencefálica (BHE), necrosis central y edema. Lamentablemente, y a pesar del avance en estas técnicas, el estadío del tumor no se averigua con certeza hasta que no se obtiene el diagnóstico histopatológico. Esto supone una gran limitación clínica y terapéutica, ya que se requiere de cirugía, o en su caso, de una biopsia estereotáxica del tejido para obtener el diagnóstico definitivo.

2.2.3 TRATAMIENTO

La terapia estándar del GBM primario o *de novo* consiste en la resección máxima de la lesión, sin afectar a otras zonas próximas, junto con radioterapia (RT) y quimioterapia concomitante. Al ser un tumor tan invasivo, la resección total es muy limitada, lo que facilita la posibilidad de recidiva tras el tratamiento. Esta terapia se conoce como el "Protocolo de Stupp", término acuñado en 2005 cuando Stupp y colaboradores demostraron que la administración de 75 mg/m^2 al día de temozolomida (TMZ), junto a la radioterapia, aumentaba la supervivencia media de los pacientes de 12,1 a 14, 6 meses en comparación con la radioterapia adyuvante (Stupp *et al.,* 2005) (**Figura 3**).

La TMZ es un agente alquilante que actúa directamente sobre el ácido desoxirribonucleico (ADN), añadiendo un grupo metilo a las bases púricas (O-6, N-7 guanina y N-3 adenina) (Zhang *et al.,* 2012). Pertenece al grupo de las nitrosureas, las cuales se tratan de unas moléculas de pequeño tamaño con estructura lipofílica que son capaces de atravesar la BHE (Villà *et al.,* 2014). Los pacientes con GBM presentan distinta sensibilidad a este fármaco, en parte dependiente del estado del promotor del gen *MGMT*, (Metilguanidina- ADN Metiltransferasa), lo que le convierte en un marcador predictivo de respuesta (Japtap *et al.,* 2005). La proteína codificada por este gen se encarga de la reparación de errores en el ADN y su funcionalidad depende del estado de metilación de su promotor, ya que cuando éste se encuentra metilado ocurre una pérdida de su expresión proteica. Por tanto, los pacientes que presenten el promotor de *MGMT* metilado responderán mejor al tratamiento que los que presenten el estado salvaje.

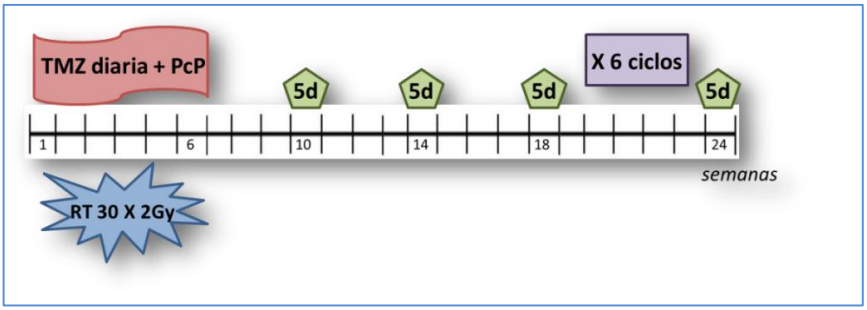

Figura 3. Terapia estándar para GBM. En el período que se administra la TMZ (75mg/m^2) junto la radioterapia (RT) se recomienda el uso de profilaxis para la pneumonia (PcP). Tras estos ciclos, se aplican 200 mg/m^2 de TMZ en períodos de 5 días cada 4 semanas. (Adaptada de Stupp *et al.,* 2007).

2.3 BARRERA HEMATOENCEFÁLICA

La barrera hematoencefálica está formada por varios componentes celulares que separan los capilares del parénquima del SNC. Uno de sus principales integrantes son las células endoteliales que recubren los vasos sanguíneos, además de los astrocitos, la microglía y los pericitos que se encuentran en la membrana basal (Do *et al.,* 2014). Las uniones estrechas entre las células endoteliales, y su interacción con el resto de componentes de la BHE aseguran su correcto funcionamiento (Luissint *et al.,* 2012). Básicamente, su competencia consiste en regular el tránsito de moléculas,

asegurando la correcta homeostasis y actividad del sistema. Dicha actividad es muy selectiva, previniendo el paso de moléculas con un peso molecular mayor de 180 Da (Petty *et al.,* 2002). Su descubrimiento fue llevado a cabo por Paul Ehrlich y Edwin E. Goldman cuando al inyectar por vía intravenosa el colorante azul tripan observaron una dispersión del mismo por todo el cuerpo, exceptuando el cerebro y la médula espinal (Hawkins *et al.,* 2005).

Aunque los pacientes diagnosticados con glioma suelen tener la BHE comprometida, los cambios en la permeabilidad dependen del tipo y tamaño del tumor. En algunas ocasiones la BHE puede estar rota en la zona central del tumor, mientras que en la periferia puede aparecer con distintas complejidades. Su ruptura permite la entrada de fluidos desde el torrente sanguíneo al parénquima cerebral, provocando una de las mayores causas de mortalidad en estos pacientes, el edema vasogénico (Ryan *et al.,* 2012).

Los métodos más comunes para evaluar la permeabilidad de la BHE se basan en la detección, dentro del SNC, de moléculas de alto peso molecular. Las proteínas endógenas comúnmente utilizadas son la albúmina y la inmunoglobulina G, ya que, debido a su gran tamaño, (69 y 150 KDa, respectivamente), en condiciones normales ninguna de ellas son capaces de atravesar la BHE. En otras ocasiones, se utilizan trazadores externos que facilitan su detección, como por ejemplo, el *Evans Blue*. Este colorante tiene una alta afinidad por la albúmina, por lo que al unirse forman un gran complejo incapaz de atravesar la BHE. Sin embargo, si la integridad de la BHE está comprometida, se puede observar un color azul dentro del SNC (Leten *et al.,* 2014). También se utilizan técnicas de imagen, como microscopía confocal *in vivo* o Resonancia Magnética Nuclear (RMN). En esta última, normalmente se utiliza como agente de contraste el Gadolinio: elemento con propiedad paramagnética que modifica los tiempos de relajación T1 y T2 permitiendo determinar el estado de la BHE. Ya que su captación por el SNC se relaciona directamente con un aumento en la permeabilidad (Wunder *et al.,* 2012).

2.4 CELULAS INICIADORAS DE TUMOR

Las células iniciadoras de tumor (CIT) o también conocidas como células madre del cáncer, consisten en una pequeña población celular dentro del tumor, a las que se las atribuye la responsabilidad del inicio del tumor, de la invasividad y de la formación de metástasis. Estas células se definen por dos características principales. La capacidad de diferenciación y la de auto-renovación. La capacidad de diferenciación o de pluri-potencialidad permite que se generen células con diferentes fenotipos, mientras que la capacidad de auto-renovación hace que las CIT sean capaces de dividirse generando células idénticas a sus progenitoras (Pointer *et al.,* 2014).

Estas células son en gran parte responsables de la recurrencia del tumor y de la resistencia a las terapias dirigidas, posiblemente por su capacidad de permanecer en estado quiescente (Singh *et al.,* 2004), y a la sobre-expresión de los transportadores ABC (cassette de unión a ATP); concretamente del ABCG2. Estos transportadores expulsan rápidamente los agentes quimioterapéuticos como, por ejemplo, la doxorubicina o el topotecan, por lo que no llegan a producir el efecto deseado (Crea *et al.,* 2009). Así mismo, se ha visto que la capacidad de auto-renovación de las CIT está ampliamente relacionada con la menor supervivencia del paciente (Laks *et al.,* 2010).

Debido a la relevancia de esta población celular en el desarrollo del cáncer, se han propuesto una variedad de métodos para su identificación. Dichos métodos tienen como objetivo principal, la identificación de nuevos marcadores moleculares que informen sobre el tipo y cantidad de CIT y ayuden de forma general a conocer mejor la biología de este tumor y de manera más específica a la estratificación de pacientes. Desafortunadamente, y pese a los esfuerzos de la comunidad científica, no existen protocolos universales para su identificación, aislamiento y caracterización. Aunque si se pueden destacar como aproximaciones más comúnmente utilizadas: la capacidad de generación de neuroesferas *in vitro,* la clasificación de células activadas por fluorescencia (FACS) mediante marcadores de superficie (como por ejemplo CD133 o CD44), la medición de la aldehído deshidrogenasa (ALDH), el método de

exclusión de Hoechst 33342 y la capacidad de formación de tumores en ratones inmunodeprimidos *(*Alamgeer *et al.,* 2013). Sin embargo, ninguno de estos métodos tiene la especificidad suficiente para distinguir entre otras células neuronales adultas (NSC) o más diferenciadas (Brescia *et al.,* 2012).

Aunque está ampliamente aceptado que se necesita un cúmulo de alteraciones tanto genéticas como epigéneticas para que tenga lugar la formación de un tumor, existen al menos dos teorías que intentan explicar el proceso de tumorogénesis.

2.4.1 MODELO ESTOCÁSTICO

El Modelo Estocástico o también conocido, como modelo de Evolución Clonal, defiende la teoría en la que una sola célula somática es la que presenta una mutación y desencadena un proceso no controlado de división celular en el que se generan nuevas alteraciones genéticas hasta que se alcanza el estado de célula tumoral (Bradshaw *et al.,* 2016). En este modelo cada célula que compone el tumor comparte las mismas características y por tanto es capaz de formar tumores primarios, es decir; los tumores se caracterizan por ser biológicamente homogéneos. En este sentido, la heterogeneidad encontrada en los tumores, se debe a la influencia de distintos factores al azar, contemplando la posibilidad de que las células cambien de estado según los factores a las que estén sometidas. Estos factores pueden ser extrínsecos; como el microambiente o la respuesta inmune, o intrínsecos; como las distintas vías de señalización o factores de transcripción (Dick *et al.,* 2009).

2.4.2 MODELO JERÁRQUICO

Por otro lado, el Modelo Jerárquico postula que sólo una pequeña población celular (CIT) es la responsable de iniciar y mantener el crecimiento del tumor, por lo que los tumores presentan distintos tipos celulares que se comportan de manera diferente, y tienen distintas características. De este modo, los tumores están organizados de forma jerárquicamente similar a un tejido normal, desde las células más primitivas, a las más diferenciadas. Las CIT se generarían por mutaciones en

células progenitoras o células madre embrionarias, adquiriendo la capacidad de propagarse y de crecer de forma incontrolada. Este hecho podría explicar la heterogeneidad observada en los procesos neoplásicos. Aunque este modelo parece ser el más aceptado en la actualidad, todavía quedan muchas cuestiones que resolver (Pietras *et al.,* 2011).

2.5 VESÍCULAS EXTRACELULARES

En los últimos años el interés por la búsqueda de marcadores moleculares a partir de biopsia líquida ha crecido exponencialmente. Dentro de los diferentes fluidos que pueden utilizarse a la hora de identificar dichos marcadores, la sangre periférica es, sin duda alguna, el más prometedor a corto y medio plazo para la mayoría de los tumores. La naturaleza de las moléculas que pueden ser utilizadas como biomarcadores es variable, aunque proteínas y, sobre todo, ácidos nucleicos, presentan mayor potencial para informar sobre la presencia de alteraciones moleculares específicas en células tumorales. Estas moléculas se pueden encontrar en tres compartimentos diferentes: circulando libremente, en el interior de células circulantes del tumor (CCT) o de vesículas extracelulares (VEs) (Strotman *et al.,* 2016). Las VEs son pequeñas estructuras rodeadas de membrana que son secretadas al espacio extracelular por todos los tipos celulares y juegan un papel importante en la comunicación de las mismas (Lee et *al.,* 2014). Su síntesis y secreción parece ser un proceso conservado, dado que no es específico de humanos, sino que aparece en otras especies como plantas, bacterias y parásitos (Yáñez-Mó *et al.,* 2015). Son elementos que participan en mecanismos de comunicación paracrina y endocrina (Tetta *et al.,* 2012). En este sentido, tienen la capacidad de transferir su contenido, formado por moléculas biológicamente activas a otras células receptoras, alterando el comportamiento de las últimas (Cvjetkovic *et al.,* 2016). Además de la comunicación celular, se les ha atribuido otras funciones como el mantenimiento de la homeostasis, la degradación o eliminación de sustancias tóxicas, la angiogénesis, la inflamación, la respuesta inmune y el desarrollo y la progresión de condiciones patológicas como es el caso de diferentes tipos de cáncer (Revenfeld *et al.,* 2014).

Estas VEs se pueden encontrar en todos los tipos de fluidos biológicos, incluyendo sangre (Fendl *et al.,* 2016), plasma (Ashcroft *et al.,* 2012), suero (Dalton *et al.,* 1975), saliva (Marzesco *et al.,* 2005), orina (Lázaro-Ibáñez *et al.,* 2014), linfa (Milasan *et al.,* 2016), líquido cefalorraquídeo (Chiasserini *et al.,* 2014), leche (Zonneveld *et al.,* 2014), líquido amniótico (Asea *et al.,* 2008) y semen (Arienti *et al.,* 2004). Desde su descubrimiento inicial en 1946 (Chargaff *et al.,* 1946), y hasta que se ha observado que su formación tiene lugar por parte de todas las células del organismo, se les ha nombrado en función de la célula o la especie de la que procedían. Así se pueden encontrar estudios en la literatura en los que aparecen descritos como dexosomas; procedentes de células dendríticas (Le Pecq et *al.,* 2005), oncosomas; procedentes de células tumorales (Minciacchi *et al.,* 2015), argosomas a los aislados en *Drosophila Melanogaster* o prostasomas, si procedían de semen (Ronquist *et al.,* 1985), entre otros. A estos últimos, se les han atribuido la función de regular algunos procesos de la activación de los espermatozoides (Stegmayr *et al.,* 1982).

Aunque de momento no se conoce el mecanismo de empaquetamiento, las VEs albergan en su interior multitud de moléculas de distintas composiciones, así como proteínas, lípidos, factores de crecimiento y/o sus receptores, proteasas, moléculas de adhesión y una diversidad de ácidos nucleicos como dsADN, ssADN (Balaj *et al.,* 2011), mtADN (Guescini *et al.,* 2010) y distintas especies de ARN, como ncARN, mARN, miARN (Deregibus *et al.,* 2012), e incluso histonas (Lee *et al.,* 2011).

En 2012, dada la necesidad de dividir los tipos de VEs, y generar un consenso a la hora de publicar literatura científica, se creó un compendio de VEs, llamado "Vesiclepedia", en el que se estableció la nomenclatura a utilizar en función de la biogénesis y el tamaño de estas VEs. Describiendo así tres subtipos: Cuerpos Apoptóticos (ABs), ectosomas o Vesículas de Shedding (SMVs) y exosomas (EXOs) (Kalra *et al.,* 2012) (**Figura 4**).

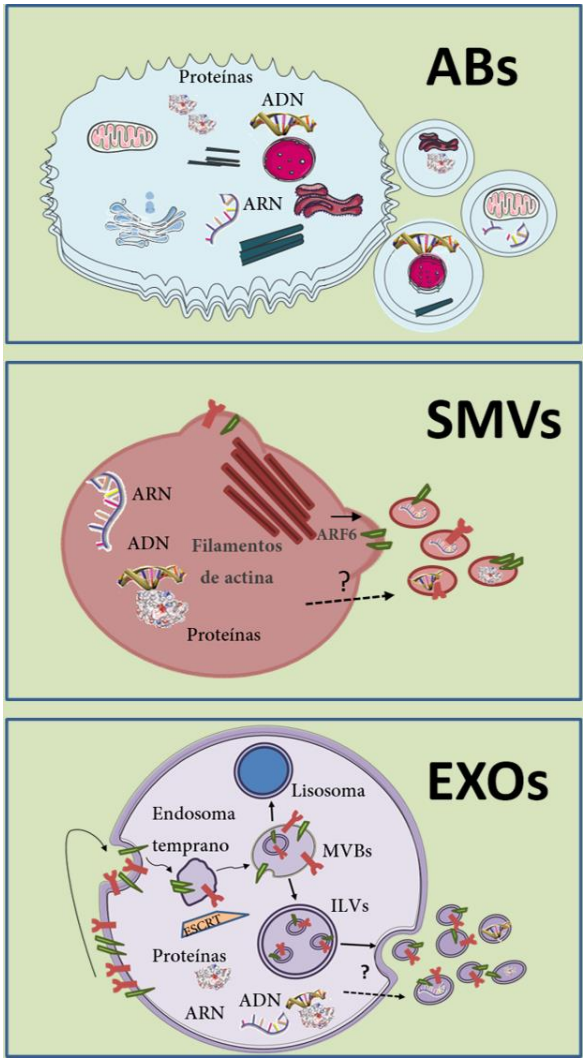

Figura 4. *Mecanismos de biogénesis de los distintos tipos de VEs.*

Los ABs son generados a partir de células apoptóticas, mientras que las SMVs se forman por evaginación de la membrana plasmática mediada por el factor ARF6. Por último, las VEs de menor tamaño (EXOs) son secretados a partir de los cuerpos multivesiculares (MVBs) formados por la vía endocítica. Se desconoce el proceso exacto de internalización del material genético dentro de las VEs.

La secreción de VEs se puede regular *in vitro* añadiendo estímulos externos. Por ejemplo, mediante la adición al medio de cultivo de colágeno, epinefrina, adenosin difosfato o ionóforos de calcio, entre otros. Del mismo modo, también se puede bloquear la generación de VEs con diversos agentes químicos, como la Imipramina, que es un inhibidor de las SMVs, DEVD (Z-Asp-Glu-Val-Asp-CH_2F), que inhibe la producción de ABs, o GW4869, un inhibidor de la esfingomielasa 2, relacionada con la liberación de EXOs (Di Trapani *et al.,* 2016).

En base a las características biológicas de las VEs, actualmente, se está extendiendo el potencial uso de las VEs como vehículos de fármacos o de ARN interferentes. Ya que se presentan como una gran alternativa frente a las partículas sintéticas debido a su origen endógeno y a la composición de su membrana, por lo que al evadir la detección del sistema inmune, generarían mayor estabilidad y menor rechazo y/o toxicidad (Lakhal *et al.,* 2011). Además, se está generalizando su uso como fuente de biomarcadores clínicos, ya que el contenido biológico de las VEs está estrechamente relacionado con la célula secretora, por ejemplo, en algunas enfermedades se han descrito biomarcadores específicos como: Glypican-1 en cáncer

de páncreas (Melo *et al.,* 2015), MAGE3/6 y TGFβ1 en cáncer de ovario (Szajnik *et al.,* 2013), CD24 en cáncer de mama (Rupp *et al.,* 2011) o CD34 en leucemia amieloide aguda (Hong *et al.,* 2014). Por lo que el uso clínico de estas VEs puede servir de apoyo tanto para el pronóstico como para el diagnóstico del paciente, así como para monitorizar la respuesta a fármacos.

2.5.1 CUERPOS APOPTÓTICOS

Son las vesículas que presentan mayor tamaño y con un rango que oscila entre 1000 nm y 4µm. Se secretan en las fases tardías de la muerte celular programada, o también llamada apoptosis. Su secreción está dirigida por la caspasa-3 que induce la reorganización del citoesqueleto y la desintegración de las células en ABs, que surgen a partir de unas protuberancias en la membrana plasmática. Se diferencian de las otras vesículas porque presentan en su interior organelas con la estructura intacta y no presentan colesterol (El Andaloussi *et al.,* 2013). Además, son característicos por tener en su membrana Trombospondina, y la proteína del complemento C3b, lo cual facilita el reconocimiento por los receptores fagocíticos. Se demostró que las células pueden liberar ácidos nucleicos en ABs durante la apoptosis protegiéndolos de la degradación (Halicka *et al.,* 2000), hecho que explica la estabilidad del ARNm observada en suero en presencia de nucleasas (Hasselmann *et al.,* 2001).

2.5.2 VESÍCULAS DE SHEDDING

Son vesículas de tamaño intermedio, de 100 a 1000nm. Se producen por evaginación de la membrana plasmática, la cual muestra una asimetría en su disposición, presentando dos monocapas. La monocapa externa, compuesta mayoritariamente por fosfatidilcolina y esfingomielina, y la cara interna o citosólica rica en fosfatidilserina (PS) y fosfatidietalonamina (Muralidharan-Chari *et al.,* 2010). Existe gran controversia acerca del proceso exacto de liberación de SMVs. Hace unos años, se postuló una teoría que defendía que la liberación de SMVs se produce cuando se desestabiliza la estructura de la membrana plasmática, dándose una translocación de PS del citosol a la cara externa, produciéndose de este modo la liberación de las vesículas, por lo que estas presentan una distribución lipídica en

sentido contrario a la disposición habitual de la membrana plasmática (Piccin *et al.,* 2007). Sin embargo, se cree que este no es el único mecanismo de liberación de SMVs, ya que hay estudios anteriores en los que aíslan y caracterizan una población de SMVs sin PS en su cara externa (Shet *et al.,* 2003). Además de caracterizarse por tener expuesto los residuos de PS en su superficie, se han asociado con regiones con altos niveles de lípidos (balsas lipídicas) y poseen otros marcadores característicos como el CD40, el factor 6 de ribosilación del ADP (ARF6), y muchas integrinas y selectinas (Kalra *et al.,* 2016). El fenotipo de las SMVs refleja la célula que lo ha secretado, y en muchas ocasiones se encuentran marcadores de linaje como por ejemplo CD14, marcador de monocitos, o el CD61, característico de plaquetas (Barteneva *et al.,* 2013).

2.5.3 EXOSOMAS

El término "exosomas" fue acuñado por Trams en 1981 cuando observó por microscopía electrónica una subpoblación de vesículas de aproximadamente 40 nm (Trams *et al.,* 1981). Sin embargo, más tarde se ha comprobado que pueden presentar un tamaño variable hasta los 150 nm. Pese a que el mecanismo exacto de biogénesis no está muy elucidado, se piensa que los EXOs se producen por invaginación de la membrana plasmática al formarse unas vacuolas intracelulares que contienen señales ubiquitinizadas. Estas vacuolas, bajo el control del Complejo de Clasificación Endosomal para el Tranporte (ESCRT), se transforman en endosomas tempranos. Éstos sufren, a continuación, una segunda invaginación y maduran en endosomas tardíos, o más conocidos como cuerpos multivesiculares (MVBs). Dichos MVBs pueden volver a ser utilizados y, por tanto, reciclados a la membrana plasmática, o ser secuestrados en vesículas intraluminares (ILVs). Sin embargo, también pueden ser degradados por la vía lisosomal, o fusionarse con la membrana plasmática y ser liberados al espacio extracelular como EXOs. Esta fusión está regulada por la familia de GTPasas Rab (Hannafon *et al.,* 2013). Cabe resaltar que también se han descrito mecanismos de formación de ILVs independientes de ESCRT, por lo que pueden existir otras vías de liberación de EXOs aún desconocidas (Stuffers *et al.,* 2009).

Basándonos en el mecanismo de biogénesis, podemos decir que los EXOs poseen por tanto la misma orientación y similar composición que la membrana plasmática rica en colesterol, ceramida y esfingomielina. Por lo que apenas poseen residuos expuestos de PS a la cara externa de la membrana, hecho que las distingue de las SMVs (Cocucci *et al.,* 2015).

Como consecuencia del complejo multiproteico ESCRT, los EXOs están enriquecidos en determinadas proteínas y tienen marcadores específicos como TSG101, Alix, la familia de las tetraspaninas; CD9, CD63 CD81, o proteínas de choque término (HSP); HSP60, HSP70, HSP90, entre otras. Este sesgo proteico, se cree que es debido a la regulación de señales de ubiqutinación de tal modo que, si sólo se produce la unión de una molécula de ubiquitina, sirve de señal para que la proteína siga la vía endocítica, y por tanto la liberación al medio extracelular en los EXOs, sin embargo, si se da una poli-ubiquitinación, la proteína queda marcada para que sea degradada por el proteasoma (Taylor *et al.,* 2011).

El aumento de estudios en estos ensayos y la necesidad de la comunidad científica de tener recopilados todos los datos relacionados con los estudios en exosomas, llevó a la creación de la base de datos ExoCarta (www.exocarta.org) en la cual se han incluido hasta la escritura de esta tesis, 286 artículos publicados en revistas indexadas, dando lugar a un total de 41.860 entradas de proteínas, 4946 entradas de mRNAs, 2838 entradas de miRNAs y 1116 entradas de lípidos. Esta base de datos contiene información de los métodos de identificación, el tipo de muestra y el organismo del que proceden los EXOs aislados en cada caso (Mathivanan *et al.,* 2010).

2.6 INTERNALIZACIÓN DE ÁCIDOS NUCLEICOS EN LAS VEs

Aunque no se conoce el mecanismo de internalización de ácidos nucleicos dentro de las VEs ni la procedencia exacta de los mismos, hay varios estudios que intentan explicar estos procesos. Por un lado, se tiene certeza de que el ADN que se encuentra en el interior de los ABs está fragmentado, lo que puede ser debido a la hipersegmentación que sufre la cromatina en las células apoptóticas de las que procede (Collins et *al.,* 1997). Además, otros autores sugieren que el ssDNA

encontrado dentro de los EXOs de las células cancerosas, puede proceder de los fallos ocurridos en la fase G_1 del ciclo celular (Balaj et al., 2011), pero esto no explicaría la presencia de dsDNA ni la representación de todo el genoma en su interior (Thakur *et al.,* 2014). Por otro lado, se han identificado secuencias conservadas en la región 3'UTR del ARN que contribuyen al reclutamiento del ARNm dentro de las VEs, por lo que sugieren que la internalización de este tipo de ácido nucleico se basa en un proceso selectivo (Bolukbasi *et al.,* 2012).

2.7 MÉTODOS DE AISLAMIENTO e IDENTIFICACIÓN

Los métodos de aislamiento de VEs a partir de medios de cultivo o de fluidos biológicos deben asegurar, en primer lugar, que no existe contaminación con otras moléculas, ya sean restos celulares, debris, u otras sustancias. Para ello se realiza una primera centrifugación de donde se obtiene el sobrenadante que se va a utilizar en los siguientes pasos y del que se van a aislar las VEs. Aunque el método por referencia o "gold standard" es la ultracentrifugación, todos los procedimientos utilizados se basan en la exclusión por tamaño o en la detección de marcadores específicos. Se incluyen distintos métodos como, por ejemplo: gradiente de sacarosa, microfiltración, cromatografía de exclusión por tamaño, precipitación con tampones orgánicos o polímeros o incluso la separación mediante métodos de afinidad inmune (Momen-Heravi *et al.,* 2013). En el caso en el que se quieran aislar los tres tipos de VEs separados en fracciones, la técnica más utilizada es la ultra-centrifugación de manera seriada y con velocidades crecientes. Sin embargo, la mayoría de estudios ignoran la fracción de las ABs, y no diferencian entre los otros dos subtipos, obteniendo una mezcla de SMVs y EXOs (Chen *et al.,* 2013; Akers *et al.,* 2013).

En este contexto, hay que tener en cuenta multitud de factores a la hora de aislar VEs, ya que algunos parámetros como la viscosidad del fluido de partida, la temperatura o el momento de almacenamiento pueden alterar el recuento final (Fendl *et al.,* 2016). En este sentido, cuando se obtienen VEs a partir de sangre periférica de pacientes, se ha descrito que el uso de anticoagulantes como EDTA o citrato hace que se reduzca el número total de VEs aisladas, ya que estos quelantes de Ca^{2+} favorecen la unión de las VEs a las plaquetas. Por el contrario, se recomienda

el uso de inhibidores de proteasas como la heparina, ya que no provoca ningún efecto en el proceso (Jayachandran *et al.,* 2012). En el caso de cultivos celulares, otro de los factores que se debe de tener en cuenta, es la utilización de suero suplementado al medio de cultivo, ya que el suero posee VEs de la especie de la que provenga y puede interferir en los siguientes experimentos. Hoy en día, cabe la posibilidad de adquirir suero comercial depleccionado previamente o se pueden eliminar la VEs mediante ultracentrifugación (Shelke *et al.,* 2014).

Una vez que se han aislado las VEs, el proceso de caracterización e identificación de estos subtipos se realiza normalmente mediante análisis morfológicos. Para ello se utilizan varios tipos de microscopía, aunque las más comunes son la Microscopía Electrónica de Transmisión y la Microscopía Crioelectrónica. Por otro lado, también es muy habitual el uso de equipamientos de rastreo y recuento de nanopartículas como el NanoSight (Nanoparticle Tracking Analysis; (NTA), o ensayos que se basan en la detección de marcadores proteicos específicos, ya sea por Western Blot o por citometría de flujo, como el MACSQuant Analyzer® o el MoFlo Astrios™ que permiten distinguir vesículas de menor tamaño que los citómetros tradicionales (Koliha *et al.,* 2016; Gardiner *et al.,* 2016).

2.8 PAPEL DE LAS VEs en el CÁNCER

Las VEs derivadas de células tumorales pueden promover la neo-angiogénesis y metástasis, ya que fomentan la liberación de metaloproteasas (MMP) encargadas de degradar la matriz extracelular y aumentan la secreción de VEGF (Yuana *et al.,* 2013). En este sentido, se ha propuesto que el ambiente ácido tumoral puede promover la lisis de la membrana de las VEs y hacer que su material esté biodisponible, y por tanto activo para las células receptoras (Taraboletti *et al.,* 2006).

De forma general, numerosos estudios atribuyen a las VEs un papel tanto en la supresión (Huber *et al.,* 2008), como en la activación del sistema inmune (Bhatnagar *et al.,* 2007). De manera específica, las VEs secretadas por células tumorales, tienen efectos inhibitorios en la respuesta inmune, ya que pueden reprimir la respuesta de los linfocitos T, e incluso inhibir la maduración de las células dendríticas en células presentadoras de antígenos. Concretamente, se ha descrito la

secreción de EXOs en células presentadoras de antígenos donde llevan en su interior el Complejo Mayor de Histocompatibilidad, por lo que pueden regular la activación de los linfocitos T (Buschow *et al.,* 2009).

Igualmente, parece que las VEs juegan un papel significativo en todos los pasos de la respuesta inmune antitumoral. En la primera fase, en la que se necesita el reconocimiento de las células tumorales por el sistema inmune innato, los EXOs expresan MICA/B en su membrana, y, por tanto, juegan un papel en la supresión de las células NK, facilitando el escape inmune y favoreciendo así la progresión del tumor (Clayton *et al.,* 2008). Cabe remarcar, que los EXOs expresan ligandos apoptóticos como FasL o TRAIL, por lo que regulan negativamente la activación de linfocitos T (Andreola *et al.,* 2002), y llevan en su membrana moléculas de adhesión como ICAM-1, que bloquean la unión entre linfocitos y células endoteliales, por lo que disminuye el reclutamiento de las células del sistema inmune adaptativo (Lee et *al.,* 2010).

2.9 VESÍCULAS EXTRACELULARES y GLIOBLASTOMA

A este respecto, Skog y colaboradores aislaron EXOs derivados de cultivos primarios de GBM en los que observaron que el mRNA presente en el interior de los EXOs era capaz de ser traducido en las células receptoras. Además de mRNA, aislaron miRNA, y concretamente, encontraron diferencias en los niveles de miRNA-21 en el interior de los EXOs de pacientes diagnosticados con GBM al compararlo con individuos sanos. Además, vieron que estos EXOs estimulaban la proliferación de otra línea celular establecida de glioma, e incluso que fomentaban la angiogénesis de células endoteliales, transportando en su interior moléculas angiogénicas tales como VEGF, angiogenina, e IL-6, entre otras. Estos mismos autores, ponen por primera vez en valor la capacidad de usar el contenido de estas VEs para obtener información acerca del diagnóstico, ya que son capaces de amplificar en las VEs del suero de pacientes, un gen frecuentemente sobre-expresado en GBM, concretamente la variante III de *EGFR* (*EGFRvIII*) (Skog *et al.,* 2008), el cual presenta una frecuencia de aparición de entre 25-64% según distintos estudios (Gan *et al.,* 2013). Este mismo gen, también se ha descrito en la membrana de los EXOs, junto a su variante salvaje y

a TGF-β1 (citoquina de carácter inmunosupresor), en pacientes con tumor cerebral (Graner *et al.,* 2009).

Así mismo, se ha intentado separar los EXOs que proceden de este tumor mediante marcadores proteicos, en concreto, la combinación de 4 marcadores específicos que aparecen con alta frecuencia en células de GBM, como son EGFR, EGFRvIII, PDPN, $IDH1^{R132H}$, permitiendo así diferenciar las VEs procedentes de controles sanos de las de pacientes diagnosticados con GBM (Shao et al., 2012). En esta misma línea, se han encontrado SMVs y EXOs procedentes de pacientes diagnosticados con GBM *de novo* que presentan un perfil distinto de expresión comparados con los individuos sanos (Noerholm *et al.,* 2012) e incluso se ha detectado un posible marcador de diagnóstico a nivel de snRNA (RNU6-1) que ya ha sido validado en una cohorte de 50 pacientes (Manterola *et al.,* 2014).

En base a todo lo expuesto y a modo de resumen, el trabajo realizado en esta tesis se presenta como un compendio de tres publicaciones en las que se pretende profundizar en la biología y el comportamiento del GBM, así como analizar el potencial uso de las VEs para el manejo clínico de los pacientes diagnosticados con gliomas.


3
Objetivos

OBJETIVOS

El trabajo presentado en la presente tesis se puede dividir en dos grandes bloques, de los que derivan los siguientes objetivos principales:

1. **Valorar la capacidad de las CIT procedentes de GBM de ser utilizadas como modelos pre-clínicos *in vitro* e *in vivo.***
   i) Aislar y caracterizar morfológica y genéticamente cultivos primarios de CIT procedentes de pacientes con GBM.
   ii) Estudiar su evolución *in vitro* a lo largo de 20 pases en cultivo.
   iii) Estudiar su evolución *in vivo* en modelos de xenoinjertos ortotópicos.
   iv) Analizar los perfiles de sensibilidad a fármacos a lo largo del tiempo en cultivo.

2. **Evaluar el uso del contenido de las VEs como fuente de biomarcardores en pacientes con gliomas.**
   i) Aislar e identificar los tres tipos de VEs: ABs, SMVs, EXOs procedentes de CIT en cultivo.
   ii) Crear un modelo animal que nos permita diferenciar las VEs procedentes del tumor.
   iii) Evaluar la capacidad de los tres tipos de VEs en atravesar la BHE intacta.
   iv) Amplificar secuencias de gADN relevantes en la biología del GBM.
   v) Identificar en el interior de las VEs un biomarcador útil en el pronóstico y diagnóstico de los pacientes con glioma.


4
Publicaciones

Como se ha detallado en la introducción, el tratamiento de los pacientes con gliomas malignos de grado IV es ineficaz, con una tasa de supervivencia que rara vez supera el año y medio. Así pues, con objeto de encontrar nuevos tratamientos más eficaces, la mayoría de los estudios en la actualidad se basan en la mejor comprensión del perfil genético de este tumor, en el conocimiento de su origen celular y los mecanismos que dirigen la iniciación, progresión, angiogénesis e invasividad que le confiere ese perfil tan agresivo. En este contexto, los cultivos primarios aislados a partir de muestras quirúrgicas parecen ser los modelos *in vitro* que mejor representa el tumor original. De este modo, el trabajo experimental desarrollado en este primer artículo se ha centrado en el aislamiento de cultivos primarios a partir de pacientes diagnosticados con GBM. Con el fin de avanzar en el conocimiento del comportamiento de las CIT in vitro y de su utilización para establecer modelos in vivo de gliomas de alto grado, se han aislado y derivado dichas células a partir de un total de 11 muestras, de las cuales hemos seleccionado 3.. Tras realizar una caracterización morfológica de dichos cultivos, hemos expandido estas líneas y evaluado sus perfiles de expresión a lo largo de 20 pases en cultivo, así como sus patrones de diseminación y crecimiento en ratones inmunodeprimidos. Además, con objeto de estudiar el perfil de respuesta sensibilidad de las mismas a diferentes tratamientos, de manera que puedan ser utilizadas para la búsqueda de marcadores de sensibilidad, hemos realizado análisis de viabilidad y toxicidad con una colección de 23 fármacos de uso común en el manejo de diferentes tumores, dirigidos a la síntesis y reparación del DNA, microtúbulos y proteosoma, así como moléculas específicas de rutas moleculares relacionadas con la biología de los tumores gliales.

“Cancer stem cells from human glioblastoma resemble but do not mimic original tumors after in vitro passaging in serum-free media”

Cancer stem cells from human glioblastoma resemble but do not mimic original tumors after *in vitro* passaging in serum-free media

Noemí García-Romero[1,*], Carmen González-Tejedo[2,*], Josefa Carrión-Navarro[3,*], Susana Esteban-Rubio[4], Gorjana Rackov[1], Vanessa Rodríguez-Fanjul[1], Jorge OliverDe La Cruz[5], Ricardo Prat-Acín[6], María Peris-Celda[6], David Blesa[7], Laura RamírezJiménez[7], Pilar Sánchez-Gómez[8], Rosario Perona[9], Carmen Escobedo-Lucea[10], Cristobal Belda-Iniesta[3], Angel Ayuso-Sacido[1,3,4]

[1]Instituto Madrileño de Estudios Avanzados, IMDEA Nanociencia, Madrid, Spain
[2]Centro Nacional de Biotecnología (CNB-CSIC), Madrid, Spain
[3]Fundación de Investigación HM Hospitales, HM Hospitales, Madrid, Spain
[4]Instituto de Medicina Molecular Aplicada (IMMA), School of Medicine, San Pablo-CEU University, Campus de Montepríncipe, Madrid Spain
[5]International Clinical Research Center, Center for Translational Medicine, St. Anne's University Hospital, Brno, Czech Republic
[6]Neurosurgery Department, Hospital Universitario la Fe de Valencia, Valencia, Spain
[7]Genetic and Genomic Unit, Fundación Centro de Investigación Príncipe Felipe, Valencia, Spain
[8]Neuro-oncology Unit, Instituto de Salud Carlos III-UFIEC, Madrid, Spain
[9]Instituto de Investigaciones Biomédicas, CIBERER, CSIC/UAM, Madrid, Spain
[10]Division of Biopharmaceutics and Pharmacokinetics, University of Helsinki, Helsinki, Finland

[*]These authors have contributed equally to this work
Correspondence to: *Angel Ayuso-Sacido,* ***email:*** *ayusosacido@gmail.com*

Keywords: *cancer stem cells, glioblastoma, genetic alterations, drug discovery, primary cell culture*
Received: *May 30, 2016* ***Accepted:*** *August 17, 2016* ***Published:*** *August 29, 2016*

ABSTRACT

Human gliomas harbour cancer stem cells (CSCs) that evolve along the course of the disease, forming highly heterogeneous subpopulations within the tumour mass. These cells possess self-renewal properties and appear to contribute to tumour initiation, metastasis and resistance to therapy. CSC cultures isolated from surgical samples are considered the best preclinical *in vitro* model for primary human gliomas. However, it is not yet well characterized to which extent their biological and functional properties change during *in vitro* passaging in the serum-free culture conditions. Here, we demonstrate that our CSC-enriched cultures harboured from one to several CSC clones from the human glioma sample. When xenotransplanted into mouse brain, these cells generated tumours that reproduced at least three different dissemination patterns found in original tumours. Along the passages in culture, CSCs displayed increased expression of stem cell markers, different ratios of chromosomal instability events, and a varied response to drug treatment. Our findings highlight the need for better characterization of CSC-enriched cultures in the context of their evolution *in vitro,* in order to uncover their full potential as preclinical models in the studies aimed at identifying molecular biomarkers and developing new therapeutic approaches of human gliomas.

INTRODUCTION

Glioblastoma (GBM) is the most common and devastating brain tumor in human adults [1], with an incidence ranging from 0.59 to 3.69 per 100 000 persons/ year [2]. The average survival does not exceed 15 months even after extensive surgery followed by radiotherapy alone or in combination with Temozolamide treatment [3-5], and just 0.05% to 4.7% of patients survive 5 years after diagnosis [6, 7].

High lethality of GBM might be partly attributed to a small population of tumour cells, termed Cancer Stem Cells (CSCs), which drive tumour initiation and maintenance [8-11]. Current approaches to treat GBM patients have little success, possibly due to the fact that the CSC subpopulation is refractory to both chemo- and

radiotherapy. Growing evidence points to CSCs as a more reliable preclinical GBM model than traditional cancer cell lines; therefore, many efforts have been made to isolate and culture CSCs in order to study their contribution to the tumorigenic processes, as well as to identify new therapeutic targets and biomarkers for diagnostics, prognostics, GBM stratification, treatment selection, and follow-up response to therapy.

CSCs display intra- and inter-tumour heterogeneity [12, 13], carry genomic and genetic alterations found in the original tumour and phenocopy their critical histopathological features when grown in serum-free media [14]. Under these culture conditions, CSC gene expression patterns resemble the original tumour more closely than those of other established tumour cell lines [15, 16]. Comparative analysis of different CSC collections reveals at least two different CSC subtypes: the first one with a proneural-like phenotype, and a highly invasive behaviour, and the second one with a mesenchymal-like phenotype and a nodular pattern with minimal invasiveness [17-19]. In addition, mRNA expression profiling and cytogenetic analysis of 48 glioma surgical samples from The Cancer Genome Atlas Research Network (TCGA) [20, 21], suggests there are four different CSC subtypes: proneural, mesenchymal, classical and neural [22], thus emphasizing the value of CSCs as preclinical models for GBMs.

CSCs are dynamic systems susceptible to evolution in culture, resulting in molecular alterations not found in the original tumours [19]. Their response to functional assays, such as tumour cell migration and dissemination, proliferation or drug sensitivity, might thus experience important changes as they evolve, affecting the reproducibility of the results as well as their capacity to model the original tumours. Therefore, in order to define the best biologically and clinically relevant conditions for a given experiment, the study of GBM CSC phenotypic and molecular dynamic in culture is essential.

Here, we present a collection of results showing that serum-free media selected CSC-enriched cultures ranging from homogeneous to quite heterogeneous populations from the original tumour. As they evolved *in vitro*, these cells displayed increasing stemness marker expression, as well as different ratios of chromosomal instability events. They reproduced at least three different dissemination patterns found in the original tumours, but exhibited irregular response to drugs between passages. Our findings highlight the need to characterize a large number of CSC-enriched cultures, both in the context of their original tumours and their *in vitro* evolution, in order to take full advantage of these preclinical tumour models for developing new therapeutic approaches.

RESULTS

Isolation and characterization of CSC cultures from human surgical samples

In order to examine the stability of CSC cultures, together with live-cell functions, we first isolated eleven CSC-enriched cultures derived from fresh surgical human GBM samples and cultured them under serumfree conditions [23]. As such, they grew as expandable sphere-like cultures showing different growing features under the optical microscope, based on which they were grouped into three clusters (Supplementary Table S1). One representative culture for each cluster was chosen for further analysis, and their CSC properties were characterized within the first 2 passages (see Supplementary Section). GBM18 grew as spheres attached to the surface that eventually detached (Figure 1A, *i*), GBM27 grew as spheres in suspension (Figure 1B, *i*) and GBM38 grew as an attached monolayer of cells in combination with spheres that eventually detached from the plate (Figure 1C, *i*). Then, with the aim of studying the evolution of CSCs *in vitro* right after their isolation, we subcultured them for up to 20 passages (18 months) without freeze-thaw cycles (Supplementary Figure S5).

Cell morphology of CSCs and tumourspheres remains stable along passages

We first examined the sphere surface and observed that all three CSC cultures displayed different cellular projection patterns that remained unchanged for all passages studied (Figure 1A, *ii*, 1B, *ii* and 1C, *ii*). Afterwards, we wondered whether the cell organization within the spheres also followed reproducible patterns. Interestingly, for all three CSC cultures, we found the presence of extracellular matrix (Figure 1A, *iii* and *iv*, 1B, *iii* and *iv* and 1C, *iii* and *iv*) and, along the number of passages, we observed an increasing number of spheres displaying wider intercellular space and a higher number of cell membrane projections, some of which interlaced, increasing the membrane surface per cell and contributing to the maintenance of the sphere architecture (Figure 1D, *i*).Next, the spheres were processed to carry out a comparative study of cell morphology intra- and interCSC culture. Serial semithin sections showed significant inter-CSC culture differences but a high grade of intraCSC culture homology. We observed that the presence of multilobular and polymorphic nuclei was a common feature for all of them. Additionally, dividing cells were observed in both the peripheral regions and the center of the tumourspheres (Supplementary Figure S6). Ultrathin sections revealed that most cells displayed the presence of differential inter-CSC culture abnormal inclusions. GBM18 showed inclusions compatible with polysaccharide deposits (Figure 1A, *v*), GBM27 showed an important number of electron dense inclusions (Figure

1B, *v*) and GBM38 a combination of polysaccharide, electron dense and lipid inclusions (Figure 1C, *v*). Finally, we also observed the alteration of the mitochondrial architecture along the passages (Figure 1A, *vi*, 1B, *vi*,

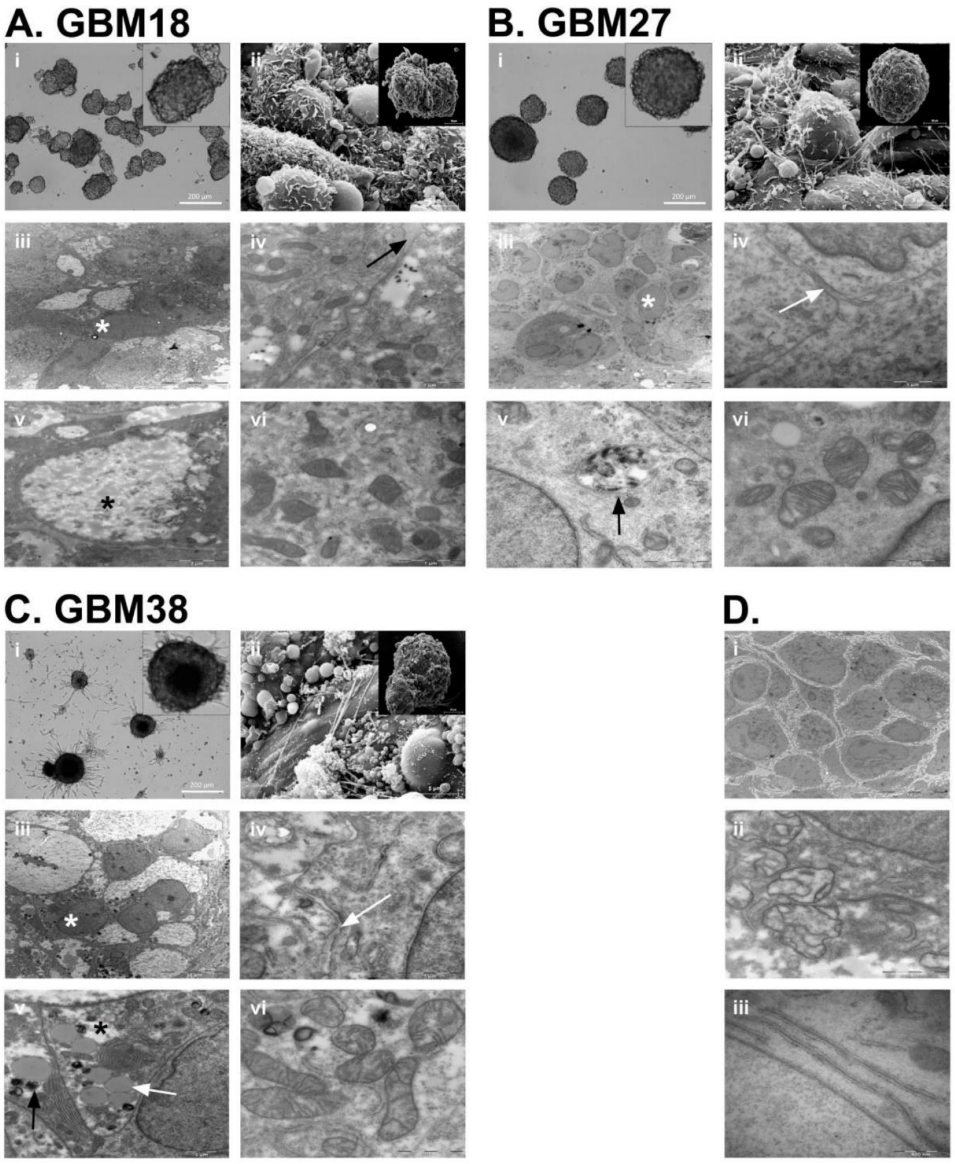

Figure 1: Neurosphere architecture and cell morphology analysis of GBM18, GBM27 and GBM38 CSC-enriched cultures. **A.** GBM18 neurosphere morphology under the OM (*i*), SEM (*ii*) and TEM (*iii-vi*). Black arrow shows extracellular matrix (*iv*), white asterisk shows clear cytoplasm cells (*iii*) and black asterisk shows representative polysaccharide intracellular deposits (5). **B.** GBM27 neurosphere morphology under the OM (*i*), SEM (*ii*) and TEM (*iii-vi*). Black arrow shows extracellular matrix (*iv*), white asterisk shows clear cytoplasm cells (*iii*) and black asterisk shows representative electro-dense intracellular deposits (*v*). **C.** GBM38 neurosphere morphology under the OM (*i*), SEM (*ii*) and TEM (*iii-vi*). White arrow shows extracellular matrix (*iv*) and representative lipid drops (*v*). Black arrow shows representative electro-dense intracellular deposits (*v*). White asterisk shows clear cytoplasm cells and black asterisk shows representative polysaccharide intracellular deposits (*iii*). **D.** Highlighted differences observed along the GBM18, GBM27 and GBM38 passages in culture: neurosphere architectural reorganization (*i*), mitochondrial crest architectural loss (*ii*) and double membrane structures (*iii*

1C, *vi* and 1D, *ii*) and the presence of double membrane structures in late passages (Figure 1D, *iii*). Interestingly, the cell morphology remained mostly unchanged for all three CSC cultures along the passages.

CSC-enriched cultures increase their stemness stage along the passages

Once we have discarded relevant changes in cell morphology within the tumorspheres, we looked into the mRNA expression of CSC markers. We found that cells in late passages from GBM18, GBM27 and GBM38 expressed higher mRNA levels of *CD133* and *CD44* while those of *SSEA1* remained unchanged (Figure 2A). Consistently, when we analysed the mRNA expression of stem cell markers such as *OCT3/4*, *BMI* and *SOX2* we found increasing values in late passages with the only exception of *SOX2* for GBM38, whose expression level remained low and even along the passages. Additionally, the mRNA expression level of adult neural stem cell

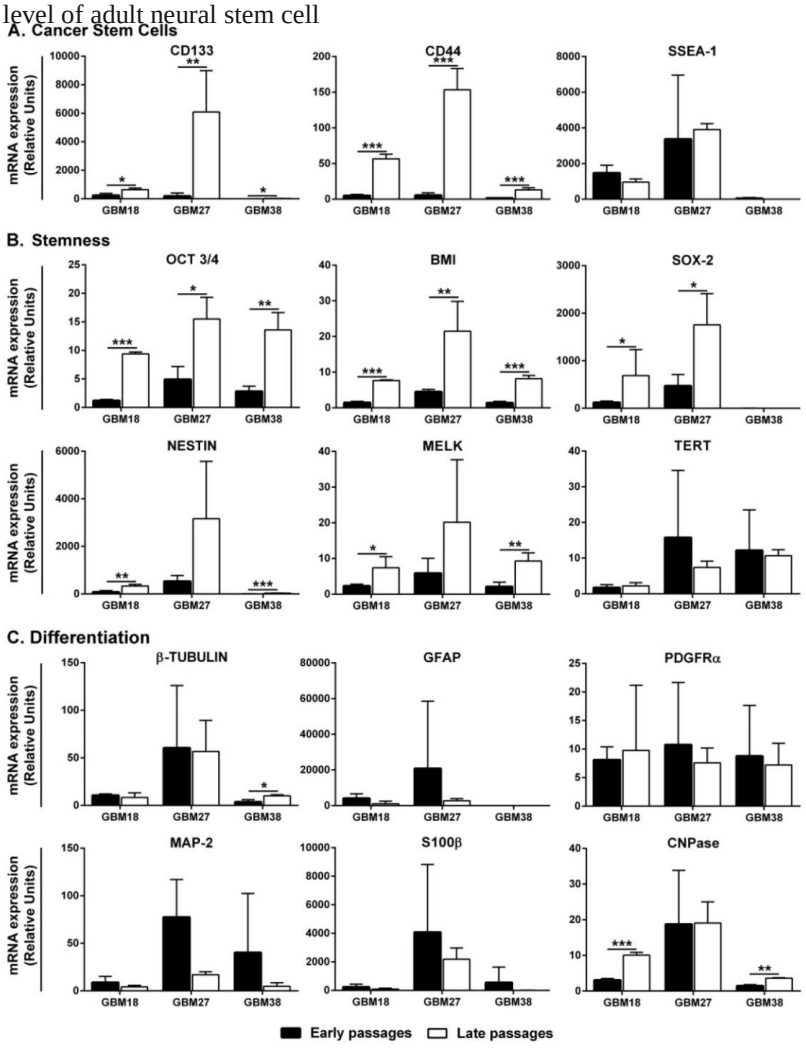

Figure 2: Gene expression analysis at early and late passages of CSC-enriched cultures. A. Cancer Stem Cell markers. **B.** Stemness markers. C. Differentiation markers. Keywords: black columns represent early passages; white columns represent late passages; for every comparative analysis, the sample with lower mRNA gene expression is given the value 1. Error bar represents Standard Deviation. *: $P \leq 0.05$; **: $P \leq 0.01$ and ***: $P \leq 0.001$.

markers, such as *NESTIN* and *MELK*, also increased in late passages, while the expression of *TERT* remained high and unchanged (Figure 2B). As the results suggested an increased stemness stage of CSC-enriched cultures along the passages, we also looked into the mRNA expression of differentiation markers for the three main neural lineages. We observed that astrocyte markers (*GFAP* and *S100β*) remained unchanged along the passages for all three CSC-enriched cultures studied. The mRNA expression of neuronal markers remained equal for GBM18 and GBM27 with a little increase of *β-III-Tubulin* in late passages of GBM38. Moreover, we did not observe significant changes in transcript levels of the early oligodendrocyte marker *PDGFRa*, while *CNPase* increased in late passages for GBM18 and GBM38 (Figure 2C).

Chromosomal instability collaborates with *in vitro* evolution of CSC-enriched cultures

Chromosomal instability is a hallmark of tumor cells, including gliomas, and the main cause of genomic alterations throughout the course of the disease. In order to evaluate the occurrence of genomic alterations in CSCs isolated from surgical samples, over their passages in culture, we carried out sequential Comparative Genomic Hibridization (CGH) assays on GBM18, GBM27 and GBM38. First, we wondered whether the chromosomal instability might be generated by the isolation and culture procedures or due to an inherent feature of CSCs. To rule out the first possibility, we set out to investigate the presence of genomic alterations in Neural Stem Cells (NSCs) isolated from surgical samples of human adult brain - normal counterpart of CSCs - under the same isolation and culture procedures used for CSCs. The analysis of CGH data showed the absence of genomic alterations in NSCs along the first 7 passages, when the cells became senescent (Supplementary Figure S7). These results demonstrated that our isolation and culture procedures did not generate chromosomal instability in human adult NSCs displaying a normal genetic background.

Then, we focused on the analysis of CGH data from all three CSC-enriched cultures – GBM18, GBM27 and GBM38- at passages 1, 5, 7, 10, 15 and 20. As expected, we observed genomic alterations due to DNA losses and gains in all three CSC-enriched cultures. Interestingly, genomic alterations identified in GBM18 remained unchanged for all passages assayed while GBM27 and, to a greater extent, GBM38 displayed chromosomal instability events along the passages (Figure 3A-3C).

In general, DNA losses outnumbered gains in all three CSC-enriched cultures. GBM18 displayed genomic alterations in 17 somatic chromosomes, including 3 DNA gains in chromosomes 3, 7 and 20, and 25 DNA losses in 15 different chromosomes (Figure 3A and Supplementary Table S4). GBM27 also displayed genomic alterations in 17 somatic chromosomes, including 11 gains in 10 chromosomes, although the total number of gains came down to 6 after the first passage. Additionally, this CSC-enriched culture exhibited a total of 26 DNA losses in 11 chromosomes along the 20 passages; being chromosomes 10 and 19 the most affected, with 6 and 5 DNA losses, respectively (Figure 3B and Supplementary Table S5). Finally, GBM38 displayed genomic alterations in all somatic chromosomes. We detected a total of 22 DNA gains in 11 chromosomes, and 28 DNA losses in 17 chromosomes, along all passages (Figure 3C and Supplementary Table S6).

Next, we wondered whether the most recurrent sites of DNA copy-number aberration described in glioma samples, containing a putative oncogene or tumor suppressor gene [24], might be also altered in CSC-enriched cultures. To address this question, we analysed the location of 19 statistically significant DNA gains and 20 DNA losses identified previously from 543 GBM solid samples by TCGA [24] (Supplementary Table S7). GBM18 displayed just 3 DNA gains, all of them at chromosome 7, including the oncogenes *EGFR*, *CDK6* and *MET*, and 2 DNA losses including *AKT1* and *AKT3*, within the set of recurrent DNA gains. On the contrary, this CSC-enriched culture showed 10 DNA losses (50%) and no DNA gains within the set of recurrent DNA losses (Figure 3A and Supplementary Tables S4 and S7). Interestingly, GBM27 and GBM38 displayed changes on DNA gains and losses throughout the passages, affecting the location of both oncogenes and tumor suppressors. GBM27 showed DNA gains affecting the location of 14 genes within the set of recurrent DNA gains at first passage, although half of them involved less than 50% of the cells. However, after the fifth passage, many DNA gains disappeared, remaining those that affected the location of *MYCN*, *SOX2*, *EGFR*, *CDK6*, *MET* and *GRB2*. Nonetheless, after the tenth passage, *MYCN* and *GRB2* DNA sequence gains persisted in less than 50% of cells. Unexpectedly, this CSC-enriched culture displayed 6 DNA gains and just 3 DNA losses within the set of recurrent DNA losses at first passage, although the DNA gains reduced to 5 after the fifth passage, affecting the location of *LSAMP*, *3q29* and *NF1*, which actually involved less than 50% of cells after the tenth passage. DNA losses affecting the location of *CDKN2A/B*, *PTEN* and 19q13.33, for all passages, and *QKI*, 10q26.3 and 15q14, in less than 50% of the cells, after the tenth passage were also detected (Figure 3B and Supplementary Tables S5 and S7). Finally, GBM38 showed DNA losses affecting chromosomes 4 and 12 in all passages, and chromosome 17 after the fifth passage, within the set of recurrent DNA gains. These DNA losses matched the location of *FGFR3*, *PDGFRa*, *CCND2*, *CDK4*, *MDM2* and *GRB2*. Surprisingly, DNA sequence gains affecting the location of *EGFR*, *CDK6* and *MET* at chromosome 7 disappeared after the tenth passage,

while others affecting *AKT3* and *MDM4* at chromosome 1 appeared from the fifth passage on. Consistent with this, the same variability was observed within the set of recurrent DNA losses. We detected 4 DNA gains at the first passage in chromosomes 3, 15 and 22, all of them affecting less than 50% of the cells. However, 3 of these DNA gains disappeared after the fifth passage and the last one after the tenth passage. Interestingly, 2 new DNA gains, affecting chromosome 1, appeared at passage 5 in 100% of the cells and remained along the 20 passages under study. We also observed the presence of 4 DNA losses in all passages, affecting the chromosome 9 (*CDKNA/B*), 10 (*PTEN* and 10q26.3) and 14 (*NPAS3*). Surprisingly, the DNA sequences gained at the first passage, affecting chromosome 22 in less than 50% of the cells, were consistently lost in 100% of the cells from the fifth passage on, and the same happened for the 2 DNA gains affecting the chromosome 3 at the first passage, which turned out to be lost at the last passage. Finally, to add on the high chromosomal instability of this CSC-enriched culture, we found 2 more DNA losses, affecting the chromosome 13 (*RB1* and 13q22.1) in less than 50% of the cells, between the passages 7 and 10 (Figure 3C and Supplementary Tables S6 and S7).

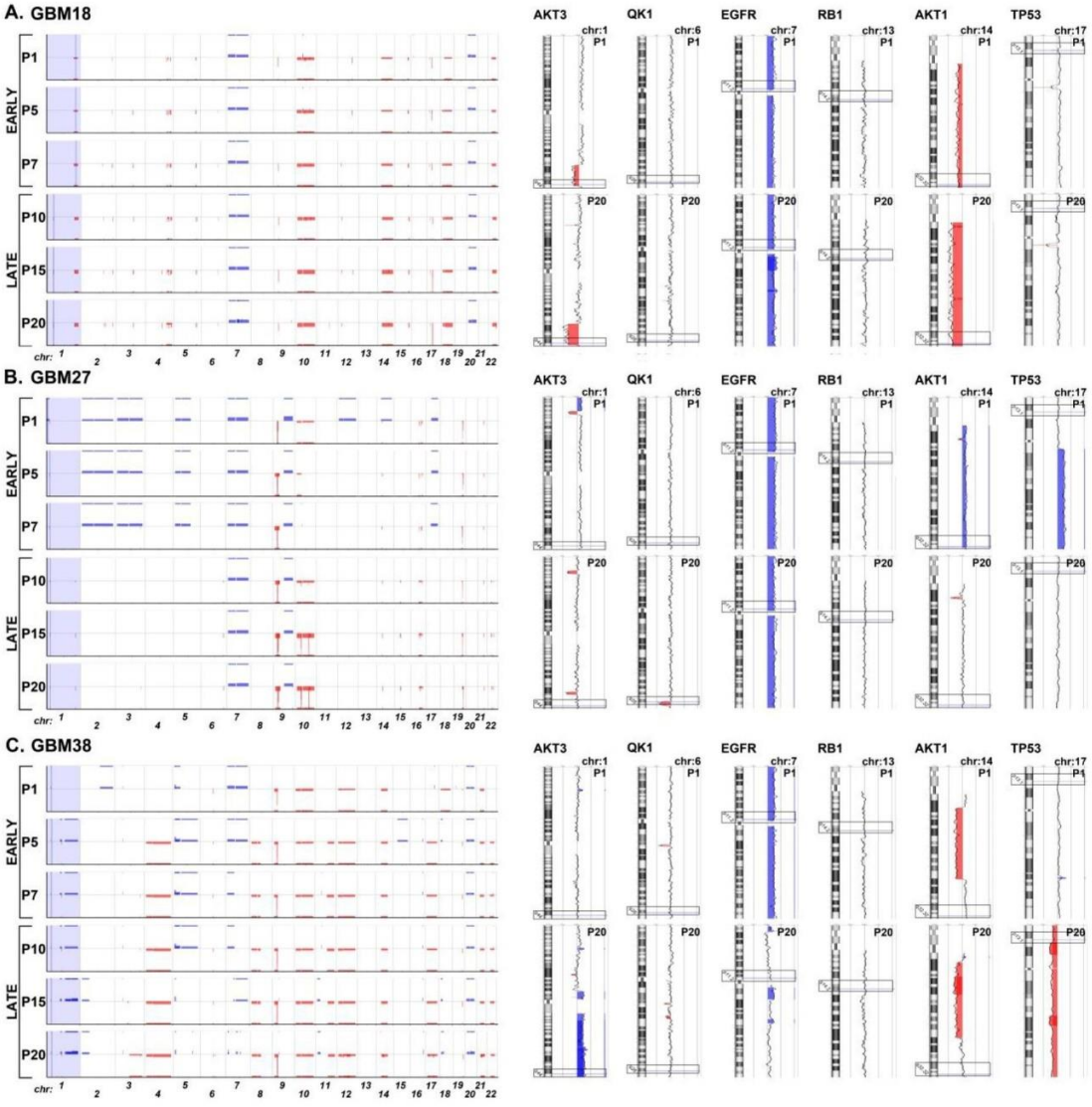

Figure 3: Graphical representation of chromosomal imbalances detected in GBM18, GBM27 and GBM38 CSCenriched cultures along the 20 first passages in culture after isolation from surgical samples. A. GBM18. **B.** GBM27. **C.** GBM38. The X-axis represents the chromosomes, while the Y-axis represents the normalized log2 Cy5(CSC)/Cy3(healthy control) fluorescence intensity thresholds -1 (loss(red)) and 1 (gain (blue)), respectively. The genes *AKT3*, *QK1*, *EGFR*, *RB1*, *AKT1* and *TP53*, frequently altered by DNA gains or losses in human gliomas, are shown as ideograms at passage 1 and 20. The clear boxes indicate the location of the gene. Blue represents DNA gains and red DNA losses.

CSC proliferation and duplication times display fluctuations along the passages

We next wondered whether the observed changes in morphology, chromosomal instability and differentiation state along the passages in culture, might influence the proliferation ratio of CSC-enriched cultures. To address this question, we carried out viability assays with early and late passages cultured *in vitro* for up to 5 days. In general, we found no significant differences in the percentage of viable cells between early and late passages of GBM27 and GBM38. Interestingly, we did observe significant differences between early and late passages of GBM18 ($P < 0.01$) (Figure 4A). GBM27 displayed the higher duplication time followed by GBM18 and GBM38, which showed the highest proliferation rate *in vitro* (Figure 4B). Then, we wanted to know whether the proliferation rate *in vitro* correlated with survival of mouse models of brain tumor xenotransplanted with these CSCs. Consistently, we found that the overall survival of xenotransplanted mice with GBM18 and GBM38 was quite similar, around 100 days, while those mice xenotransplanted with GBM27 displayed longer overall survival with an average of 220 days (Figure 4C).

In vivo migration and dissemination patterns of CSCs remain unchanged along passages

To evaluate the ability of these CSC-enriched cultures to recapitulate the original tumor features, we carried out orthotopic transplantations within the striatal brain of adult nude mice. Staining with anti-human Vimentin, to expose human cells, revealed the *in vivo* migration and invasion capacity of these three CSCenriched cultures. At the time of diagnosis, GBM18 and GBM27 were clinically described as highly disseminating, while GBM38 was described as nodular (Figure 5A, 1-3). Consistent with clinical description, GBM18 formed a nodular-like tumor mass; however, the nodular boundaries were not well defined. The cells migrated out of the nodular tumor mass and invaded the neighbouring tissues, reaching the contralateral hemisphere at both early and late passages (Figure 5A, 1). Interestingly, GBM27 CSCs disseminated through the mouse brain and invaded the contralateral hemisphere at both early and late passages (Figure 5A, 2). On the contrary, GBM38 CSCs remained within the ipsilateral hemisphere forming a nodularlike tumor mass, with well-defined boundaries, also at both early and late passages (Figure 5A, 3). We found GBM18 CSCs surrounding blood vessels in the striatum, but not GBM27 CSCs. Both GBM18 and GBM27 CSCs seemed to accumulate along the ventricular wall and use the myelin fiber tracks within the striatum and the *corpus callosum* to migrate (Figure 5 and Supplementary Figure S8). In order to find a molecular signature that explained this histological finding, we studied the mRNA expression of genes related to migration and invasiveness. Consistently, the mRNA expression of *CD90*, *CD144*, *CD24*, *CD73* and *OLIG2* was higher in GBM27 followed by GBM18 and GBM38. Interestingly, the expression levels of *CD90*, *CD144*, *CD166*, *CD24* and *CD73*, were significantly increased in the late passages of GBM27, as well as *OLIG2* to a lesser extent. Similar results were observed when we analysed *CD90*, *CD24*, *CD73* and *OLIG2* for GBM18 and *CD166* and *CD73* for GBM38. However, the higher mRNA expression of migration and invasiveness markers at late passages did not translate into an increased migration of CSCs *in vivo* (Figure 5B).

The CSCs response to drugs evolves in vitro

Once we confirmed that all CSC-enriched cultures, regardless the passage in culture, reproduced the migration and dissemination patterns *in vivo*, we wanted to know whether the time in culture influenced their sensitivity to a panel of drugs currently used in both clinical trials and clinical practice against GBM. To address this question, we carried out functional viability assays with three different early and late passages for all CSC-enriched cultures (Figure 6). The IC_{50} as well as the percentage of cell survival at 10 µM were calculated by lineal interpolation to compare drug sensitivity between early and late passages. We found that all three CSC cultures showed significant differences between early and late passages in both the IC_{50} and the viability at 10 µM for at least 20% of the assayed drugs. Interestingly, late passages

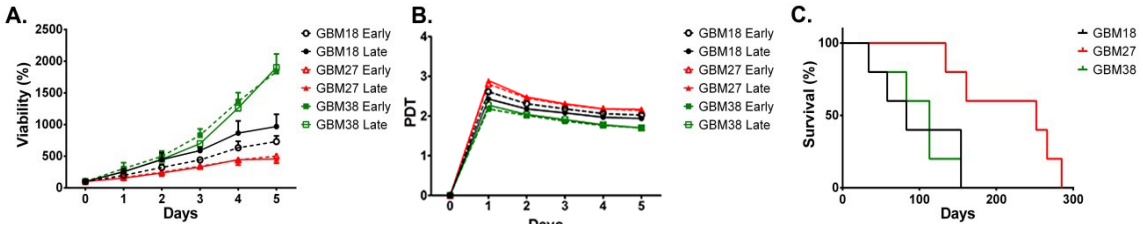

Figure 4: Viability of early and late passages of CSC-enriched cultures and average survival of mouse models of their respective brain tumor xenotransplats. A. Viability assay for early and late passages of GBM18, GBM27 and GBM38. **B.** Duplication time for early and late passages of GBM18, GBM27 and GBM38. **C.** Kaplan-meier survival curves for mice xenotransplated with GBM18, GB27 and GBM38.

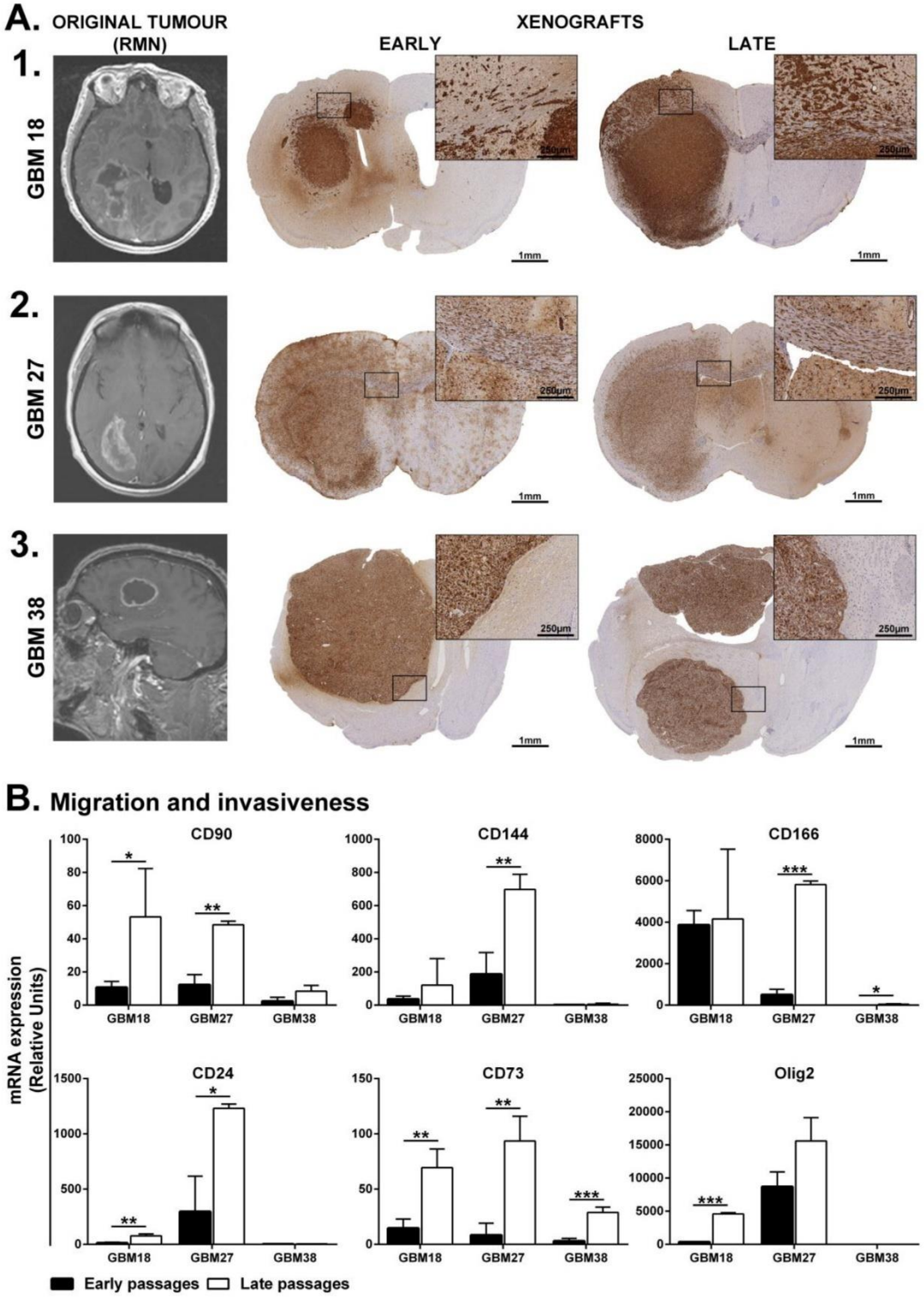

Figure 5: Brain dissemination patterns of early and late CSCs isolated from human samples. A. MRI from the original tumor and mouse model of brain tumor xenotransplated with GBM18 (A1), GBM27 (A2) and GBM38 (A3) at early and late passages. GBM18 and GBM27 are clinically defined as highly disseminated while GBM38 as nodular. Squared regions are shown at higher magnification. **B.** Gene expression analysis of migration and invasiveness markers at early and late passages of CSC-enriched cultures. Keywords: black columns represent early passages; white columns represent late passages; Error bar represents Standard Deviation. *: $P \leq 0.05$; **: $P \leq 0.01$ and ***: $P \leq 0.001$.

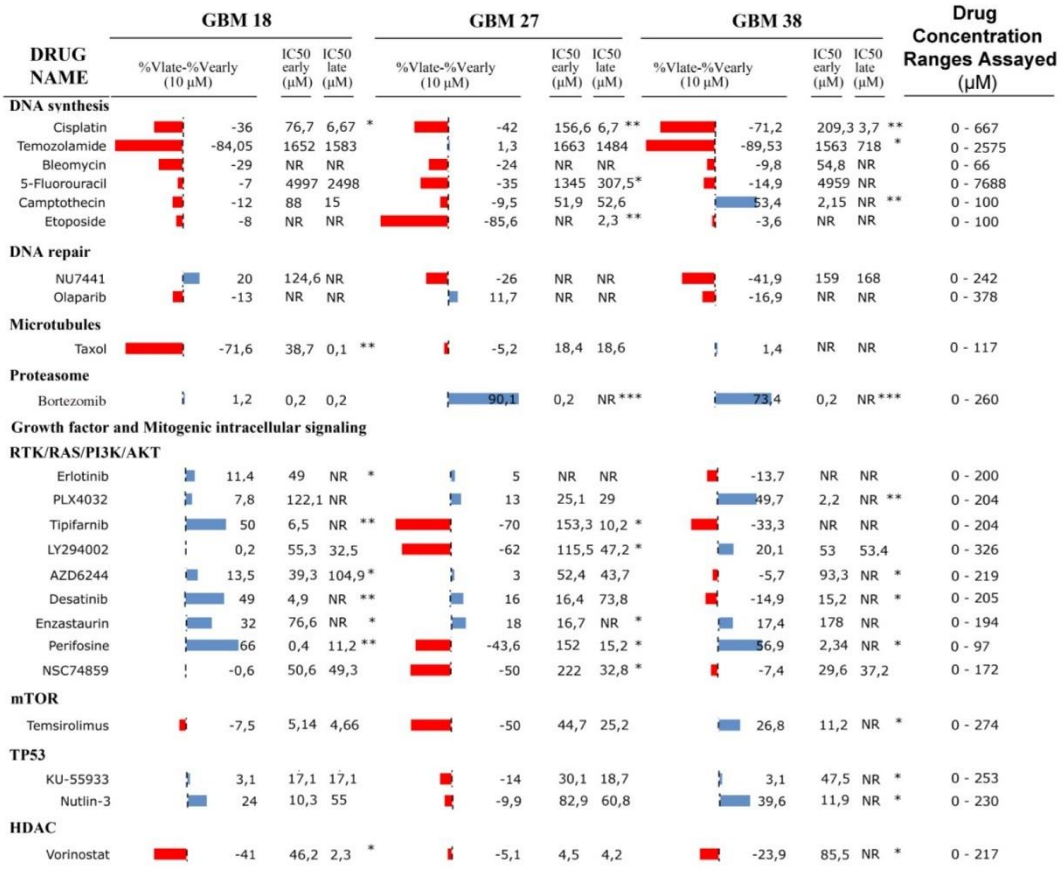

Figure 6: Drug sensitivity panel of early and late CSCs isolated from human samples. For every CSC-enriched culture viability differences (% viability at late passages - % viability at early passages), as well as the viability at IC_{50} for early and late passages are shown. Keywords: red bars mean that early passages are more sensitive than late passages; blue bars mean that early passages are less sensitive than late passages; asterisks represent differences between early and late IC_{50} by * (one), ** (two) or *** (three) orders of magnitude.

were significantly more sensitive to cisplatin. In the same line, we observed that all three CSC cultures displayed higher sensitivity to drugs interfering with DNA synthesis at late passages, with the only exception of camptothecin for which GBM38 showed an IC_{50} at least 10 times higher at late passages. However, there were no differences between early and late passages when we assayed drugs that interfered with DNA repair. GBM18 and GBM27 displayed sensitivity to taxol but there were important differences between both CSC cultures. While the IC_{50} between early and late passages of GBM27 was quite similar, late passages of GBM18 displayed an IC_{50} more than 50 times lower than early passages. The three CSC cultures were sensitive to bortezomib; however, GBM27 and GBM38 were significantly more sensitive at early passages. Then, we assayed a collection of drugs targeting growth factors and cell signalling pathways. We observed an IC_{50} more than 10 times lower at early passages of GBM18 for tipifarnib, desatinib and perifosine, and the opposite for vorinostat. GBM27 also displayed significant differences between late and early passages for perifosine, enzastaurin and tipifarnib. Finally, we found significant differences between early and late passages of GBM38 for PLX4032 and to a lesser extent for desatinib, perifosine, temsirolimus and Nutlin-3 (Figure 6).

DISCUSSION

The percentage of surgical samples from which we were able to isolate expandable CSC cultures, as well as the different growth patterns observed, is consistent with previous works [11, 17, 18]. These patterns apparently did not change along the passages when observed under the OM. However, a closer analysis under the EM revealed morphological changes common to all three CSCs, as well as more specific features for each of them. For all analyzed
CSC lines, TEM confirmed common architectural reorganization of spheres and a higher number of disrupted mitochondrial crests over the passages. The widening of intercellular spaces, together with the increase of membrane surface per cell, probably played a role in permitting the access of fresh nutrients to internal cells as well as the clearance of residual metabolites. Additionally, the alteration of mitochondrial cytoarchitecture might be compatible

with a progressive selection of glycolysis for glucose metabolism *in vitro* [25]. In this regard, the ability of CSCs isolated from human gliomas to use multiple pathways for energy production has been recently demonstrated, suggesting that CSCs might be refractory to treatments targeting individual metabolic pathways [26]. Moreover, we observed abnormal deposits of different types of macromolecules in all three CSC lines, probably as a result of altered metabolic pathways. In this regard, the deposit volume might be related to the differentiation stage; the clear cytosolic cells, found within the sphere, might thus correspond to the most undifferentiated CSC subpopulation. Interestingly, for all analysed CSC lines, the morphology of most cells within the spheres was highly homogeneous, which suggests a clonal origin of these cells.

In line with the homogeneous cell morphology within each CSC line, the analysis of specific molecular marker expression along the passages revealed a striking similarity between the analysed CSC lines. These results support the uniform presence of differentiated cells within the tumorspheres along the passages, and are consistent with the observation that cytosolic cells were overloaded with aberrant deposits. Furthermore, these results suggest a positive selection of CSCs with more prominent stemness stage. Our data thus confirm previous genomic analyses of CSC lines from different passages, which showed that CSC biological replicates grouped together when compared with other samples [15, 17, 27]. However, the relative expression of specific biomarkers between the passages has not been previously reported.

In the last few years, several groups have published a collection of data demonstrating the existence of intra-tumor heterogeneity in human glioblastoma [12, 13, 28]. Consistent with these reports, we found that most chromosomal alterations affected 100% of the cell populations along the 20 passages after isolation. This finding, together with the morphologically homogeneous intra-tumoral CSCs, points to a clonal origin for the tumor cells present in primary cultures. Interestingly, our CGH analysis shows that the current protocols for CSC enrichment and culture, under serum-free conditions, randomly generate both homogeneous and heterogeneous populations of CSCs. We observed DNA gains, affecting less than 50% of the population, in the first passage of GBM27 and GBM38 cells that disappeared a few passages later, which might suggest the presence of clones less prone to survival or competitiveness than other clones *in vitro*. Additionally, DNA gains and losses affecting less than 50% of the population showed up at different passages, and then either disappeared or remained underrepresented in the total population. Finally, for these two CSC-enriched cell lines, we also observed new DNA gains and losses, affecting 100% of the population, at different passages. On the contrary, CGH analysis showed no significant changes for the GBM18 homogenous population. All together, these results suggest that a heterogeneous population of CSC-enriched cell lines evolve *in vitro* as they do *in vivo*, although essential differences in microenvironment cues probably drive the evolution process in different directions. We found that CSC-enriched cultures displayed similar duplication times, meaning that the chromosomal instability and gene expression variability observed along passages did not translate into significant proliferation changes *in vitro*. Interestingly, mouse models of brain tumor xenotransplated with GBM27, that displayed the higher duplication time *in vitro*, showed the longest average survival. This result suggests a link between low proliferation *in vitro* and *in vivo*, however other parameters like the brain dissemination pattern, may also influence and more experiments with a higher number of CSC- lines will be needed to clarify this question.

Notably, the dissemination pattern of CSCs through the parenchymal brain in mice remained unchanged along the passages - resembling the original tumors -. This finding suggests the presence of either specific mutations or, most probably, coordinated molecular alterations, passed on from the original clone, responsible for the migration and dissemination. Consistently, other authors observed no changes in the dissemination patterns *in vivo* from different passages of CSCs [11, 17]. However, considering that CSCs also evolve *in vitro*, it is important to note that new alterations affecting essential molecules in migration pathways along the passages *in vitro* might modify the dissemination pattern *in vivo*. Importantly, we showed three different patterns of dissemination *in vivo* for CSCs isolated from human glioma samples. GBM27 displayed a highly disseminating pattern, longer overall survival and higher expression of *OLIG2*, consistent with the CSC type I described by Günther *et al.*,, and the proneural phenotype [29]. On the contrary, GBM18 and GBM38 displayed a nodular dissemination pattern and similar overall survival, which resemble the CSC type II , and the mesenchymal phenotype [16, 17, 29, 30]. However, GBM18 showed irregular boundaries, with cells migrating out of the main tumor mass, and significantly higher *OLIG2* expression than GBM38. Therefore, the disseminated, nodular and semi-nodular preclinical *in vivo* models of GBM constitute three separated tumor behaviours that might need different therapeutical approaches.

Supporting the idea of *in vitro* evolution of CSCenriched cultures, we also observed significant variations in the IC_{50} for a number of drugs along the first 20 passages in culture. These variations affected both homo (GBM18) and heterogeneous (GBM27 and GBM38)

CSC-enriched cultures. The *in vitro* DNA gains and losses might thus not be enough to explain the drug-sensitivity variations, and genetic and/or epigenetic

alterations along the passages might also play a role. These results suggest that reliable functional experiments need to be performed on well-characterized CSC-enriched cultures within a limited number of passages.

Altogether, the CSC-enriched cultures from surgical samples are now the most reliable preclinical models of human high-grade glial tumors. However, these models are far from mimicking the original tumors. Indeed, these cultures evolve *in vitro* acquiring new features as a result of their intrinsic instability and microenvironment cues. Therefore, in order to take advantage of the whole potential of these preclinical tumor models to develop new therapeutic approaches, it will be essential to isolate a large number of CSC-enriched cultures and characterize them not only in the context of their original tumors but also their evolution *in vitro*.

MATERIALS AND METHODS

Isolation and culture of CSCs from human GBM samples

Cancer stem cells were isolated from human fresh GBM samples. Tissue samples were obtained from patients operated at the Neurosurgery department (Hospital la Fe, Spain). Permission to use this material was obtained from the ethical review board in Hospital la Fe and Principe Felipe Research Center, and written informed consent was obtained from patients. GBM CSCs and normal brain parenchyma cells were cultured in media containing: DMEM/F-12 (Gibco, 11039), Non Essential Amino Acids (10mM; Gibco, 11140), Hepes (1M; Gibco, 15630), D-Glucose (45%; Sigma, G8769), BSA-F5 (7,5%; Gibco, 15260), Sodium Pyruvate (100mM; Gibco, 11360), L-Glutamine (200mM; Gibco, 25030), AntibioticAntimycotic (100x; Gibco, 15240), N_2 Supplement (100x; Gibco, 17502), Hydrocortisone (1µg/µl; Sigma, H0135), Tri-iodothyronine (100µg/ml; Sigma, T5516), EGF (25ng/ µl; Sigma, E9644), bFGF (25ng/µl; Sigma, F0291) and Heparin (1µg/µl; Sigma, H3393).

Tumorsphere morphological analysis

To evaluate possible changes in both the sphere architecture and cell morphology, we separated 12 spheres of 150 µm diameter from each CSC culture at different time points (Supplementary Figure S5) and further analysed them by optical microscopy (OM), Screening Electronic Microscopy (SEM) and Transmission Electronic Microscopy (TEM). Tumorspheres were fixed with 3.5% glutaraldehyde (Electron Microscopy Science, Hatfield, USA) for 1 h at 37°C. Afterwards, they were embedded in 3% agar drops and postfixed with 1% osmium tetroxide (Sigma), rinsed, dehydrated, and embedded in araldite (Durcupan, Sigma). For brain tissue analysis, at the appropriate time points, mice were deeply anesthetized with an intraperitoneal injection of Ketamine (100mg/kg) and Medetomidine (0,5mg/kg), and transcardially perfused with a 0.9% NaCl solution followed by a 2% paraformaldehyde/2.5% glutaraldehyde solution (PFA/GA, Electron Micoscopy Sciences, Hatfield, PA) in PBS. Brains were removed, post-fixed in PFA/GA overnight and rinsed in cold PBS (5x10 min). After fixation, brains were cut into 200 µm sections on a vibratome (Leica VT-1000), rinsed, dehydrated and embedded in araldite (Durcupan, Sigma). For both types of samples, tumorspheres and brain tissue slides, semithin sections (1.5 µm) were cut with a diamond knife and lightly stained with 1% toluidine blue (Panreac, Barcelona, Spain). Semithin sections were detached from the glass slide by repeated freezing (liquid nitrogen) and thawing and re-embedded in an araldite block. The block with semithin sections was cut in ultrathin (0.05 µm) sections with a diamond knife, stained with lead citrate, and examined under a Tecnai Spirit Electron Microscope (FEI). Photographic images were taken with a Morada camera (Soft Image System, Munster, Germany).

RT and QRT-PCR

For RT-PCR, total RNA was isolated using RNeasy Mini or Micro kit (QIAGEN) following the manufacturer's recommendations. One µg of RNA was used for cDNA synthesis (High-Capacity cDNA Reverse Transcription Kit; Applied BioSystems). Samples were amplified with specific primers and the Paq5000 polymerase (Stratagene), in a Mastercycler (Eppendorf). QRT-PCR was run in a LightCycler 480 Instrument (Roche). For each experiment, controls were performed in which reverse transcriptase was omitted from the cDNA reaction mixture and template DNA was omitted from the PCR mixture.

Cancer stem cell differentiation

Cells were plated for 10 days on 8-well chamber slides (Nalgene Nunc, 177402) coated with Matrigel Basement Membrane Matrix (2mg/ml; BD, 356234) in growth factor-free media supplemented with 10% FBS. Cells were then fixed in 4% paraformaldehyde.

Immunocytochemistry

Cells were fixed in 4% paraformaldehyde for 20 min, washed with PBS and incubated in 0.2% Triton X-100/PBS for 20min at 37ºC and 10min at RT. Cells incubated with BrdU were treated with 1N HCl for 30 min at 37ºC and neutralized in 0.1M borate buffer, pH 8.5 for 5min at RT. After treatment with 5% normal goat serum/0.1% Triton X-100/PBS for 15min, cells were incubated overnight at 4ºC with the following primary antibodies: BrdU (mouse monoclonal, 1:100,

Dako), GFAP (rabbit polyclonal, 1:1000, Dako), SOX2 (goat, 1:50, Chemicon), Nestin (rat, 1:100, Chemicon), Tuj1 (chicken, 1:500, Sigma) and CNPase (mouse monoclonal, 1:400, Abcam). Cells were then incubated 1h with the corresponding Alexa Fluor conjugated secondary antibodies (1:500) and treated with DAPI (1:1000, Sigma) for 15min. Coverslips were mounted in Fluorsave Reagent (Calbiochem, 345789).

Immunohistochemistry

Formalin-fixed paraffin-embedded sections were stained (as per the manufacturer's staining protocol) with the Bond Polymer Refine Detection Kit on a Bond-max™ fully automated staining system (Leica Microsystems GmbH, Germany), using a mouse monoclonal antibody against human Vimentin (1:500, Santa Cruz Biotechnology).

Genomic DNA microarray

Genomic DNA was quantified by spectrophotometry (NanoDrop ND1000, NanoDrop Technologies, Wilmington, Delaware USA). Integrity of DNA was assessed by 0.8% agarose gel electrophoresis. Nonamplification labeling of DNA (direct method) was obtained following the 'Agilent Oligonucleotide ArrayBased CGH for Genomic DNA Analysis' protocol
Version 4.0 (Agilent Technologies, Palo Alto, California USA. p/n G4410-90010). 500 ng of experimental and pool female reference genomic DNA samples were fragmented in a restriction digestion step. Digestion was confirmed and evaluated by DNA 7500 Bioanalyzer assay. Cyanine 3-dUTP and cyanine 5-dUTP were used for fluorescent labeling of test and reference digested gDNAs respectively, using the 'Agilent Genomic DNA Labeling Kit PLUS' (Agilent p/n 5188-5309) according to the manufacturer's instructions. Labeled DNA was hybridized with Human Genome CGH Microarray 44K (Agilent p/n G4426B-014950) containing 43,000+ coding and noncoding human sequences. Arrays were scanned in an Agilent Microarray Scanner (Agilent G2565BA) according to the manufacturer's protocol and data extracted using Agilent Feature Extraction Software 9.5.3.1 following the Agilent protocol CGH-v4_95_Feb07 ('Lowess Only' normalization correction dye bias method instead of 'Linear Only') and the QC Metric Set CGH_ QCMT_Feb08.

Xenografts

All mouse experiments were approved by and performed according to the guidelines of the institutional animal care committee of Principe Felipe Research Center in agreement with the European Union and national directives. An average of 75.000 cells were stereotactically injected into the striatum of the right brain hemisphere (0 mm anterior and 2,5 mm lateral to the bregma; 3,5 mm intraparenchymal) of 9 week-old NUDE mice (Charles River Laboratories). Mice were euthanized when they presented neurological symptoms or a significant loss of weight.

MTS assays

The viability of early and late CSC-enriched culture *in vitro* as well as their sensitivity to different drugs was assessed using the MTS assay. Briefly, single-cell suspensions of CSCs were plated in a 96-well plate, 3000 cells/well in a final volume of 80 µl/well. For the viability assay, they were allowed to grow up to 5 days and analyzed every 24 hours. For drug sensitivity assays, the cells were allowed to grow and to form spheres for 4 days. Cultures were then treated with 20 µl/well of media (control cells), vehicle (DMSO or water) or increasing concentrations of each drug for 72h. 20 µl/well of MTS (CellTiter 96 AQueous One Solution Cell Proliferation Assay, Promega) was added to the culture media, incubated at 37ºC for 3 hours and absorbance was measured at 490 nm. Sensitivity was assessed by comparing the absorbance values of drug-treated cells with vehicle-treated cells and with the absorbance values of control cells (untreated cells) for each treatment group. Each treatment group was repeated in quadruplicate and each experiment in duplicate. Lines were classified as sensitive if their viability decreased or remained unchanged compared with controls.

Statistical analysis

Statistical analyses were performed using a 2-tailed Student *t* test. Data are presented as means ± standard deviation and were calculated using the software package GraphPad Prism v. 5.0. Statistical values of $p > 0.05$ were not considered significant.

ACKNOWLEDGMENTS

We thank the histology core facility at IMMA (Facultad de Medicina, Universidad San Pablo-CEU), the Electronic Microscopy and Genetic and Genomic Core Facilities at Centro de Investigación Príncipe Felipe, and the Biobank Hospital la Fe.

CONFLICTS OF INTEREST

The authors declare no competing financial interests.

GRANT SUPPORT

We are grateful for the financial support from PI10/01069, PI14/00077, and the 'Miguel Servet Program'
CP11/00147 (AAS), PI-01495 (RP), and PI12/00775) (PSG) from Fondo de Investigaciones Sanitarias, Instituto de Salud Carlos III, Spain, supported by

FEDER funds, and Ministerio de Economía y Competitividad, Red Temática de Investigación Cooperativa en Cáncer (RTICC) (RD12/0036/0027) (PSG).

Author contributions

N.G.R., C.G.T., J.C.N., S.E.R., and A.A.S. conceived, designed and performed research with assistance from C.B.I., C.E.L., R.P., P.S.G., M.P.C.,
R.P.A., J.O.C., and V.R.F. All authors contributed to the general discussion and comments on the manuscript. N.G.R., J.C.N., and A.A.S. wrote the manuscript with inputs from G.R., P.S.G., and C.B.I.

REFERENCES

1. Louis DN, Ohgaki H, Wiestler OD, Cavenee WK, Burger PC, Jouvet A, Scheithauer BW, Kleihues P. The 2007 WHO classification of tumours of the central nervous system. Acta Neuropathol. 2007; 114: 97–109.

2. Ostrom QT, Bauchet L, Davis FG, Deltour I, Fisher JL, Langer CE, Pekmezci M, Schwartzbaum JA, Turner MC, Walsh KM, Wrensch MR, Barnholtz-Sloan JS. The epidemiology of glioma in adults: A state of the science review. Neuro Oncol. 2014; 16: 896–913.

3. R. Stupp, W. P. Mason MJ van den B et al., "Radiotherapy plus concomitant and adjuvant temozolomide for glioblastoma." New Engl J Med vol 352, no 10. 2005; pp. 987–96.

4. Stupp R, Hegi ME, Gilbert MR, Chakravarti A. Chemoradiotherapy in malignant glioma: Standard of care and future directions. J Clin Oncol. 2007; 25: 4127–36.

5. Darefsky AS, King JT, Dubrow R. Adult glioblastoma multiforme survival in the temozolomide era: A populationbased analysis of Surveillance, Epidemiology, and End Results registries. Cancer. 2012; 118: 2163–72.

6. Sant M, Minicozzi P, Lagorio S, Børge Johannesen T, Marcos-Gragera R, Francisci S. Survival of European patients with central nervous system tumors. Int J Cancer. 2012; 131: 173–85.

7. Ostrom QT, Gittleman H, Farah P, Ondracek A, Chen Y, Wolinsky Y, Stroup NE, Kruchko C, Barnholtz-sloan JS. N E U RO - O N CO LO GY CBTRUS Statistical Report: Primary Brain and Central Nervous System
Tumors Diagnosed in the United States in 2006-2010. 2013; iil–56.

8. Singh SK, Clarke ID, Terasaki M, Bonn VE, Hawkins C, Squire J, Dirks PB. Identification of a Cancer Stem Cell in Human Brain Tumors. Cancer Res [Internet]. 2003; 63: 5821–8.

9. Singh SK, Hawkins C, Clarke ID, Squire JA, Bayani J, Hide T, Henkelman RM, Cusimano MD, Dirks PB. Identification of human brain tumour initiating cells. Nature [Internet]. 2004; 432: 396–401.

10. Ignatova TN, Kukekov VG, Laywell ED, Suslov ON, Vrionis FD, Steindler DA. Human cortical glial tumors contain neural stem-like cells expressing astroglial and neuronal markers in vitro. Glia. 2002; 39: 193–206.

11. Galli R, Binda E, Orfanelli U, Cipelletti B, Gritti A, Vitis S De, Fiocco R, Foroni C, Dimeco F, Vescovi A. Isolation and Characterization of Tumorigenic, Stem-like Neural Precursors from Human Glioblastoma Isolation and Characterization of Tumorigenic, Stem-like Neural Precursors from Human Glioblastoma. Cancer Res. 2004; 64: 7011–21.

12. Sottoriva A, Spiteri I, Piccirillo SGM, Touloumis A, Collins VP, Marioni JC, Curtis C, Watts C, Tavaré S. Intratumor heterogeneity in human glioblastoma reflects cancer evolutionary dynamics. Proc Natl Acad Sci U S A [Internet]. 2013; 110: 4009–14.

13. Piccirillo SGM, Combi R, Cajola L, Patrizi a, Redaelli S, Bentivegna a, Baronchelli S, Maira G, Pollo B, Mangiola a, DiMeco F, Dalprà L, Vescovi a L. Distinct pools of cancer stem-like cells coexist within human glioblastomas and display different tumorigenicity and independent genomic evolution. Oncogene. 2009; 28: 1807–11.

14. Joo KM, Kim J, Jin J, Kim M, Seol HJ, Muradov J, Yang H, Choi Y La, Park WY, Kong DS, Lee J Il, Ko YH, Woo HG, et al., Patient-Specific Orthotopic Glioblastoma Xenograft Models Recapitulate the Histopathology and Biology of Human Glioblastomas In Situ. Cell Rep [Internet]. The Authors; 2013; 3: 260–73.

15. Lee J, Kotliarova S, Kotliarov Y, Li A, Su Q, Donin NM, Pastorino S, Purow BW, Christopher N, Zhang W, Park JK, Fine HA. Tumor stem cells derived from glioblastomas cultured in bFGF and EGF more closely mirror the phenotype and genotype of primary tumors than do serumcultured cell lines. Cancer Cell. 2006; 9: 391–403.

16. Li A, Walling J, Kotliarov Y, Steed ME, Ahn SJ, Rosenblum M, Mikkelsen T, Zenklusen JC, Fine HA. Genomic Changes and Gene Expression Profiles Reveal That Established Glioma Cell Lines Are Poorly Representative of Primary Human Gliomas. Molecular Cancer Research. 2008; 6: 21–31.

17. Günther HS, Schmidt NO, Phillips HS, Kemming D, Kharbanda S, Soriano R, Modrusan Z, Meissner H, Westphal M, Lamszus K. Glioblastoma-derived stem cellenriched cultures form distinct subgroups according to molecular and phenotypic criteria. Oncogene. 2008; 27: 2897–909.

18. Marziali G, Signore M, Buccarelli M, Grande S, Palma A, Biffoni M, Rosi A, D'Alessandris QG, Martini M, Larocca LM, De Maria R, Pallini R, Ricci-Vitiani L. Metabolic/ Proteomic Signature Defines Two Glioblastoma Subtypes With Different Clinical Outcome. Sci Rep. 2016; 6;1-13.

19. Wakimoto H, Mohapatra G, Kanai R, Curry WT, Yip S, Nitta M, Patel AP, Barnard ZR, Stemmer-Rachamimov AO, Louis DN, Martuza RL, Rabkin SD. Maintenance of primary tumor phenotype and genotype

in glioblastoma stem cells. Neuro Oncol. 2012; 14: 132–44.

20. Phillips HS, Kharbanda S, Chen R, Forrest WF, Soriano RH, Wu TD, Misra A, Nigro JM, Colman H, Soroceanu L, Williams PM, Modrusan Z, Feuerstein BG, et al., Molecular subclasses of high-grade glioma predict prognosis, delineate a pattern of disease progression, and resemble stages in neurogenesis. Cancer Cell. 2006; 9: 157–73.

21. Verhaak RGW, Hoadley KA, Purdom E, Wang V, Qi Y, Wilkerson MD, Miller CR, Ding L, Golub T, Mesirov JP, Alexe G, Lawrence M, O'Kelly M, et al., Integrated Genomic Analysis Identifies Clinically Relevant Subtypes of Glioblastoma Characterized by Abnormalities in PDGFRA, IDH1, EGFR, and NF1. Cancer Cell [Internet]. Elsevier Ltd; 2010; 17: 98–110.

22. Xie Y, Bergström T, Jiang Y, Johansson P, Marinescu VD, Lindberg N, Segerman A, Wicher G, Niklasson M, Baskaran S, Sreedharan S, Everlien I, Kastemar M, et al., The Human Glioblastoma Cell Culture Resource: Validated Cell Models Representing All Molecular Subtypes. EBioMedicine. 2015; 2: 1351–63.

23. Ayuso-Sacido, A., Roy, N.S., Schwartz, T.H., Greenfield, J.P., Boockvar, J.A. Long-term expansion of adult human brain subventricular zone precursors. Neurosurgery. 2008; 62, 223–229.

24. Brennan, C.W. et al., The somatic genomic landscape of glioblastoma. Cell. 2013; 155, 462–477.

25. Warburg O, P.K., Negelein E üeber den Stoffwechsel der Tumoren. Biochem Z. 1924; 319–344.

26. Vlashi E, Lagadec C, Vergnes L, Matsutani T, Masui K, Poulou M, Popescu R, Della Donna L, Evers P, Dekmezian C, Reue K, Christofk H, Mischel PS, et al.

Metabolic state of glioma stem cells and nontumorigenic cells. Proc Natl Acad Sci U S A [Internet]. 2011; 108: 16062–7.

27. Beier D, Hau P, Proescholdt M, Lohmeier A, Wischhusen J, Oefner PJ, Aigner L, Brawanski A, Bogdahn U, Beier CP. CD133+ and CD133- glioblastoma-derived cancer stem cells show differential growth characteristics and molecular profiles. Cancer Res. 2007; 67: 4010–5.

28. Meyer M, Reimand J, Lan X, Head R, Zhu X, Kushida M, Bayani J, Pressey JC, Lionel AC, Clarke ID, Cusimano M, Squire JA, Scherer SW, et al., Single cell-derived clonal analysis of human glioblastoma links functional and genomic heterogeneity. Proc Natl Acad Sci U S A [Internet]. 2015; 112: 851–6.

29. Nevo I, Woolard K, Cam M, Li A, Webster JD, Kotliarov Y, Kim HS, Ahn S, Walling J, Kotliarova S, Belova G, Song H, Bailey R, et al., Identification of molecular pathways facilitating Glioma cell invasion in situ. PLoS One. 2014; 9.

30. Xie Y, Bergström T, Jiang Y, Johansson P, Marinescu VD, Lindberg N, Segerman A, Wicher G, Niklasson M, Baskaran S, Sreedharan S, Everlien I, Kastemar M, et al., The Human Glioblastoma Cell Culture Resource: Validated Cell Models Representing All Molecular Subtypes. EBioMedicine. 2015; 2: 1351–63.

Cancer stem cells from human glioblastoma resemble but do not mimic original tumors after *in vitro* passaging in serum-free media

SUPPLEMENTARY MATERIALS

Isolation and characterization of CSC-enriched cultures from human GBM

Cells derived from fresh surgical human GBM samples were isolated and cultured under the same serumfree conditions used for neural stem cells isolated from human adult brain [2]. About 55% of GBM samples (11 out of 20) rendered expandable cell cultures. Consistent with a previous work reported by Günther *et al.*,, [3] we observed that CSC-enriched cell lines cultured under these conditions showed different growing features that can be grouped into three clusters: spheres attached to the surface that eventually detached (cluster 1), spheres growing in suspension (cluster 2) and attached monolayer of cells in combination with spheres that eventually detached from the plate surface (cluster 3) (Supplementary Table S1). For the purpose of the present work, we randomly took one representative CSC-enriched culture from each group (Figure 2).

To rule out the possibility that these cells were normal progenitor cells, we performed a Comparative Genomic Hibrydization (CGH) analysis on total DNA isolated from the first passage in culture. All three cell lines exhibited loss of heterogeneity (LOH) in chromosome 10 and duplication of chromosome 7, among other chromosomal alterations. All these alterations are hallmarks of glioblastoma (Supplementary Figure S1).

The selected CSC-enriched cultures were grown under differentiation conditions, giving rise to cells expressing astrocyte, oligodendrocyte and neuron markers. We found an important number of cells coexpressing several lineage-restricted markers, which have been previously reported and regarded as another feature of brain tumor cells (Immunocytochemistry assay results for GBM18 shown as example in Supplementary Figure S2). Then, we studied the expression of CSC markers together with stemness and differentiation gene markers. We first designed and validated a collection of primers targeting the selected gene markers (Supplementary Table S2). We observed that GBM18 and GBM27 expressed *CD133*, *SSEA1*, *CD44* and *CD90* genes, all of them reported in the literature to label CSCs subpopulations, in addition of stemness genes also found in adult NSCs. Interestingly, we found no expression of *CD133* and *SSEA1*, and a very low expression of *Nestin* in GBM38 (Supplementary Figure S3). Further analysis of GBM38 CGH showed a LOH at 4p15.32 and 11q21, the chromosomal locations of *CD133* and *SSEA1* respectively (Supplementary Table S3). Finally, we observed equal expression of neuronal markers *MAP-2* and *βIII-Tub* in all three CSC-enriched cell lines while the astrocytic marker *GFAP* was just expressed in GBM18 and GBM27, and oligodendrocyte markers *CNPase* and *PDGFRα* were highly expressed in GBM18 and GBM38 (Supplementary Figure S3). Finally, using Shotgun proteomics, we studied these markers at the protein level. We observed the presence of CD44, Nestin, βIII-Tub, MAP2, and CNPase in all three CSC-enriched cultures. Additionally, we detected SOX2 and GFAP in GBM18 and GBM27 and PDGFRα in GBM18 and GBM38. The presence of GFAP and SOX2, in GBM18 and GBM27 and Nestin, in all three CSCs-enriched cultures, was also confirmed by immunocytochemistry (Supplementary Figure S4).

SUPPLEMENTARY FIGURES AND TABLES

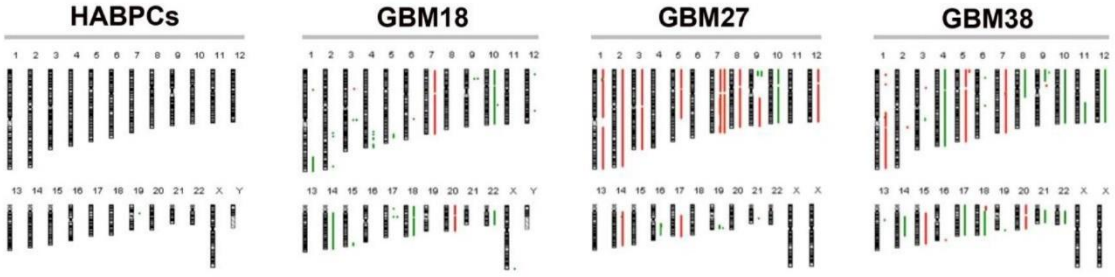

Supplementary Figure S1: Graphical karyotipe representation of the GBM18, GBM27 and GBM38 CSC-enriched cultures by Comparative Genomic Hybridisation at passage 2. The chromosomal abnormalities are compatible with GBM. Human Adult Brain Progenitor Cells (HABPCs), isolated from surgical tissue, at passage 1, were used to evaluate the influence of culture conditions on chromosomal instability Keywords: Green line indicates DNA loss and Red line indicates DNA gain.

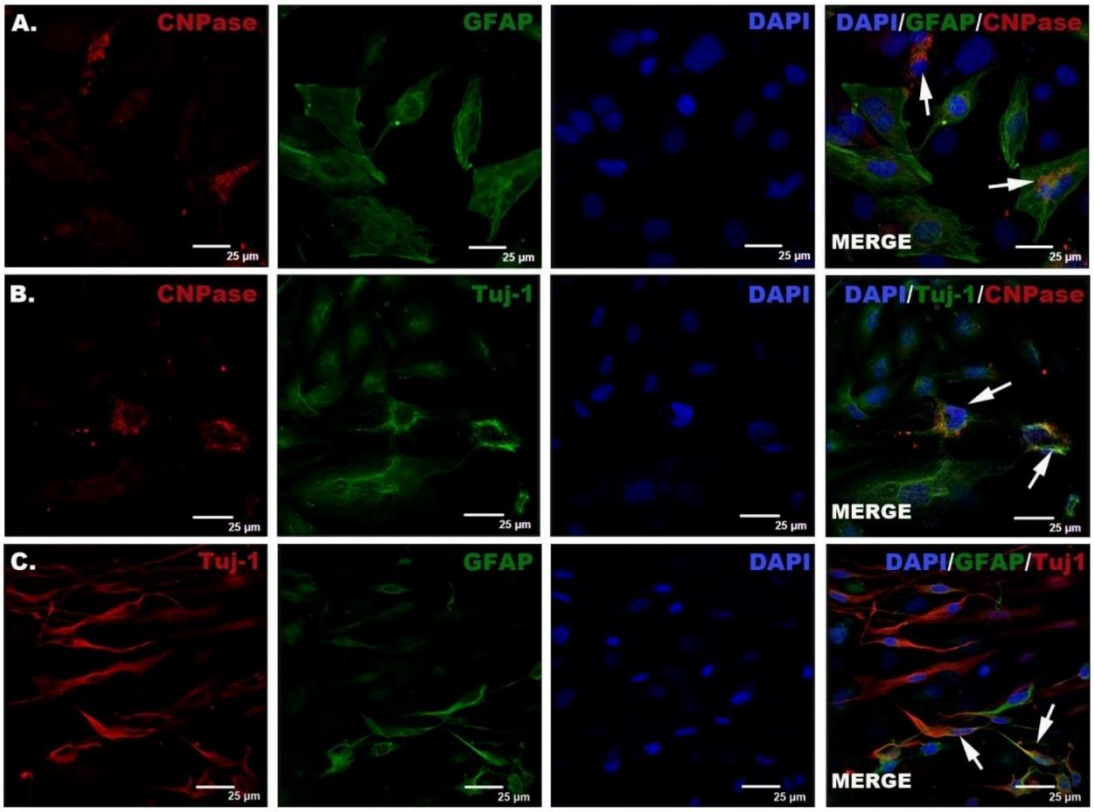

Supplementary Figure S2: Spontaneous differentiation of CSCs induced by serum addition to culture media for ten days. The pictures represent the results for GBM18. **A.** GFAP and CNPase co-expression; **B.** Tuj-1 and CNPase co-expression and **C.** Tuj-1 and GFAP co-expression. White arrows represent cells co-expressing markers.

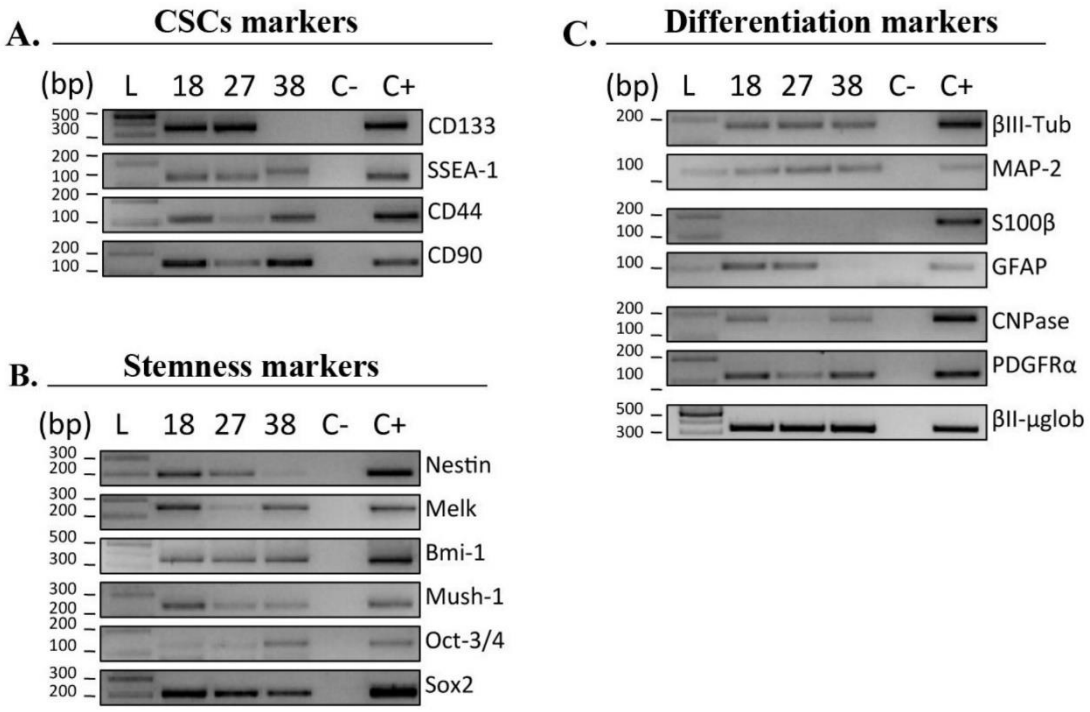

Supplementary Figure S3: A. mRNA expression pattern of GBM18, GBM27 and GBM38 for CSC. Stemness **B.** and differentiation markers **C.** The assay indicates presence or absence of the markers.

A.

Type of marker	Uniprot ACC	Entry Name	Protein Name	Gene Symbol	GBM18			GBM27			GBM38		
					Exclusive unique peptides	Total unique peptides	Sequence coverage (%)	Exclusive Unique peptides	Total unique peptides	Sequence coverage (%)	Exclusive Unique peptides	Total unique peptides	Sequence coverage (%)
CSCs	O43490	PROM1_HUMAN	Antigen AC133	PROM1	-	-	-	-	-	-	-	-	-
	P16070	CD44_HUMAN	CD44 antigen	CD44	1	8	3%	1	5	10%	1	5	3%
	P22083	FUT4_HUMAN	Fucosyltransferase 4	FUT4	-	-	-	-	-	-	-	-	-
STEMNESS	Q01860	PO5F1_HUMAN	Oct-3/4	POU5F1	-	-	-	-	-	-	-	-	-
	P35226	BMI1_HUMAN	BMI-1	BMI1	-	-	-	-	-	-	-	-	-
	P48431	SOX2_HUMAN	SOX-2	SOX2	1	1	5%	2	3	26%	-	-	-
	P48681	NEST_HUMAN	Nestin	NES	16	49	10%	85	49	52%	1	1	2%
	Q14680	MELK_HUMAN	hMELK	MELKV4	-	-	-	-	-	-	-	-	-
	O14746	TERT_HUMAN	HEST2	TERT	-	-	-	-	-	-	-	-	-
DIFFERENTIATION	Q13509	TBB3_HUMAN	Tubulin beta-3 chain	TUBB3	0	17	21%	3	18	60%	1	23	26%
	P14136	GFAP_HUMAN	GFAP	GFAP	6	16	17%	27	14	56%	-	-	-
	P16234	PGFRA_HUMAN	PDGFR-alpha	PDGFRA	2	2	4%	-	-	-	1	1	3%
	P11137	MTAP2_HUMAN	MAP-2	MAP2	1	1	0%	4	4	3%	2	2	2%
	P04271	S100B_HUMAN	Protein S100-B	S100B	-	-	-	-	-	-	-	-	-
	P09543	CN37_HUMAN	CNPase	CNP	4	7	16%	17	10	38%	2	6	8%

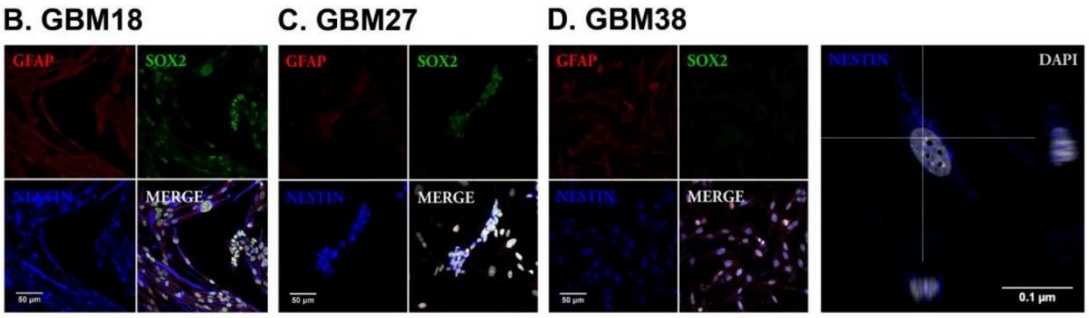

Supplementary Figure S4: Cancer stem cells, stemness and differentiation markers identified in total proteome of GBM18, GBM27 and GBM38 by shotgun proteomics analysis and confocal microscopy images showing SOX2, GFAP and Nestin immunocytochemistry analysis in CSC-enriched culture cells at late passages. **A**. Whole cell lysates were digested with trypsin and fractionated by reverse-phase chromatography at basic pH prior to LC-MS/MS (liquid chromatography coupled to tandem mass spectrometry) analysis in a 5600 TripleTOF system (AB SCIEX). Uninterpreted MS/MS data were searched against a human database (UniprotKB, 2013) concatenated with reversed sequences as decoy (containing 73,704 sequences, 36,852 forward sequences), using an in-house licensed Mascot v2.4 search engine. Data analysis was performed using Scaffold (v 4.4.5, Proteome Software), applying a False Discovery Rate (FDR) below 1% at the peptide level. **B**. GBM18. **C.** GBM27. **D.** GBM38. GFAP (red), SOX2 (green), Nestin (blue) and Nuclei (grey). Keywords: *Type of marker*: Classification of protein markers identified by shotgun proteomics; *Uniprot ACC:* accession number of the identified proteins based on Swiss-Prot database; *Entry Name*: the protein ID of the identified proteins based on Swiss-Prot database; *Protein Name*: the name of identified proteins based on Swiss-Prot database; *Gene symbol*: the gene name of the identified proteins based on Swiss-Prot database; *Exclusive Unique Peptides*: the number of different amino acid sequences, regardless of any modification, that are associated with a single protein (as defined by Scaffold software); *Total Unique Peptides*: number of different amino acid sequences that are associated with a specific protein, including those shared with other proteins (as defined by Scaffold software); *Percentage sequence coverage*: the percentage of all the amino acids in the protein sequence that were detected in the sample (as defined by Scaffold software).

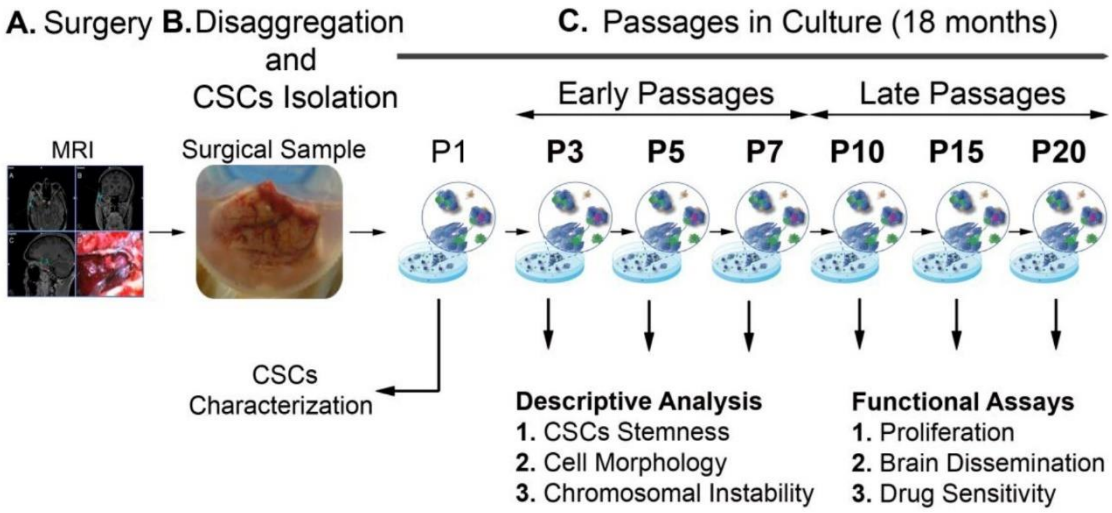

Supplementary Figure S5: Diagram depicting the experimental design and assays on CSC-enriched cultures isolated from surgical human glioma samples. A. Standard image of intraoperative MRI indicating the location from where the tumor sample is resected. **B.** Image of regular surgical sample after resection conserved in PBS before processing. **C.** Schematic representation of early and late passages of CSC-enriched culture as well as the different descriptive analyses and assays conducted with the indicated passages. The growth patterns of each CSC culture were conserved along the 20 passages *in vitro*.

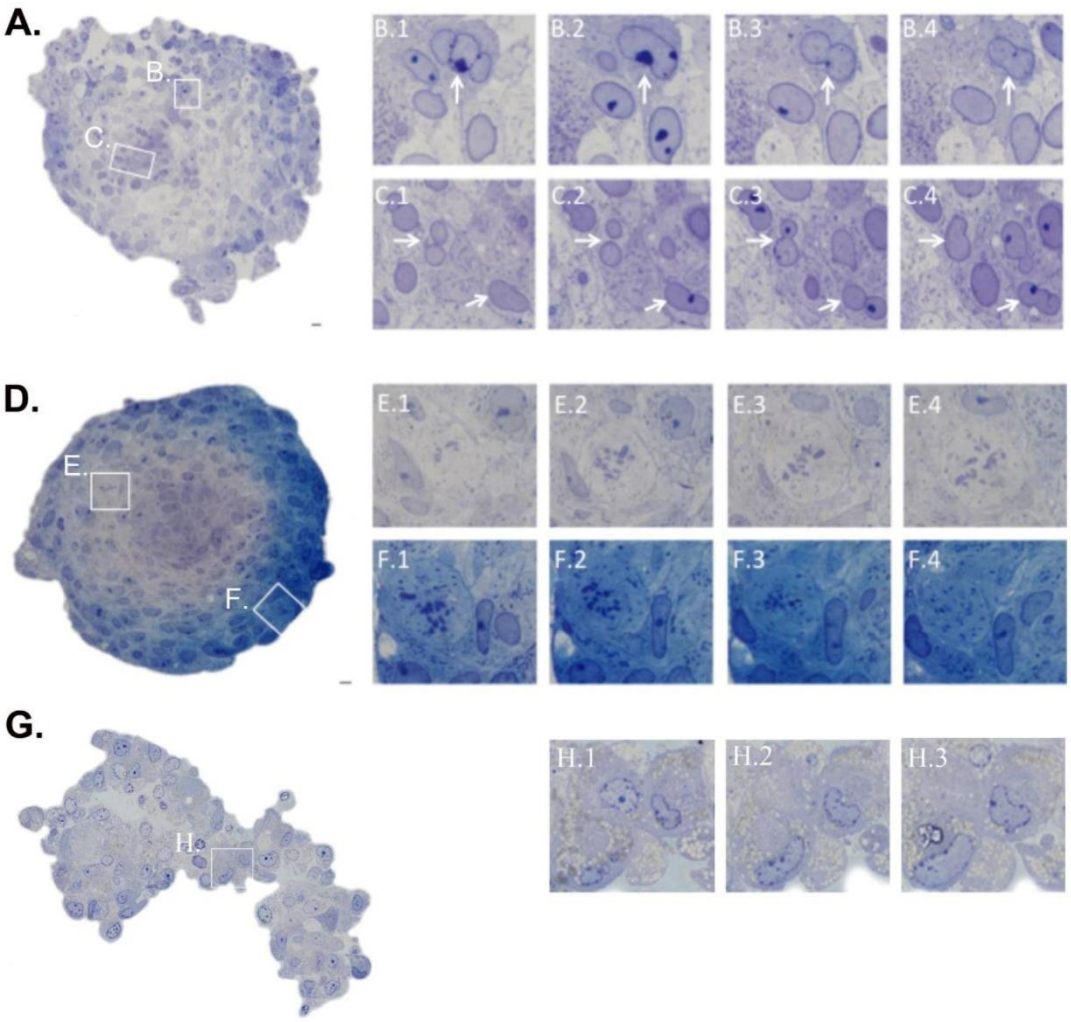

Supplementary Figure S6: Semithin sections of tumorspheres stained with toluidine blue. A. GBM18 tumorsphere. **B1-B4** and **C1-C4**. The white squares show polymorphic nuclei revealed by serial images. The white arrows indicate the location of the nuclei; **D.** GBM27 sphere. **E1-E4** and **F1-F4**. The white squares show dividing cells located both at the periphery and inside the tumorsphere, and appear magnified in the serial sections. **G.** GBM38 sphere. **H1-H3**. The white squares show cells carrying a huge number of lipid inclusions all over the cells. Scale bars represent 10 μm.

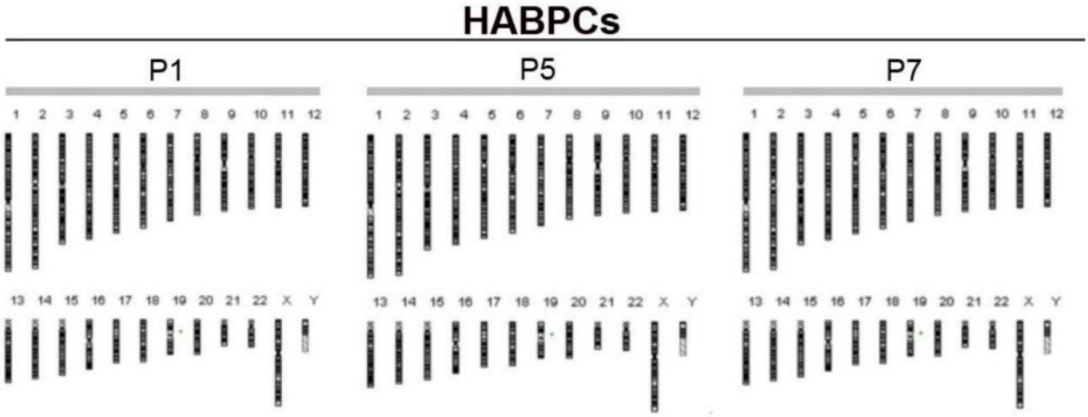

Supplementary Figure S7: Graphical karyotype representation of Human Adult Brain Progenitor Cells (HABPCs), isolated from adult human brain white matter of patients receiving temporal lobectomy for the treatment of intractable epilepsy. Comparative Genomic Hybridization was performed on passages 1, 5 and 7. Chromosomal aberrations were absent until the cells became quiescent, which demonstrates the low influence of the isolation procedure and culture conditions on chromosomal instability in non-transformed cells. Keywords: Green line indicates DNA loss.

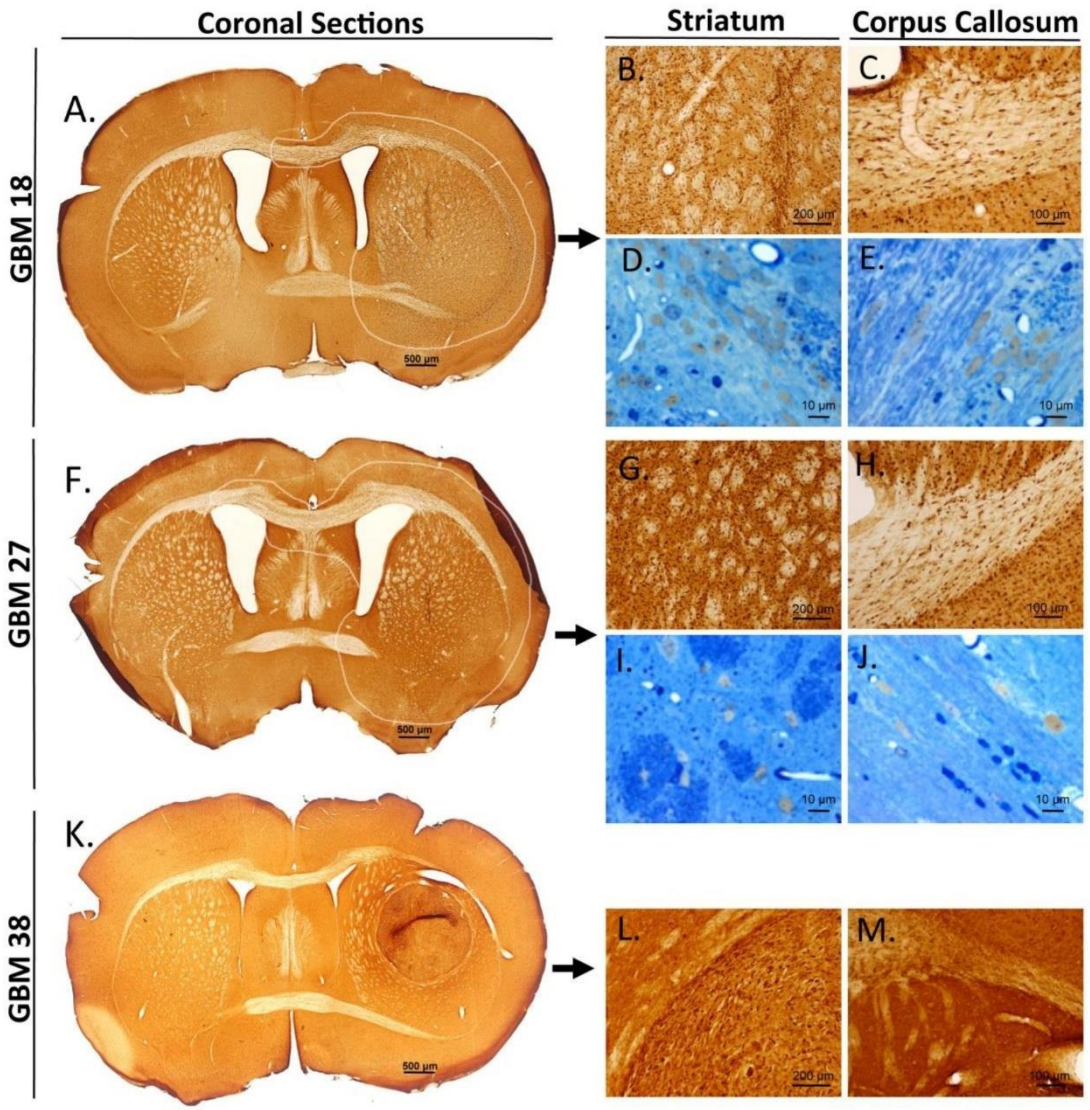

Supplementary Figure S8: Brain dissemination pattern of CSCs isolated from human samples. Human cells are revealed by immunostaining with anti-human nuclei. Mice were sacrificed 4 weeks after xenotrasplantation with **A.** GBM18, **F.** GBM27 and **K.** GBM38 without clinical evidences of tumor. Both GBM18 and GBM27 CSC-enriched cultures utilize myelin fibers to disseminate through the parenchymal brain as observed on 50 µm sections stained with DAB **B, C, G** and **H.** and semi-thin sections counterstained with toluidine blue **D, E, I** and **J.** The GBM38 CSC-enriched culture grew as a nodular tumor with well-defined boundaries from very early stages **L, M.**

Supplementary Table S1: Surgical samples used to derive cancer-stem cells. Keywords: GBM: Glioblastoma; AA: Anaplastic Astrocitoma; ODG: Oligodendroglioma. Grouped according to *in vitro* growth patterns (*vide supra*).

See Supplementary File 1

Supplementary Table S2: List of primers targeting specific genes designed and validated in our laboratory in the context of previous or present works. For all cases, cell lines expressing the gene of interest were utilized for primers validation.

See Supplementary File 2

Supplementary Table S3: CSC gene markers used in the present work and their chromosomal location and dotation within the CSC-enriched cultures GBM18, GBM27 and GBM38. Keywords: LOH (loss of heterogeneity).

See Supplementary File 3

Supplementary Table S4: List of chromosomal alterations in GBM18, by Comparative Genomic Hybridization, along the first 20 passages in culture. Keywords: white square, deletions; grey square, amplifications; -2, homozygous deletion; -1, heterozygous deletion and +1, heterozygous amplification.

See Supplementary File 4

Supplementary Table S5: List of chromosomal alterations in GBM27, by Comparative Genomic Hybridization, along the first 20 passages in culture. Keywords: white square, deletions; grey square, amplifications; -2, homozygous deletion; -1, heterozygous deletion; +2, homozygous amplification, +1, hetrerozygous amplification and *, less than 50% of cells.

See Supplementary File 5

Supplementary Table S6: List of chromosomal alterations in GBM38, by Comparative Genomic Hybridization, along the first 20 passages in culture. Keywords: white square, deletions; grey square, amplifications; -2, homozygous deletion; -1, heterozygous deletion; +2, homozygous amplification, +1, heterozygous amplification and *, less than 50% of cells.

See Supplementary File 6

Supplementary Table S7: Statistically significant DNA sequence gains (19) and losses (20) identified on GBM solid samples by TCGA and analysed in CSC-enriched cultures over the first 20 passages in culture. Keywords: N, normal; G, gained; L, lost; HL, heterogeneity lost and *, less than 50% of cells.

See Supplementary File 7

Supplementary File 1

Sample	Age	Diagnostic	Primary Culture	Group
13	59	GBM	-	-
7	65	GBM	-	-
14	71	GBM	**Yes**	1
35	63	GBM	**Yes**	3
15	61	AA	**Yes**	2
16	65	GBM	-	-
18	59	GBM	**Yes**	1
32	45	GBM	-	-
22	45	GBM	**Yes**	2
29	56	GBM	**Yes**	2
27	61	GBM	**Yes**	2
37	56	GBM	-	-
35	58	GBM	-	-
5	61	AA	-	-
33	50	ODG	**Yes**	3
43	56	GBM	**Yes**	1
51	63	GBM	-	-
53	39	AA	**Yes**	2
56	57	AA	-	-
38	63	GBM	**Yes**	3

Supplementary File 2

Gene name	Protein name	Primers (5'-3')	Amplicon size (pb)	Control
β2M	Beta-2-microglobulin	CTCGCGCTACTCTCTCTTTCTG	335	U87
		GCTTACATGTCTCGATCCCACT		
CD90	Thymocyte differentiation antigen 1	CGCTCTCCTGCTGCTAACAGTCTT	120	U87
		CAGGCTGAACTCGTACTGGA		
BM1	B lymphoma Mo-MLV insertion region 1 homolog	GGAGACCAGCAAGTATTGTCCCCTTTTG	320	U87
		CATTGCTGCTGGGCATCCGTAAG		
CD133	Prominin 1	TCTCTATGTGGTACAGCCG	350	U87
		TGATCCGGGTTCTTACCTG		
GFAP δ	Glial fibrillary acidic protein isoform delta	AGTGGTAAAGGTGGTGAGTCCT	126	human GBM
		GTCCAGGCACAGCGAGAC		
MELK	*Maternal embryonic leucine zipper kinase*	CTTGGATCAGAGGCAGATGTTTGGAG	248	human GBM
		GTTGTAATCTTGCATGATCCAGG		
NESTIN	Nestin	GAGAGGGAGGACAAAGTCCC	251	U87
		TCCCTCAGAGACTAGCGCAT		
SOX2	Sex determining region Y-box 2	GCACATGAACGGCTGGAGCAACG	206	human GBM
		TGCTGCGAGTAGGACATGCTGTAGG		
CD44	Receptor for hyaluronic acid (HA)	AGAAGGTGTGGGCAGAAGAA	116	U87
		AAATGCACCATTTCCTGAGA		
GFAP α	Glial fibrillary acidic protein isoform alpha	TGCGGTCCCTTCTTACTCAC	232	U373
		CCTCCCAGTCCCATCTCTG		
S100B	S100 calcium binding protein B	TGCGAGTTCTGATGGAGTTG	160	U373
		TGCGAGTTCTGATGGAGTTG		
TUBB3	Beta- III tubulin	GAGGAAGAGGGCGAGATGTA	166	U87
		GAGGGGAAAGCAGGGTGT		
MAP2	Microtubule-associated protein 2	ATTCCGAGGTTCCAACACAC	102	U87
		ACCAGCCATTGAAGAAATGC		
PDGFRα	Platelet-derived growth factor receptor subunit a	ATAATCCCCACAGGCACATT	118	human oligodendro glioma tissue
		TCACACATTCACCACACCATT		
CNPase	2', 3'-cyclic nucleotide 3'-phosphodiesterase	CAGGACCGCCAAAGAATG	172	
		GGAAAGGAGGGGAGTGAGAC		
Mush-1	Mushashi	GATGGTCACTCGGACGAAGAA	149	U87
		CAAACCCTCTGTGCCTGTTG		
Oct 3/4	POU transcription factor	CAAAAACCCTGGCACAAACT	128	U87
		CCTGTCTCCGTCACCACTCT		
SSEA-1	stage-specific embryonic antigen 1	GGCAGAAAACCAGGAATCAG	126	Leukocytes
		ACTTGGCTCCTTTCCCTGA		
TERT	Telomerase reverse transcriptase	GCGTTTGGTGGATGATTTCT	254	U87
		AGCTGGAGTAGTCGCTCTGC		
CD144	vascular endothelial-cadherin (VE-cadherin)	TCGTCATGGACCGAGGTT	87	human adipose tissue
		TTGGTTAAAACAAACAAGTCAGTGT		
CD166	Activated leukocyte adhesion molecule	ATTGAAGTTTTATTTGGCAGGAA	102	human adipose tissue
		GGCTTAGCCATGCAAAACA		
CD24	Heat Stable Antigen (HSA)	TTGGGAAGTGAAGACTGGAAG	119	human adipose tissue
		GTTCTAAATGTGGCTATTCTGATCC		
CD73	5'-nucleotidase	CTTAACGTGGGAGTGGAACC	102	human adipose tissue
		TCTAGCTGCCATTTGCACAC		
ABCG2	ATP-binding cassette sub-family G member 2	GGGTTCTCTTCTTCCTGACGACC	389	U87
		TGGTTGTGAGATTGACCAACAGACC		

Supplementary File 3

CSCs gene markers	Location	GBM18	GBM27	GBM38
CD133	4p15.32	OK	OK	LOH(-1)
SSEA-1	11q21	OK	OK	LOH(-1)
CD44	11q23.3	OK	OK	OK
CD90	11p13	OK	OK	OK

Supplementary File 4

Chr. #	Cytoband	UCSC hg18 Start	UCSC hg18 Stop	Size (Mb)	GBM18 P1	GBM18 P5	GBM18 P7	GBM18 P10	GBM18 P15	GBM18 P20
chr1	p33	49403959	49860501	0,46	**-1**	**-1**	**-1**	**-1**	**-1**	**-1**
chr1	q32.3 - q44	2,1E+08	2,45E+08	34,37	**-1**	**-1**	**-1**	**-1**	**-1**	**-1**
chr2	q24.2	1,6E+08	1,6E+08	0,43	**-1**	**-1**	**-1**	**-1**	**-1**	**-1**
chr2	q37.1	2,34E+08	2,34E+08	0,79	**-1**	**-1**	**-1**	**-1**	**-1**	**-1**
chr3	p21.31	47553726	47602749	0,05	**+1**	**+1**	**+1**	**+1**	**+1**	**+1**
chr3	q13.31	1,17E+08	1,18E+08	0,43	**-2**	**-2**	**-2**	**-2**	**-2**	**-2**
chr3	q13.33	1,21E+08	1,21E+08	0,16	**-1**	**-1**	**-1**	**-1**	**-1**	**-1**
chr4	q25	1,14E+08	1,14E+08	0,14	**-1**	**-1**	**-1**	**-1**	**-1**	**-1**
chr4	q31.23 - q31.3	1,5E+08	1,51E+08	1,85	**-1**	**-1**	**-1**	**-1**	**-1**	**-1**
chr4	q32.1	1,56E+08	1,58E+08	1,77	**-1**	**-1**	**-1**	**-1**	**-1**	**-1**
chr4	q32.2 - q32.3	1,64E+08	1,65E+08	0,34	**-1**	**-1**	**-1**	**-1**	**-1**	**-1**
chr4	q32.3	1,66E+08	1,69E+08	2,27	**-1**	**-1**	**-1**	**-1**	**-1**	**-1**
chr4	q34.3	1,8E+08	1,81E+08	1,07	**-1**	**-1**	**-1**	**-1**	**-1**	**-1**
chr4	q35.1 - q35.2	1,83E+08	1,88E+08	5,18	**-1**	**-1**	**-1**	**-1**	**-1**	**-1**
chr5	q33.3 - q34	1,57E+08	1,64E+08	7,10	**-1**	**-1**	**-1**	**-1**	**-1**	**-1**
chr6	q22.31	1,19E+08	1,19E+08	0,34	**-1**	**-1**	**-1**	**-1**	**-1**	**-1**
chr7	p22.3 - q36.3	149268	1,59E+08	158,45	**+1**	**+1**	**+1**	**+1**	**+1**	**+1**
chr9	p21.3	21968146	21980722	0,01	**-2**	**-2**	**-2**	**-2**	**-2**	**-2**
chr10	p15.3 - q26.3	138206	1,35E+08	135,12	**-1**	**-1**	**-1**	**-1**	**-1**	**-1**
chr11	q14.1	78303246	79188879	0,89	**-1**	**-1**	**-1**	**-1**	**-1**	**-1**
chr12	p13.2 - p13.1	12393482	12669535	0,28	**-1**	**-1**	**-1**	**-1**	**-1**	**-1**
chr12	q23.1	99130349	99228987	0,10	**-1**	**-1**	**-1**	**-1**	**-1**	**-1**
chr14	q11.2 - q32.33	19508845	1,06E+08	86,82	**-1**	**-1**	**-1**	**-1**	**-1**	**-1**
chr15	q26.1 - q26.3	90198224	97613657	7,42	**-1**	**-1**	**-1**	**-1**	**-1**	**-1**
chr17	p13.1	7401533	7517547	0,12	**-1**	**-1**	**-1**	**-1**	**-1**	**-1**
chr17	q11.2	26338949	26783160	0,44	**-2**	**-2**	**-2**	**-2**	**-2**	**-2**
chr18	p11.32 - q23	170029	76083258	75,91	**-1**	**-1**	**-1**	**-1**	**-1**	**-1**
chr20	p13 - q13.33	18380	62363774	62,35	**+1**	**+1**	**+1**	**+1**	**+1**	**+1**
chr22	q11.1 - q13.33	14433473	49525130	35,09	**-1**	**-1**	**-1**	**-1**	**-1**	**-1**
chrX	q28	1,53E+08	1,54E+08	1,44	**-1**	**-1**	**-1**	**-1**	**-1**	**-1**

Supplementary File 5

Chr. #	Cytoband	UCSC hg18 Start	UCSC hg18 Stop	Size (Mb)	GBM27 P1	GBM27 P5	GBM27 P7	GBM27 P10	GBM27 P15	GBM27 P20
chr1	p36.33 - p36.1	2554068	22913633	22,36	**+1***					
chr1	p36.12 - p35.3	23113417	27820370	4,71	**-1**	**-1**	**-1**	**-1**	**-1**	**-1**
chr1	p35.3-q44	27960490	2,47E+08	219,16	**+1***					
chr1	q41 - q42.12	2,2E+08	2,24E+08	3,90				**-1***	**-1***	**-1***
chr2	p25.3-q37.3	208595	2,43E+08	242,48	**+1***	**+1**	**+1**	**+1***	**+1***	**+1***
chr3	p26.3-q29	224527	1,99E+08	199,06	**+1**	**+1**	**+1**	**+1***	**+1***	**+1***
chr5	p15.33-q23.2	148043	1,23E+08	122,51	**+1**	**+1**	**+1**	**+1***	**+1***	**+1***
chr6	q26 - q27	1,64E+08	1,68E+08	3,83				**-1***	**-1***	**-1***
chr7	p22.3 -q36.3	149068	1,59E+08	158,45	**+1***	**+1**	**+1**	**+1**	**+1**	**+1**
chr8	p23.3 -q24.3	445082	1,46E+08	145,76	**+1***					
chr9	p24.3 -p22.1	204167	19540325	19,34		**-1**	**-1**	**-1**	**-1**	**-1**
chr9	p22.1 - p21.3	19587033	24874189	5,29	**-2**	**-2**	**-2**	**-2**	**-2**	**-2**
chr9	p21.3 - p13.1	25081725	39277118	14,20		**-1**	**-1**	**-1**	**-1**	**-1**
chr9	q13 - q34.3	70327267	1,4E+08	69,75	**+2**	**+1**	**+1**	**+1**	**+1**	**+1**
chr10	p15.3 - p11.21	138206	38166900	38,03	**-1***	**-1***	**-1***	**-1***	**-1***	**-1***
chr10	p11.23 - p11.2	230768143	33431691	2,66				**-2***	**-2***	**-2***
chr10	p11.22-p11.21	33531030	38468194	4,94				**-1***	**-1***	**-1***
chr10	q11.21 -q26.3	44669560	1,34E+08	89,78	**-1***	**-1***	**-1***	**-1***	**-1***	**-1***
chr10	q23.2 - q23.31	89540133	90814414	1,27				**-2***	**-2***	**-2***
chr10	q23.31- q26.3	90955266	1,34E+08	43,49				**-1***	**-1***	**-1***
chr12	p13.33 - q24.33	179123	1,32E+08	132,01	**+1**					
chr14	q11.2 - q32.33	19508845	1,05E+08	85,52	**+1***					
chr14	q12	28684841	29767186	1,08	**-1**	**-1**	**-1**	**-1**	**-1**	**-1**
chr15	q14 - q15.1	32511272	38445780	5,93				**-1***	**-1***	**-1***
chr16	q12.1	47505319	48408783	0,90	**-1**	**-1**	**-1**	**-1**	**-1**	**-1**
chr16	q12.1 - q22.1	50843158	68534348	17,69	**-1**	**-1**	**-1**	**-1**	**-1**	**-1**
chr16	q22.3 - q23.1	73148905	75674285	2,53	**-1**	**-1**	**-1**	**-1**	**-1**	**-1**
chr17	q11.2 - q25.3	26663307	78623230	51,96	**+1**	**+1**	**+1**	**+1***	**+1***	**+1***
chr19	q13.32	50975367	53079022	2,10	**-1**	**-1**	**-1**	**-1**	**-1**	**-1**
chr19	q13.33	55600649	56342690	0,74					**-1***	**-1***
chr19	q13.33	55600449	55704086	0,10	**-1**	**-1**	**-1**	**-1**	**-1**	**-1**
chr19	q13.33 - q13.4	156275383	58646276	2,37	**-1**	**-1**	**-1**	**-1**	**-1**	**-1**
chr19	q13.33	56392998	56687199	0,29	**-2**	**-2**	**-2**	**-2**	**-2**	**-2**

chr21	q22.11	33246346	33799862	0,55	**-1***	**-1**	**-1**	**-1**	**-1**	**-1**
chr22	q11.1 - q11.22	15835035	21010211	5,18				**-1***	**-1***	**-1***
chr22	q12.3 - q13.1	33442011	37176202	3,73				**-1***	**-1***	**-1***

Supplementary File 6

Chr. #	Cytoband	UCSC hg18 Start	UCSC hg18 Stop	Size (Mb)	GBM38 P1	GBM38 P5	GBM38 P7	GBM38 P10	GBM38 P15	GBM18 P20
chr1	p36.13	17483078	17914454	0,33	**+1**	**+1**	**+1**	**+1**	**+1**	**+1**
chr1	p34.3 - p34.2	36835076	39875175	3,04	**+1**	**+1**	**+1**	**+1**	**+1**	**+1**
chr1	p21.1 -q44	#######	247179291	141,04		**+1**	**+1**	**+1**	**+1**	**+1**
chr1	p13.1	1,17E+08	117379771	0,27	**-1**	**-1**	**-1**	**-1**	**-1**	**-1**
chr2	p25.3-q22.1	29193	141703284	141,67		**-1***	**-1***			
chr2	p25.3 - p16.1	208795	56540075	56,51					**+1**	**+1**
chr2	p16.1-q37.3	57384961	242690037	185,31					**-1**	**-1**
chr2	q22.1 - q22.2	1,42E+08	144035497	2,70	**+1**	**+1**	**+1**	**+1**		
chr2	q22.1 - q37.3	1,42E+08	242169652	100,41	**+1**					
chr3	p21.31	45516991	45964687	0,45	**+1**	**+1**	**+1**	**+1**	**+1**	**+1**
chr3	p12.3-p11.1	76211888	90264177	14,05	**-1***	**-1***	**-1***			
chr3	q11.2-q29	95088205	199288217	104,20	**+1***					**-1**
chr4	p16.3-q35.2	62447	191121344	191,06	**-1***	**-1**	**-1**	**-1**	**-1**	**-1**
chr5	p15.33 - p15.2	148043	9683273	9,53	**+2**	**+2**	**+2**	**+2**	**+2**	**+2**
chr5	q31.2	1,38E+08	137879815	0,41					**+1**	**+1**
chr5	p15.2 - q35.3	10120817	180617107	170,50	**+1**	**+1**	**+1**	**+1**		
chr6	p25.3-q27	204528	170734227	170,53			**-1***	**-1***		
chr6	p22.1	27882726	27988302	0,11	**-1**	**-1**	**-1**	**-1**		
chr6	q15	87855835	88919083	0,89	**-1**	**-1**	**-1**	**-1**	**-1**	**-1**
chr6	q24.3	1,46E+08	146097565	0,21				**-1***	**-1**	**-1**
chr7	p22.3 - q36.3	149268	158781397	158,63	**+1**	**+1**	**+1**	**+1**		
chr7	p22.1	5993160	6344349	0,29					**+1**	**+1**
chr7	q11.21-q21.11	62153588	79562970	17,41					**+1**	**+1**
chr8	p23.3 - q13.2	181530	70029837	69,85		**-1**	**-1**	**-1**	**-1**	**-1**
chr9	p24.3 - p21.1	204367	28735046	28,53	**-1**	**-1**	**-1**	**-1**	**-1**	**-1**
chr9	p21.3	21844914	21999182	0,15	**-2**	**-2**	**-2**	**-2**	**-2**	**-2**
chr10	p15.3 -q26.3	138206	135254513	135,12	**-1**	**-1**	**-1**	**-1**	**-1**	**-1**
chr11	p15.5 - p14.3	192958	22892819	22,49					**+1**	**+1**
chr11	p15.1-q14.1	21322916	84398989	63,08		**-1***	**-1***	**-1***		
chr11	q14.1 - q25	82843821	133761259	49,31		**-1**	**-1**	**-1**	**-1**	**-1**
chr12	p13.33 -q24.33	49967	132278059	132,23	**-1**	**-1**	**-1**	**-1**	**-1**	**-1**
chr13	q12.11-q34	18601703	114077122	95,48			**-1***	**-1***		
chr13	q13.1	31574116	31738692	0,16	**-1**	**-1**	**-1**			

chr14	q12 - q31.1	28974471	78816279	49,84	**-1**	**-1**	**-1**	**-1**	**-1**	**-1**
chr15	q11.2 - q26.3	20418129	100168859	81,06	**+1***	**+1***	**+1***			
chr16	q24.2	85927761	86371915	0,96	**+1**	**+1**	**+1**	**+1**	**+1**	**+1**
chr17	p13.3- q25.3	84287	78623230	78,57		**-1**	**-1**	**-1**	**-1**	**-1**
chr17	q23.2	57344164	58191068	0,85	**+1**					
chr18	p11.32 - q23	170229	76083117	75,91	**-1**					
chr18	p11.32 -q11.2	170229	17760271	18,46		**+1***	**+1***	**+1***	**+1**	**+1**
chr18	q11.2-q23	18770696	76083117	57,31		**-1***	**-1***	**-1***		
chr19	q13.43	63043564	63784382	0,74	**-1**	**-1**	**-1**	**-1**	**-1**	**-1**
chr20	p13 - q13.33	18580	62363633	62,35	**+1**	**+1**	**+1**	**+1**	**+1**	**+1**
chr21	q11.1 - q22.3	10013263	46892352	36,88	**-1**	**-1**	**-1**	**-1**	**-1**	**-1**
chr22	q11.1 - q13.33	15908242	49335558	35,09	**+1***	**-1**			**-1**	**-1**
chr22	q11.1 - q13.2	15908242	40007382	25,57			**-1**	**-1**		
chr22	q13.2	40064271	41312679	1,25			**+1**	**+1**		
chr22	q13.2 - q13.33	41336148	49525130	8,19			**-1**	**-1**		
chrX	p22.33-q28	2782031	153475911	150,69					**-1**	**-1**

Supplementary File 7

Genes	Chr #	GBM18							GBM27							GBM38					
		P1	P5	P7	P10	P15	P20		P1	P5	P7	P10	P15	P20		P1	P5	P7	P10	P15	P20
Gains																					
PRDM2	1	N	N	N	N	N	N		G*	N	N	N	N	N		N	N	N	N	N	N
MDM4	1	N	N	N	N	N	N		G*	N	N	N	N	N		N	G	G	G	G	G
AKT3	1	L	L	L	L	L	L		G*	N	N	N	N	N		N	G	G	G	G	G
MYCN	2	N	N	N	N	N	N		G*	G	G	G*	G*	G*		N	L*	L*	N	N	N
SOX2	3	N	N	N	N	N	N		G*	G	G	G	G	G		G*	N	N	N	N	L
FGFR3	4	N	N	N	N	N	N		N	N	N	N	N	N		L*	L	L	L	L	L
PDGFRA	4	N	N	N	N	N	N		N	N	N	N	N	N		L*	L	L	L	L	L
EGFR	7	G	G	G	G	G	G		G*	G	G	G	G	G		G	G	G	G	N	N
CDK6	7	G	G	G	G	G	G		G	G	G	G	G	G		G	G	G	G	N	N
MET	7	G	G	G	G	G	G		G	G	G	G	G	G		G	G	G	G	N	N
MYC	8	N	N	N	N	N	N		G*	N	N	N	N	N		N	N	N	N	N	N
CCND2	12	N	N	N	N	N	N		G	N	N	N	N	N		L	L	L	L	L	L
CDK4	12	N	N	N	N	N	N		G	N	N	N	N	N		L	L	L	L	L	L
MDM2	12	N	N	N	N	N	N		G	N	N	N	N	N		L	L	L	L	L	L
IRS2	13	N	N	N	N	N	N		N	N	N	N	N	N		N	N	L*	L*	N	N
AKT1	14	L	L	L	L	L	L		G	N	N	N	N	N		N	N	N	N	N	N
HYDIN	16	N	N	N	N	N	N		N	N	N	N	N	N		N	N	N	N	N	N
GRB2	17	N	N	N	N	N	N		G	G	G	G*	G*	G*		N	L	L	L	L	L
CCNE1	19	N	N	N	N	N	N		N	N	N	N	N	N		N	N	N	N	N	N
Losses																					
1p36.31	1	N	N	N	N	N	N		N	N	N	N	N	N		N	G	G	G	G	G
1p36.23	1	N	N	N	N	N	N		N	N	N	N	N	N		N	G	G	G	G	G
CDKN2C	1	N	N	N	N	N	N		G	N	N	N	N	N		N	N	N	N	N	N
LSAMP	3	HL	HL	HL	HL	HL	HL		G	G	G	G*	G*	G*		G*	N	N	N	N	L
3q29	3	N	N	N	N	N	N		G	G	G	G*	G*	G*		G*	N	N	N	N	L

4q35.1	4	L	L	L	L	L	L		N	N	N	N	N	N		L*	L	L	L	L	L
QKI	6	N	N	N	N	N	N		N	N	N	L*	L*	L*		N	N	N	N	N	N
CDKN2A/B	9	HL	HL	HL	HL	HL	HL		HL	HL	HL	HL	HL	HL		HL	HL	HL	HL	HL	HL
PTEN	10	L	L	L	L	L	L		L*	L*	L*	L*	L*	L*		L	L	L	L	L	L
10q26.3	10	L	L	L	L	L	L		N	N	N	L*	L*	L*		L	L	L	L	L	L
12p13.1	12	L	L	L	L	L	L		G	N	N	N	N	N		N	N	N	N	N	N
RB1	13	N	N	N	N	N	N		N	N	N	N	N	N		N	N	L*	L*	N	N
13q22.1	13	N	N	N	N	N	N		N	N	N	N	N	N		N	N	L*	L*	N	N
NPAS3	14	L	L	L	L	L	L		G*	N	N	N	N	N		L	L	L	L	L	L
15q14	15	N	N	N	N	N	N		N	N	N	L*	L*	L*		G*	G*	G*	N	N	N
16p12.1	16	N	N	N	N	N	N		N	N	N	N	N	N		N	N	N	N	N	N
TP53	17	L	L	L	L	L	L		N	N	N	N	N	N		N	L*	L*	L*	L*	L*
NF1	18	HL	HL	HL	HL	HL	HL		G	G	G	G*	G*	G*		N	N	N	N	N	N
19q13.33	19	N	N	N	N	N	N		L	L	L	L	L	L		N	N	N	N	N	N
22q13.32	22	L	L	L	L	L	L		N	N	N	N	N	N		G*	L	L	L	L	L

“The use of peripheral extracellular vesicles for identification of molecular biomarkers in a solid tumor mouse model”

En el anterior trabajo de esta tesis, hemos podido comprobar la gran heterogeneidad que presentan los pacientes diagnosticados con glioblastoma, ya que su perfil genético además de variar entre pacientes, evoluciona a lo largo del tiempo, lo que impide que las terapias actuales sean efectivas.

Por tanto, es importante desarrollar técnicas que permitan evaluar la evolución de dichos tumores, a tiempo real, a lo largo del curso de la enfermedad. En este sentido, la identificación de biomarcadores a partir de biopsia líquida cumpliría perfectamente los requerimientos de esta nueva aproximación. Dentro de los diferentes compartimentos, en los que se pueden aislar e identificar biomarcadores en sangre periférica, una de las posibilidades de biopsia líquida más prometedoras, son las VEs, las cuales transportan el contenido genético de las células tumorales productoras protegido mediante una membrana vesicular. Sin embargo, no se conoce demasiado acerca de los procesos de biogénesis, ni de los mecanismos de captación de material genético dentro de estas VEs. Así como se desconoce su capacidad para atravesar la BBB, incluso en los casos en que ésta se encuentra intacta y llegar al torrente sanguíneo. Así pues, para profundizar más en la biología de formación de estas VEs y de su potencial utilización como fuente de biomarcadores moleculares, necesitábamos crear modelos animales que reprodujeran algunas de las características de los gliomas humanos e implementar las técnicas de aislamiento de VEs a partir de sangre periférica.

En este contexto, en nuestro laboratorio hemos creado varios modelos animales de tumores cerebrales gliales, en ratones inmunodeprimidos (nude) xenotrasplantados con CIT aisladas de GBM humano. En estos modelos, somos capaces de detectar VEs que provienen del tumor de una forma indirecta, mediante el análisis de secuencias de ADN.

The use of peripheral extracellular vesicles for identification of molecular biomarkers in a solid tumor mouse model

Noemí García-Romero[1,2*], Gorjana Rackov[1,2*], Cristobal Belda-Iniesta[2], Angel Ayuso-Sacido[1,2,3].

[1] Instituto Madrileño de Estudios Avanzados, IMDEA Nanociencia, Madrid, Spain.

[2] Fundación de Investigación HM Hospitales, Hospital de Madrid Group, Madrid, Spain.

[3] Instituto de Medicina Molecular Aplicada (IMMA), School of Medicine, San Pablo-CEU University, Campus de Montepríncipe, Madrid Spain.

* These authors contributed equally to this work.

Abstract

Extracellular vesicles (EVs) have been increasingly recognized as a potential source of disease biomarkers, since they contain a multitude of biologically active protein, DNA and RNA species, and they can be retrieved from circulating blood of patients. Here, we describe a protocol for DNA extraction from exosomes, shedding microvesicles and apoptotic bodies isolated from peripheral blood in a mouse xenograft model of solid tumor. In this model, human DNA isolated from tumor-derived EVs can be readiliy distinguished from the one of the host, which is of particular interest for studies aimed at molecular characterization of tumor biomarkers.

Key words

extracellular vesicles, glioblastoma, xenograft, biomarkers, peripheral blood

1. Introduction

Historically, the release of cellular material encapsulated in membrane vesicles was considered as a way of discarding harmful molecules or useless signaling mediators, as exemplified by the transferrin receptor removal during erythropoiesis [1, 2]. Recent data, nonetheless, suggest that these extracellular vesicles (EVs) are more than mere "molecular trash". Rather, they are now considered as units of information, which play important roles in medium and long-range intercellular communication. EV cargo contains a multitude of bioactive molecules such as lipids, nucleic acids (DNA, mRNA, miRNA) and cellular proteins, including oncogenes and active oncoproteins originating from malignant cells [3]. Moreover, EVs can be isolated from diverse body fluids: blood, urine, saliva, bronchoalveolar fluid, amniotic fluid, breast milk, semen, cerebrospinal fluid and bile [4, 5], thereby offering a unique source of disease-related biomarkers.

Molecular characterization of malignant cells is of great importance for disease diagnosis and prediction of its progress, as well as for evaluation of therapy effectiveness. However, cancer cells can only be accessed through invasive procedures such as biopsy or surgical removal of tumor tissue, which complicates frequent or long-term monitoring of molecular markers of tumor progression. In addition, tumors are often composed of heterogeneous cell populations such that different regions of tumor mass are bearing different oncogenic mutations, hence the biopsy may fail to provide representative molecular profile. To bypass these obstacles, EVs isolated from peripheral blood can be analyzed for the presence of tumor-associated biomarkers, such as mutated DNA, mRNA or proteins. Here, we describe a method to isolate EVs

from peripheral blood and detect tumor-associated biomarkers in a mouse model xenotransplanted with human glioma cancer stem cells (CSCs) (Fig. 1). Of interest, cargo present in EVs derived from human tumor cells can be readily distinguished from those of the host, which makes this model suitable for studying tumor-associated biomarkers present within EVs in other types of xenograft models as well.

2. Materials

2.1 Cancer Stem Cell (CSCs) isolation from solid tumor and culture

All materials and solutions coming in contact with the cells must be sterile, and proper sterile procedures should be employed.

1. Scalpels (immerse in 70% ethanol).
2. 100 × 15-mm petri dishes (BD Falcon).
3. Glass Pasteur pipettes.
4. Hank's Balanced Salt Solution (HBSS), with or without calcium and magnesium.
5. PIPES Buffer.
6. L-Cysteine/EDTA solution. Preparation: In 500ml water (MilliQ), dissolve 2.04 g EDTA (55mM final concentration) and 4.829 g L-Cysteine hydrochloride (14mM final concentration); sterilize using 0.22-µm filter.
7. Papain solution (10 mg/ml).
8. Solution for enzymatic digestion: mix 3.1 ml Pipes Buffer, 1.4 ml Papain (10 mg/ml) and 0.5ml L-Cystein/EDTA solution. Heat to 37ºC.
9. DNaseI.
10. Defined Proliferative Medium: Dulbecco's modified Eagle's medium/F12 (DMEM/F-12) supplemented with non-essential amino acids (10mM), HEPES (1M), D-glucose (45%), bovine serum albumin (BSA)-fraction V (7,5%), sodium pyruvate (100mM), L-Glutamine (200mM), antibiotic/antimycotic (100x), N_2 supplement (100x), hydrocortisone (1µg/µl), triiodothyronine (100µg/ml), epidermal growth factor (EGF) (25ng/µl), basic fibroblast growth factor (bFGF) (25ng/µl) and heparin (1µg/µl).
11. Fetal Bovine Serum (FBS).

2.2 Xenograft model

1. 9-week-old athymic nude mice of approximately 20 g weight (Charles River).
2. Hemocytometer.
3. Isofluorane anesthesia (3,5% in 70% N_2O: 30% O_2).
4. Stereotaxic frame (Stoelting).
5. Ophthalmic ointment.
6. 70% ethanol, H_2O_2, betadine, and surgical sterile instruments.
7. PBS (Phosphate Buffered Saline).
8. High-speed micro drill.
9. Hamilton syringe.
10. 1 cc syringe.
11. 21 and 22 gauge needles.
12. Manual or programmable Syringe Pump.
13. Surgical glue (Histoacryl®).
14. Matrigel™ Basement Membrane Matrix.
15. Caliper to measure tumor dimension.

2.3 Peripheral blood isolation

1. Surgical platform.
2. Surgical scissors.
3. 1.5 ml microcentrifuge tubes.
4. 1 cc syringe.
5. 23 gauge needles.

6. 70% ethanol.

7. Benchtop centrifuge.

2.4 Extracellular vesicles isolation

1. PBS (Phosphate Buffered Saline).

2. Polycarbonate or polyallomer tube.

3. Ultracentrifuge and swinging-bucket rotor.

3. Methods

3.1 CSCs isolation from solid tumor and cell culture

Cancer stem cell (CSC) hypothesis postulates that a subpopulation of tumor cells is responsible for tumor initiation, invasive growth and metastasis formation. These cells possess the capacity of self-renewal and they generate heterogeneous cancer cell lineages within tumor. In most cases, existing therapies do not eradicate CSCs, which remain quiescent and retain the ability to regenerate tumor. There are several methods for CSC identification and isolation: a) assessment of their ability to grow as floating spheres in serum-free medium, b) fluorescence-activated cell sorting (FACS) according to CSC-specific cell surface markers, c) detection of side population phenotype by Hoechst 33342 exclusion, and d) aldehyde dehydrogenase (ALDH) activity assay (Fig. 2).

1. Wash biopsy specimens in HBSS with Ca^{2+} and Mg^{2+}.
2. Remove necrotic areas and mechanically dissociate the tissue using two scalpels in a Petri Dish (*see* **Note 1**).
3. Add four volumes of HBSS without Ca^{2+} and Mg^{2+} and transfer to a 15-ml tube.
4. Wait 2 minutes or until the precipitate has settled, and remove the supernatant.
5. Repeat steps 3 and 4 one more time.
6. Add one volume of Pipes Buffer, resuspend gently and spin 15 sec at 1500 rpm.
7. Remove the supernatant and resuspend the pellet in 2.5 ml of the solution for enzymatic digestion.
8. Add 10 U/ml of DNAseI and incubate at 37°C for 30 min with rotation.
9. Centrifuge 5 min at 1500 rpm at RT and aspirate the supernatant.

10. Prepare three Pasteur pipettes with decreasing diameters of fire-polished tips.
11. To dissociate into single cells, gently pipette the sample starting with the pipette of the largest diameter, and then switch to the other two pipettes of decreasing diameter. Pipette slowly up and down 10 times with each pipette.
12. Resuspend the cells in 9 ml of Defined Proliferative Media and filter through 70-µm cell strainer.
13. To inactivate papain activity, add 500 µl of FBS.
14. Centrifuge at RT 10 min at 1500 rpm and discard supernatant.
15. Add 10 ml of Defined Proliferative Media and repeat previous step.
16. Resuspend the cells in 4,5 ml of Defined Proliferative Media and plate 1,5 ml per well in a 6-well tissue culture plate.
17. Incubate the cells in a humidified 37 °C, 5% O_2 and 5% CO_2 incubator. Change the medium every 3 days.

3.2 Xenograft model

3.2.1 Orthotopic model (brain location)

1. Immediately prior to implantation, disaggregate the cells and resuspend 10^5 cells in Defined Proliferative Media (*see* **Note 2**).
2. Position the isofluorane-anasthetized mice in a stereotaxic frame with a mouth holder (*see* **Note 3**).
3. Apply ophthalmic ointment to the mice eyes to keep the moist.
4. Make a midline incision overlying the top of the skull (Fig. 3).
5. Clean the area with H_20_2 swabs to remove the meninges.

6. Mark the position of the injection site: the striatum of the right brain hemisphere (0 mm anterior and 2.5 mm lateral to the bregma; 3.5 mm intraparenchymal).
7. Drill a burr-hole at this point through the skull without breaking the dura.
8. Clean the area with betadine solution.
9. Inject 5 µl of CSC suspension into the hole with a Hamilton syringe (22 G needle) over 5 min (*see* **Note 4**).
10. Withdraw the needle after 5 min to avoid misplacing the cells.
11. Close the wound with surgical glue (*see* **Note 5**).
12. Return the mouse to its cage after it recovers from anesthesia (*see* **Note 6**).

3.2.2 Heterotopic model (flanks location)

1. Disaggregate the cells by gentle mixing, resuspend 2-3 x10^6 cells in 1:1 Defined Proliferative media and Matrigel (*see* **Note 7**) and place on ice.
2. Inject 250 µl of the mixture into the subcutaneous space in the mice flank, using a 1 cc syringe with 21 G needle. (*see* **Note 8**)
3. Tumor volumes need to be measured with a caliper at least twice a week.

3.3 Peripheral blood collection

1. Observe mice once or twice per week for tumor growth and symptoms. Blood should be collected after approximately 12 weeks in orthotopic and 4 weeks in heterotopic model (*see* **Note 9**).
2. This procedure requires general anesthesia and posterior animal sacrifice.

3. Place the mouse ventral side up at the working platform, disinfect the abdomen with 70% ethanol and make a ventral midline incision (2cm) with surgical scissors.
4. Remove the skin aside to expose the abdominal cavity.
5. Find the inferior vena cava, which is located between the kidneys, lying laterally on the right side of abdominal aorta.
6. Use a 1cc syringe with a 23 G needle and introduce carefully into the vein. Apply suction and wait until blood appears in the syringe (*see* **Note 10**). Repeat until blood flow ceases (up to 1 ml can be obtained) (*see* **Note 11**).
7. Centrifuge 10 min at 1500 × *g* to obtain plasma (*see* **Note 12**). Store plasma at -80°C or continue with the protocol.

3.4 Isolation of extracellular vesicles

Extracellular vesicles (EVs) are categorized into three main classes: 1) shedding microvesicles (derived by outward budding of plasma membrane), 2) exosomes (derived by inward budding of endosomal membrane), and 3) apoptotic bodies (originating from apoptotic blebs during apoptosis) [6]. All three types of EVs contain DNA, which can be used for biomarker detection. Recently, several methods for isolation and purification of EVs have been developed, including antibody-coated beads (Exosome-Streptavidine for Isolation/Detection from Invitrogen, ExoPureimmunobeadsTM from BioVison), microfluidic devices, precipitation techologies (total exosome isolation from Invitrogen, ExoQuickTM from SystemBiosciences, miRCURYTM from EXIQON, ExoPureTMReagent from BioVision), or filtration technologies. Most of these platforms are optimized for

exosome isolation, they are not suitable for isolation of large amounts of EVs and captured EVs may not retain functionality after elution from the beads [7]. Here, we describe differential centrifugation protocol, which is the gold standard for EV isolation and purification. This protocol involves several centrifugation and ultracentrifugation steps, although it may lead to inconsistencies in recovery of EVs because of different biofluid viscosity.

1. Centrifuge plasma samples 5 min at 1200 × *g* to remove cellular debris (*see* **Note 13**).
2. Transfer the supernatant to a specific centrifuge tube (*see* **Note 14**) and centrifuge for 20 min at 8000 × *g*.
3. Transfer the supernatant to a new tube and resuspend the pellet in PBS to obtain apoptotic bodies (*see* **Note 15**).
4. Centrifuge this supernatant 20 min at 25000 × *g*. Transfer the supernatant to a new tube and resuspend the pellet in PBS to obtain shedding microvesicles.
5. Ultra-centrifuge the remaining supernatant 90 min at 117000 × *g* to obtain exosomes.
6. Repeat the ultracentrifugation step and store the EV samples at -20°C until use or continue with the protocol (*see* **Note 16**).

3.5 gDNA biomarkers

1. Treat EV samples with DNase I (54 Kunitz/ml) for 30 min at 37°C to remove DNA contamination.
2. Perform Polymerase Chain Reaction (PCR) of a housekeeping gene to ensure DNaseI activity and analyze PCR products on 1,8 % agarose gel (*see* **Note 17**).

3. Extract DNA from each EVs fraction using a DNeasy Blood and Tissue Kit (Qiagen) using manufacturer's recommendations.

4. Detect gene mutations, minority alleles, point mutations, small deletions or amplifications, and fusion genes with clinical or biological value.

4. Notes

1. Fresh human tissue must be processed within 12 h after extraction.
2. Volume and cell concentration can be adjusted depending on the assay.
3. All animal experiments must be approved by and performed according to the guidelines of the Institutional Animal Care Committee.
4. Clean the syringe with 70% ethanol, MilliQ H_20 and PBS before and after its use, by drawing up multiple times.
5. Instead of surgical glue, sterile silk sutures could be used.
6. Mice should be placed in an electric blanket to recover from anesthesia in order to maintain corporal temperature.
7. All experiments with Matrigel need to be carried out at 4 °C, since it solidifies at room temperature and at -20 °C. Matrigel should be thawed out in ice or at 4 °C overnight. Matrigel that has solidified cannot be re-used. Syringes and material that contacts the Matrigel must be kept cold. When pipetting Matrigel, do not make any bubbles.
8. Anesthesia is recommended but not required for this procedure; its application facilitates the experiment and minimizes stress in mice.
9. Tumor growth depends on multiple factors such as origin of CSCs, animal model of choice, growth factors, etc.
10. If blood stops flowing, rotate the needle and pull it out lightly.
11. In case that vein collapses, an alternative assay can be performed, such as cardiac puncture [8].

12. There is no consensus regarding to the choice between serum and plasma [9], although some authors have postulated that more EVs can be recovered from serum than plasma [10].

13. All steps must be performed in a laminar flow cell culture hood and all centrifugations must be performed at 4 °C. *g*-force data are estimated for an Optima-LE 90K ultracentrifuge, 50.2 Ti rotor, Beckman Coulter. To convert *g* force to RPM, the following formula should be used: Relative Centrifuge Force (RCF) or *g*-force = 1.12 x R x $(RPM/1000)^2$. R-rotor radius (mm), RPM-revolutions per minute.

14. Polycarbonate or pollyallomer sterile tubes are needed depending of the ultracentrifuge rotor used.

15. Volume of PBS to resuspend the pellet depends on the starting volume and EVs concentration.

16. It is desirable to store in small aliquots, since one freeze and thaw cycle reduces the number of EVs up to 15% [11].

17. No amplification products should be detected in agarose gel. If so, repeat DNaseI treatment, to remove DNA contamination.

Figure legends

Fig. 1. Schematic view of the glioblastoma xenograft model and isolation of peripheral blood EVs by differential centrifugation.

Fig. 2 Approaches for CSC identification and isolation. (**a**) CSCs form clonal spheres when plated in soft agar. (**b**) CSCs express cell-specific markers that distinguish them from non-CSC populations. (**c**) Side population analysis by FACS. The Hoechst 33342 dye is measured at two wavelengths for detection of Hoechst blue and red fluorescence. (**d**) To determine ALDH activity, cells are stained with fluorescent ALDH substrate and analyzed by flow cytometry. CSCs are characterized by low side scatter and high ALDH activity.

Fig. 3 An anesthetized mouse positioned in a stereotaxic frame with a midline incision at the top of the skull. Meninges are removed by cleaning the area with swabs soaked in H_20_2.

Acknowledgment

This work was supported in part by grants from Health Research Fund (Fondo de Investigaciones Sanitarias, FIS), Carlos III Health Institute (PI10/01069, CP11/00147, and PI14/00077), Plan Estatal I + D + I 2013–2016, and Ministerio de Economía y competitividad (RTC-2015-3846-1) (AAS). The funders had no role in study design, data collection and analysis, decision to publish, or preparation of the manuscript.

References

1. Harding C, Heuser J, Stahl P (1983) Receptor-mediated endocytosis of transferrin and recycling of the transferrin receptor in rat reticulocytes. J Cell Biol 97:329–339
2. Pan BT, Teng K, Wu C, et al (1985) Electron microscopic evidence for externalization of the transferrin receptor in vesicular form in sheep reticulocytes. J Cell Biol 101:942–948
3. Al-Nedawi K, Meehan B, Rak J (2009) Microvesicles: Messengers and mediators of tumor progression. Cell Cycle 8:2014–2018
4. Chaput N, Théry C (2010) Exosomes: immune properties and potential clinical implementations. Semin Immunopathol 1–22
5. Raposo G, Stoorvogel W (2013) Extracellular vesicles: Exosomes, microvesicles, and friends. J Cell Biol 200:373–383
6. Borges FT, Reis L a, Schor N (2013) Extracellular vesicles: structure, function, and potential clinical uses in renal diseases. Braz J Med Biol Res 46:824–30
7. Momen-Heravi F, Balaj L, Alian S, et al (2013) Current methods for the isolation of extracellular vesicles. Biol Chem 394:1253–1262
8. Doeing DC, Borowicz JL, Crockett ET (2003) Gender dimorphism in differential peripheral blood leukocyte counts in mice using cardiac, tail, foot, and saphenous vein puncture methods. BMC Clin Pathol 3:3
9. Witwer KW, Buzás EI, Bemis LT, et al (2013) Standardization of sample collection, isolation and analysis methods in extracellular vesicle research. J Extracell vesicles 2:1–25
10. James GN, Thoi LL, McManus LM, Reimann TA (1982) Isolation of human platelet membrane microparticles from plasma and serum. Blood 60:834–841.
11. Jayachandran M, Miller VM, Heit J a., Owen WG (2012) Methodology for isolation, identification and characterization of microvesicles in peripheral blood. J Immunol Methods 375:207–214

Figures

Fig. 1 Schematic view of the glioblastoma xenograft model and isolation of peripheral blood EVs by differential centrifugation.

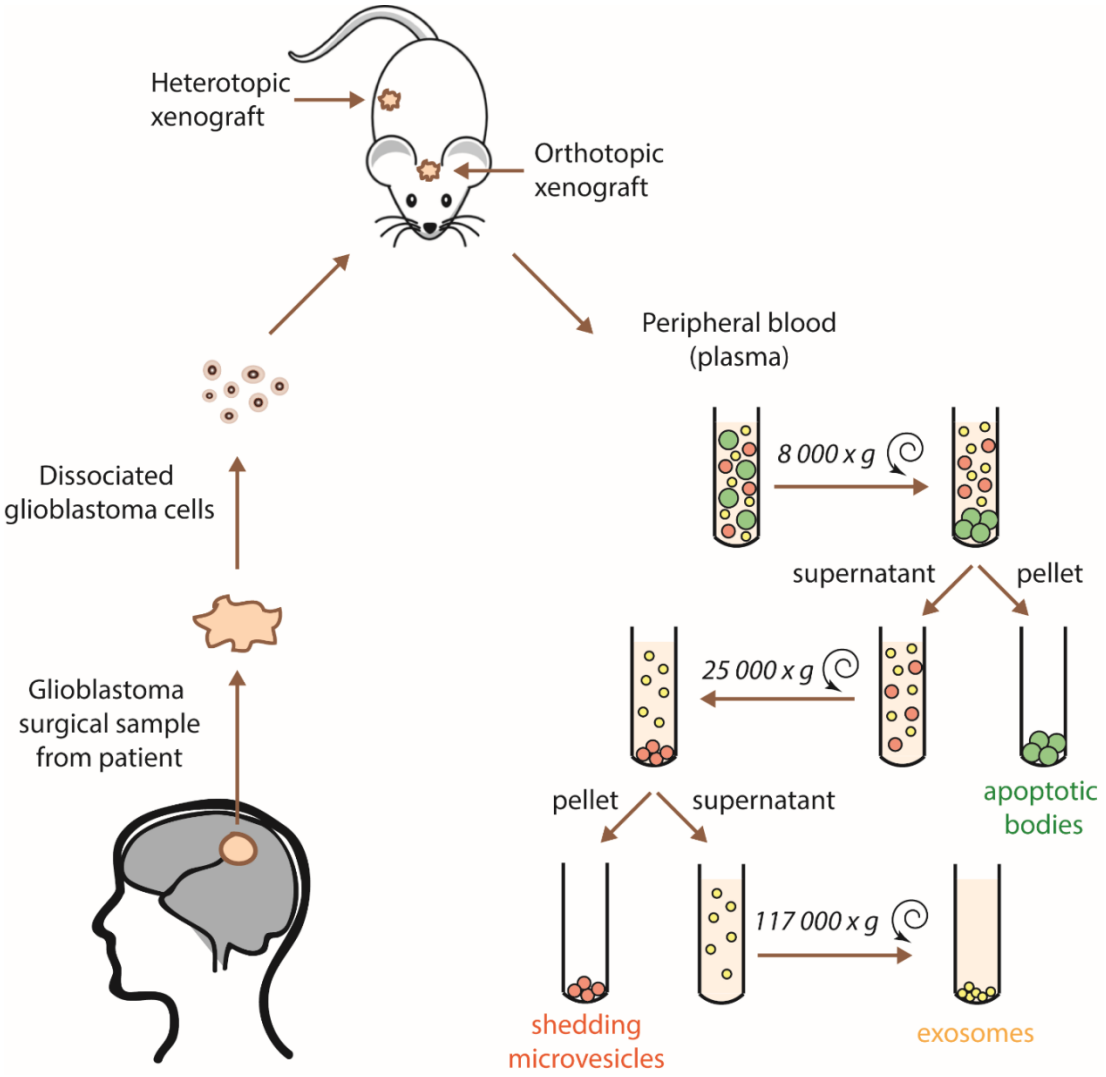

Fig. 2 Approaches for CSC identification and isolation.

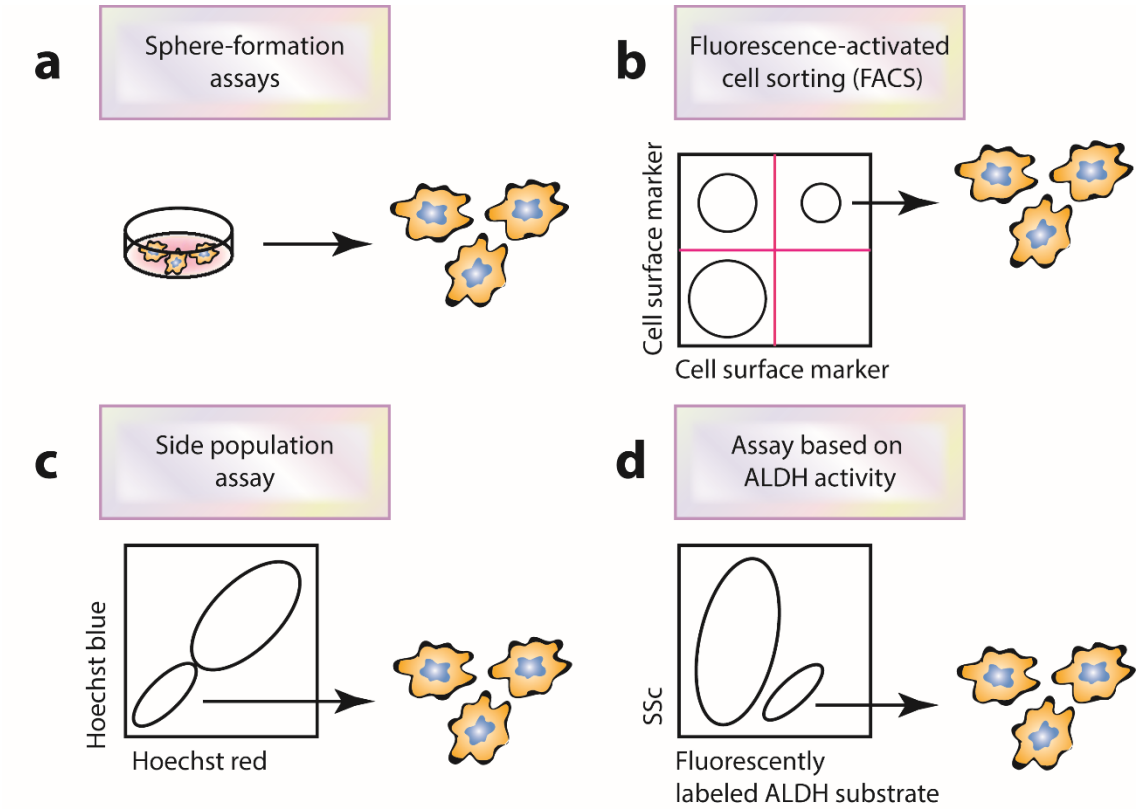

Fig. 3 An anesthetized mouse positioned in a stereotaxic frame with a midline incision at the top of the skull.

“DNA sequences within glioma-derived extracellular vesicles can cross the intact Blood-Brain Barrier and be detected in peripheral blood of patients ”

Con el fin de poder utilizar el contenido de las VEs como fuente de biomarcadores en el contexto de tumores gliales, lo primero que necesitábamos saber es si estas VEs eran capaces de atravesar la BHE incluso si ésta se encontraba intacta, como ocurre en la mayoría de gliomas de bajo grado. Para ello, precisábamos de CIT que reprodujeran tumores cerebrales gliales con la BHE intacta. Con este fin, utilizamos las líneas GBM27 y GBM38 que presentaban un patrón de crecimiento *in vivo* infiltrativo y nodular respectivamente.

Por lo que, tras validar nuestros modelos animales, escogimos el modelo de crecimiento difuso, que además presentaba una BHE intacta, para los siguientes ensayos. En este modelo, hemos sido capaces de encontrar todos los tipos de VEs procedentes del tumor (cuerpos apoptóticos, vesículas de shedding y exosomas) en el torrente sanguíneo del ratón, de forma indirecta, en base a la presencia de secuencias de ADN humano. Demostrando por primera vez, que las VEs son capaces de atravesar la BHE intacta. Una vez comprobado esto, nos preguntamos si estos resultados serían reproducibles en humanos. Para ello nos centramos en la secuencia del gen *IDH1*, que aparece mutado en un alto porcentaje de gliomas de bajo grado y, en menor medida, en gliomas de alto grado. Y analizamos muestras de tejido tumoral y sangre periférica de una cohorte de 21 pacientes, 20 de los cuales fueron diagnosticados con tumores gliales de distinto grado. En dicha cohorte, hemos identificado secuencias de *IDH1* mutadas a partir de VEs aisladas de sangre periférica de pacientes con gliomas de bajo grado y BHE intacta, en un porcentaje similar al obtenido analizando el tejido tumoral. Además, hemos identificado la misma secuencia de *IDH1* mutado en el 40% de gliomas de alto grado, incluidos aquellos en los que la muestra de tejido tumoral también había dado positivo. Para llevar a cabo la identificación de secuencias de *IDH1* mutado en VEs aisladas de sangre periférica, se implementó además un nuevo procedimiento que actualmente está protegido bajo patente.

DNA sequences within glioma-derived extracellular vesicles can cross the intact Blood-Brain Barrier and be detected in peripheral blood of patients

Noemí García-Romero[1,2,*], Josefa Carrión-Navarro[1,3,*], Susana Esteban-Rubio[1,3,*]Elisa Lázaro-Ibáñez[4], María Peris-Celda[5], Marta M. Alonso[6], Juan Guzmán-DeVilloria[7], Carlos Fernández-Carballal[8], Ana Ortiz de Mendivil[1], Sara García-Duque[1], Carmen Escobedo-Lucea[4], Ricardo Prat-Acín[9], Cristóbal Belda-Iniesta[1,3], Angel Ayuso-Sacido[1,2,3]

[1] Fundación de Investigación HM Hospitales, HM Hospitales, Madrid, Spain
[2] IMDEA Nanoscience, Madrid, Spain
[3] Facultad de Medicina (IMMA), Universidad San Pablo-CEU, Madrid, Spain
[4] Division of Pharmaceutical Biosciences, Faculty of Pharmacy, University of Helsinki, Helsinki, Finland
[5] Department of Neurological Surgery, University of Pittsburgh School of Medicine, Pittsburgh, PA, USA
[6] Clínica Universidad de Navarra, CIMA, Pamplona, Spain
[7] Servicio de Radiodiagnóstico, Hospital General Universitario Gregorio Marañón, Madrid, Spain
[8] Servicio de Neurocirugía, Hospital General Universitario Gregorio Marañón, Madrid, Spain
[9] Departamento de Neurocirugía, Hospital Universitario la Fe, Valencia, Spain
[*] These authors have contributed equally to this work

Correspondence to: *Angel Ayuso-Sacido,* ***email:*** *ayusosacido@gmail.com*

Keywords: *extracellular vesicles, brain tumors, blood-brain barrier, biomarkers*

Received: *September 20, 2016* ***Accepted:*** *November 07, 2016* ***Published:*** *November 26, 2016*

ABSTRACT

Tumor-cell-secreted extracellular vesicles (EVs) can cross the disrupted blood-brain barrier (BBB) into the bloodstream. However, in certain gliomas, the BBB remains intact, which might limit EVs release. To evaluate the ability of tumor-derived EVs to cross the BBB, we used an orthotopic xenotransplant mouse model of human glioma-cancer stem cells featuring an intact BBB. We demonstrated that all types of tumor cells-derived EVs– apoptotic bodies, shedding microvesicles and exosomes – cross the intact BBB and can be detected in the peripheral blood, which provides a minimally invasive method for their detection compared to liquid biopsies obtained from cerebrospinal fluid (CSF). Furthermore, these EVs can be readily distinguished from total murine EVs, since they carry human-specific DNA sequences relevant for GBM biology. In a small cohort of glioma patients, we finally demonstrated that peripheral blood EVs cargo can be successfully used to detect the presence of $IDH1^{G395A}$, an essential biomarker in the current management of human glioma

INTRODUCTION

Primary malignant brain tumors account for 3% of adult cancer deaths and are the second cause of tumoral mortality in children [1]. High-grade gliomas are the most common primary malignant brain tumors in adults. Despite advances in treatment, the median patient survival rate is 12 to 15 months, as tumor eventually recurs in all patients [2].

Gliomas are commonly detected through clinical assessment and imaging techniques. However, the final diagnosis relies on the histological analysis of the biopsy tissue, in accordance with the WHO current standard for glioma diagnostic. Recently published molecular pathology-based glioma classification drastically improved tumor diagnostics and prognostics, essentially through the detection of the $IDH1^{R132H}$ mutation [3, 4].

With the current treatment protocol, tissue specimens are suitable for the evaluation of tumor histopathology at the very beginning of the disease, but they do not allow molecular evolution assessment of the tumor along the course of the disease, which is critical for improving patient survival [5]. Thus, the last few years have seen a marked increase in using liquid biopsies for monitoring cancer genetics, by analyzing circulating cells, nucleic acids, or extracellular vesicles (EVs) released from tumors [6]. The EVs are present in readily accessible biofluids [7–9] and they carry lipids [10], proteins [11], and distinct species of nucleic acids [12–14] originating from donor cells. According to the Vesiclepedia nomenclature [15], three types of EVs can be distinguished: apoptotic bodies (ABs), shedding microvesicles (SMVs), and exosomes (EXOs). All of these EVs might be useful to identify the tumor molecular profile at any time, using minimally invasive procedures.

The amount and proportion of these circulating tumor-derived EVs might be determined by the integrity of the BBB, as well as the tumor size and distribution. Recent studies have demonstrated that EXOs administered intranasally [16] or injected through the tail vein in mice [17] can cross the BBB and deliver their cargo within the parenchymal brain, but the barrier's integrity was not discussed in these studies. Therefore, it remains unknown wheter EVs of glioma cells can cross an intact BBB into blood vessels.

Tumoral mutated sequences have been recently detected in circulating DNA (ctDNA) and EVs extracted from cerebrospinal fluid (CSF) [18, 19]. However, CSF extraction through lumbar puncture is an invasive procedure and not recommended in patients with high intracraneal pressure (commonly present in brain tumors). In addition, bearing this in mind, additional efforts to develop a blood-based liquid biopsy method for GBM patients are required.

To investigate the ability of tumor-derived EVs to cross an intact BBB, we used an orthotopic xenotransplant model of human cancer stem cells (hCSCs), previously described and characterized in our laboratory, which produces a disseminated braintumor phenotype featuring an intact BBB [20]. Using this model, we showed that all three types of EVs derived from human brain tumor cells can cross the undisrupted BBB and reach the bloodstream. These EVs carried human genomic-DNA (gDNA) sequences corresponding to those of the xenotransplanted cells, and could be isolated and enriched from peripheral blood (Figure 1). In a cohort of glioma patients with undisrupted BBB, we demonstrated that peripheral blood EV cargo can be successfully used to detect

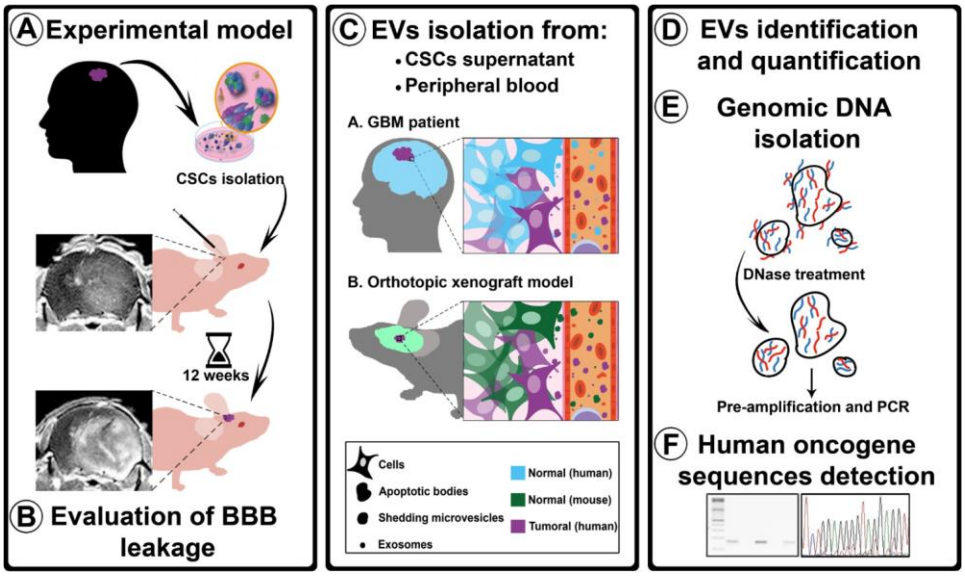

Figure 1: Experimental procedure flowchart. A. Isolated hCSCs from 2 GBM patients were xenotransplanted in athymic mice. After 12 weeks, the animals were transcardially perfused. **B.** BBB permeability was evaluated using three assays: MRI, Evans Blue staining, and albumin extravasation. **C.** EVs (ABs, SMVs, and EXOs) were isolated from hCSCs-enriched culture supernatants and from mouse peripheral blood. **D.** EVs were identified using TEM, tracking analysis, and CD63 tetraspanin quantification. **E.** To ensure that the analyzed DNA was confined within the EVs, supernatants and plasma were treated with DNase before gDNA isolation; after the isolation, gDNA was pre-amplified before performing PCR analysis with human-specific primers. **F.** Sequences detected were sequenced to confirm their human origin.

the presence of specific mutations, such as IDH1^{G395A}. This finding provides evidence that liquid biopsies can successfully improve the current management of brain tumors.

RESULTS

GBM xenograft model with intact BBB

Our first aim was to evaluate the capacity of EVs secreted by glioma cells to cross normal BBB into the bloodstream. For this purpose, we used an orthotopic xenotransplant model of hCSCs culture (GBM27), which developed an infiltrative brain-tumor phenotype featuring an intact BBB in nude mice. We compared this model to a second orthotopic xenotransplant model of hCSCs culture (GBM38) that generated a nodular brain tumor featuring a disrupted BBB in nude mice.

(Supplementary Figure S1). We performed stereotactic transplants of 1 × 105 cells from GBM27 and GBM38 into the striatum of mice. Twelve weeks later we evaluated the functional competence of the BBB through 3 distinct procedures (Supplementary and Figure S2).

First, we evaluated the BBB integrity in the xenotransplant models GBM27 and GBM38 as well as in control mice (Figure 2A and Supplementary Figure S2A) with MRI images. On GBM38 xenograft tumor, we observed an enhancement in T1-weighted images with Gadolinium-based contrast agent, a sensitive marker of blood-brain barrier disruption (Gd-DTPA-BMA; Omniscan, Amersham Health, Oslo, Norway). Conversely, no enhancement of Gd-DTPA was observed on the GBM27 tumor suggesting an intact BBB. Control mice showed no MRI abnormalities

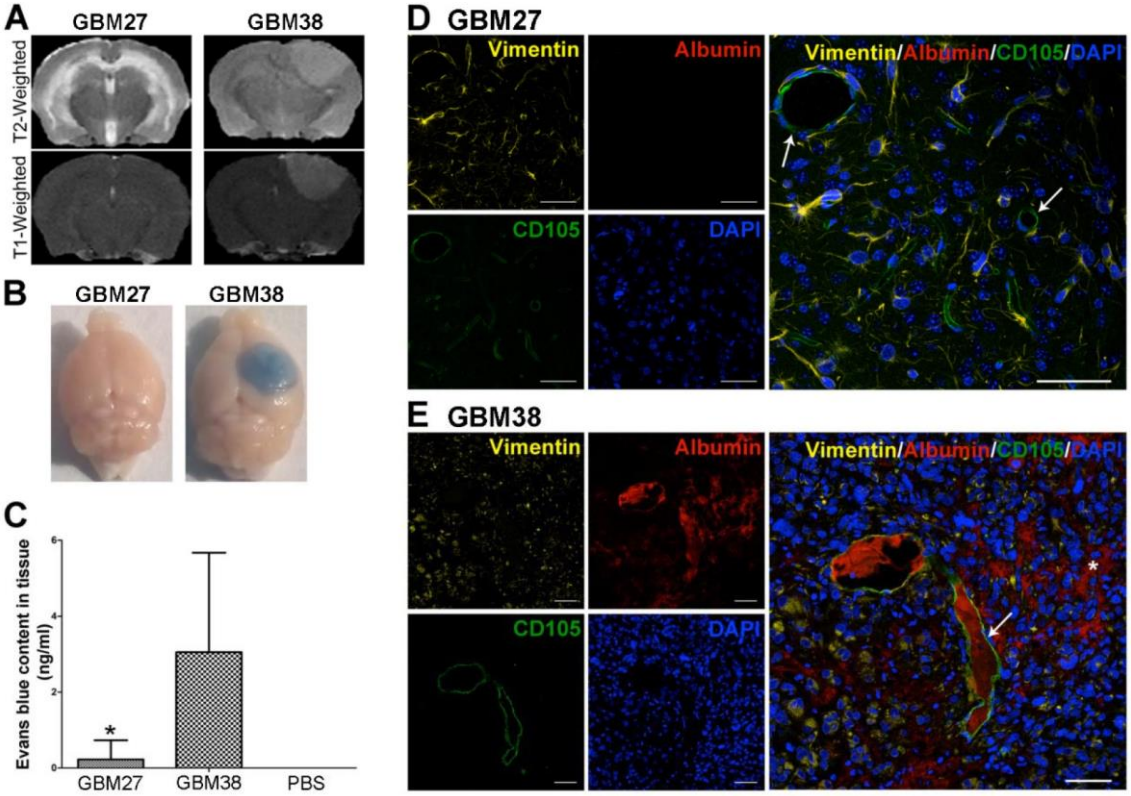

Figure 2: Evaluation of BBB leakage in two GBM models: GBM27 presents an intact BBB. A. Representative T2- and T1weighted images of GBM27 and GBM38. The GBM27 tumor xenotransplant T2-weighted image depicts diffuse hyperintense infiltrative involvement. GBM38 xenograft tumor showed well-defined borders. T2-weighted images revealed a hyperintense mass compressing ventricular structures. GBM27 features an intact BBB, as revealed by the lack of any contrast enhancement. GBM38 shows a homogeneous enhancement, suggesting that the BBB integrity is compromised. **B.** Evans Blue extravasation. Examination of the brains of perfused animals previously stained with Evans Blue confirmed BBB disruption in the GBM38 model. **C.** Quantification of Evans Blue extravasation. *P <0.05. **D-E.** Immunofluorescence staining of human vimentin (yellow), mouse CD105 (green), and mouse albumin (red). Nuclei were stained with DAPI (blue). GBM27 presents no sign of albumin staining throughout the tissue, which indicates that the BBB is intact. GBM38 features a leaky BBB, as shown by albumin spreading (white asterisk) from the blood vessels (white arrows) through the tissue. Total slides with anti-human vimentin are shown in Fig S1. Scale bar: 50 µm.

To verify these findings, we visualised and quantified the amount of Evans Blue present in the parenchymal brain after its injection through the tail vein. This test showed that Evans Blue extravasation was significantly increased in the mice xenotransplanted with GBM38 cells compared to the GBM27 xenotransplanted ones ($p < 0.05$) (Figure 2BC), which confirmed that BBB was intact in GBM27 xenotransplants. No Evans Blue dye was detected in control brains (Supplementary Figure S2B). Finally, to demonstrate the functional competence of the BBB, we also analysed albumin extravasation using immunofluorescence (Figure 2D and E). Considerable albumin diffusion from blood vessels into the parenchymal brain of GBM38 xenotransplanted mice was observed (Figura 2D). Consistently, no albumin extravasation was detected in GBM27 xenotransplants nor in control mice (Figure 2 and Supplementary Figure S2D).

Our rsults confirmed that the GBM27 orthotopic xenotransplant model of hCSCs culture displays an intact BBB.This allowed us to examine whether tumor-derived EVs can cross intact BBB to the bloodstream.

Morphological visualization and size distribution of EVs

After demonstrating the suitability of our model, we studied whether all three types of EVs could be isolated and enriched from hCSCs (GBM27) culture supernatant as well as from plasma of xenotransplanted mice. EVs were isolated and enriched using centrifugation techniques, and then visualized using transmission electron microscopy (TEM) (Figure 3A and Supplementary Figure S3A). TEM images revealed the typical morphology and expected diameter ranges of

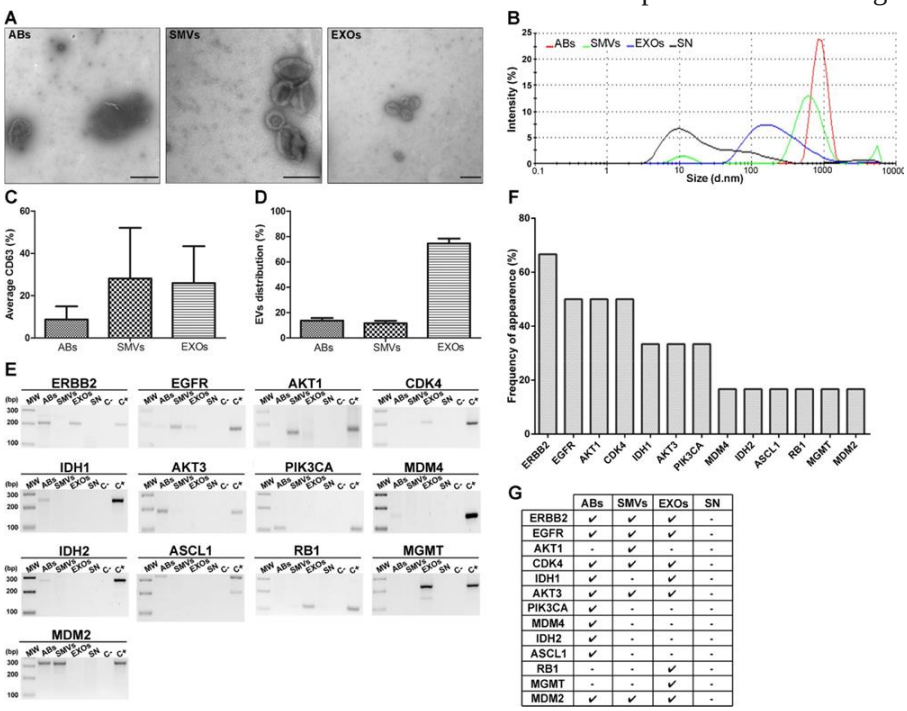

	ABs	SMVs	EXOs	SN
ERBB2	✔	✔	✔	-
EGFR	✔	✔	✔	-
AKT1	-	✔	-	-
CDK4	✔	✔	✔	-
IDH1	✔	-	✔	-
AKT3	✔	✔	✔	-
PIK3CA	✔	-	-	-
MDM4	✔	-	-	-
IDH2	✔	-	-	-
ASCL1	✔	-	-	-
RB1	-	-	✔	-
MGMT	-	-	✔	-
MDM2	✔	✔	✔	-

Figure 3: Morphological characterisation of EVs isolated from hCSCs supernatant from GBM27 and gDNA isolation.

A. Transmission electron microscopy images. ABs (500 nm to 1 µm), SMVs (500–150 nm) and EXOs (150–60 nm). **B.** Size distribution of EVs, as measured using Nanosizer tracking analysis. **C.** Quantification of the tetraspanin cell-surface glycoprotein CD63. **D.** Relative distribution of EVs. **E.** Most representative sequences analyzed are present in EVs isolated from GBM27 cells. **F.** Histogram showing the frequency of occurrence of target sequences after 6 consecutive experiments. **G.** Presence of *ERBB2*, *CDK4*, *AKT3*, and *MDM2* sequences in all types of EVs. The remaining sequences were found randomly in ABs, SMVs, and EXOs. No sequences were detected in the supernatant. Scale bars: 1 µm (ABs), 0.2 µm (SMVs and EXOs).

the ABs (>1 μm), SMVs (~200 nm), and EXOs (~100 nm). To confirm the enrichment of the different fractions of EVs from GBM27 cells, we analyzed them using a Zetasizer: the AB fraction ranged from 2000 to 500 nm in size, the SMV fraction showed an average size of 600 nm, and the EXO fraction displayed a main peak at 180 nm (Figure 3B). The supernatant also showed a small 10-nm peak, compatible with the presence of proteins. These results confirmed the utility of the protocol used to isolate EVs from the supernatant. Although these images and sizes were consistent with the presence of all three types of EVs, we also quantified the relative expression of tetraspanin CD63. The results indicated similar CD63 expression in SMVs and EXOs and a considerably lower expression in ABs (Figure 3C). Lastly, EVs distribution was quantified using TEM: the EXO fraction was almost 4 times larger than the AB and SMV fractions in the hCSCs supernatant (Figure 3D). A similar trend was observed in the case of EVs isolated from mouse plasma (Supplementary Figure S3B).

EVs from hCSCs contain gDNA

The presence of human gDNA in EVs was verified using a collection of primers specifically designed and validated to amplify human gDNA sequences (Supplementary Figure S4). We detected all the gDNA sequences assayed, except for *CDKN2a*, *PTEN*, and *TP53* sequences (Figure 3E). Then, we speculated whether the lack of PCR-amplification of these gene sequences might be related to the existence of chromosomal aberrations. Accordingly, we examined the chromosomal status of GBM27 cells using comparative genomic hybridisation (CGH). The CGH analysis revealed loss of heterozygosity of chromosome 9 at p21.3, chromosome 10 at q23.1 and chromosome 17 at position p13.1, which respectively affect the *CDKN2a*, *PTEN* and *TP53* locations (Supplementary Figure S5).

Interestingly, gDNA sequences relevant for the GBM biology were detected in all three types of EVs. Certain sequences appeared in all EVs, such as *ERBB2*, *EGFR*, *CDK4*, *AKT3*, and *MDM2*, whereas *IDH1* was detected only in ABs and EXOs, and a few sequences appeared exclusively in one type of EV: *PIK3CA*, *MDM4*, *IDH2*, and *ASCL1* in ABs, *AKT1* in SMVs, and *MGMT* and *RB1* in EXOs (Figure 3E-G). Nevertheless, we observed a 70,4% frequency of bias in this assay, which was independent of our experimental procedure (Supplementary Figure S6).

hCSC-derived EVs cross the intact BBB into the bloodstream

The GBM27 orthotopic xenotransplant model was used to analyze whether all three types of GBM27derived EVs can carry relevant human gDNA sequences, cross the undisrupted BBB and reach the bloodstream. We hypothesised that if this was the case, we should be able to detect relevant human gDNA sequences within the pool of EVs (both mouse and human) isolated from peripheral blood. Thus, we isolated and separated all three types of EVs from plasma obtained from the inferior vena cava, isolated total DNA from each type of EV and performed PCR assays to specifically amplify human gDNA sequences. PCR-amplification products of the expected sizes were obtained for *AKT3* from ABs, *PIK3CA* from ABs and SMVs, and *MDM4* and *EGFR* from EXOs. Multiple sequence alignment showed a complete homology among these sequences and their counterparts from the supernatants of hCSCs-enriched cultures (Figure 4).

IDH1^{G395A} gDNA sequences successfully identified within EVs isolated from peripheral blood of human glioma patients regardless of BBB integrity

Having detected tumor-specific gDNA sequences within EVs isolated from peripheral blood in a mouse model with intact BBB, we next wondered whether glioma-derived EVs could be detected in the bloodstream of patients, regardless of the BBB integrity. To accomplish this, we screened peripheral blood EVs from 21

patients (20 diagnosed with low- and high-grade glioma and 1 brain metastasis) for the presence of IDH1 mutations, the most relevant mutation for human glioma diagnostic and prognostic [3] (Table 1). To investigate BBB integrity, we used the analysis of contrast acquisition in T1-weighted images, which takes advantage of the incapacity of gadolinium contrast agent to cross the intact BBB. In addition, we used Dynamic Contrast-Enhanced (DCE) MRI to longitudinally measure the vascular constant transfer K^{trans}, which reflects BBB permeability (Supplementary Figure S7). The results revealed 3 patients (HGUGM002, HGUGM003 and HGUGM007) with an intact BBB, in contrast to the remaining 18 patients that showed a disrupted BBB (Table 1). Next, we assayed for the presence of $IDH1^{R132H}$ on surgical solid samples by IHC (the Standard of Gold technique) and conventional PCR. IHC gave positive results for 3 low-grade (HGUGM003, HGUGM007 and HM001) and 1 high-grade (HGUGM008) glioma (Table 1). Consistent with these results, $IDH1^{G395A}$ was also detected by conventional PCR on these 3 lowgrade glioma samples.

Furthermore, this technique detected $IDH1^{G395A}$ in an additional low-grade glioma sample (HGUGM002), while it was negative for the high-grade glioma HGUGM008. Finally, we extracted total DNA from EVs from peripheral blood obtained immediately before surgery. As a first approach, we used conventional PCR to amplify IDH1 gDNA sequences, however, $IDH1^{G395A}$ was observed in none of the low-grade gliomas, and only in 4 of the high-grade glioma samples, including HGUGM008, for which the presence of $IDH1^{R132H}$ was detected on a surgical solid sample by IHC (Table 1).

Considering these results, we hypothesized that $IDH1^{G395A}$ sequences might be underrepresented within EVs compared to $IDH1^{wt}$. To solve this problem, we tested the fast ColdPCR technique, which, in our hands, is able to enrich and detect $IDH1^{G395A}$ when its relative representation is at least as low as 10% of total IDH1 sequences (Supplementary Figure S8). We used fast ColdPCR on solid samples, for which the results were similar to those obtained by conventional PCR. Notably, when we used fast ColdPCR on DNA isolated from peripheral blood EVs, we detected the presence of $IDH1^{G395A}$ in 47.6% of the samples included in the cohort. Within the low-grade gliomas, $IDH1^{G395A}$ was identified in 80% of the samples, matching our previous results from IHC and conventional PCR on solid samples. Interestingly, within high-grade gliomas, we also detected $IDH1^{G395A}$ in 40% of the samples, including those previously detected by conventional PCR. The same technique identified only $IDH1^{wt}$ on DNA isolated from peripheral blood EVs of a patient diagnosed with adenocarcinoma brain metastasis, used as a negative control.

These results support the idea that EVs secreted by brain tumor cells can cross the BBB, whether intact or disrupted, and enters the bloodstream. Therefore, the analysis of their cargo might be useful as a biomarker not only for high-grade gliomas but also for low-grade gliomas, most of which conserve an intact BBB.

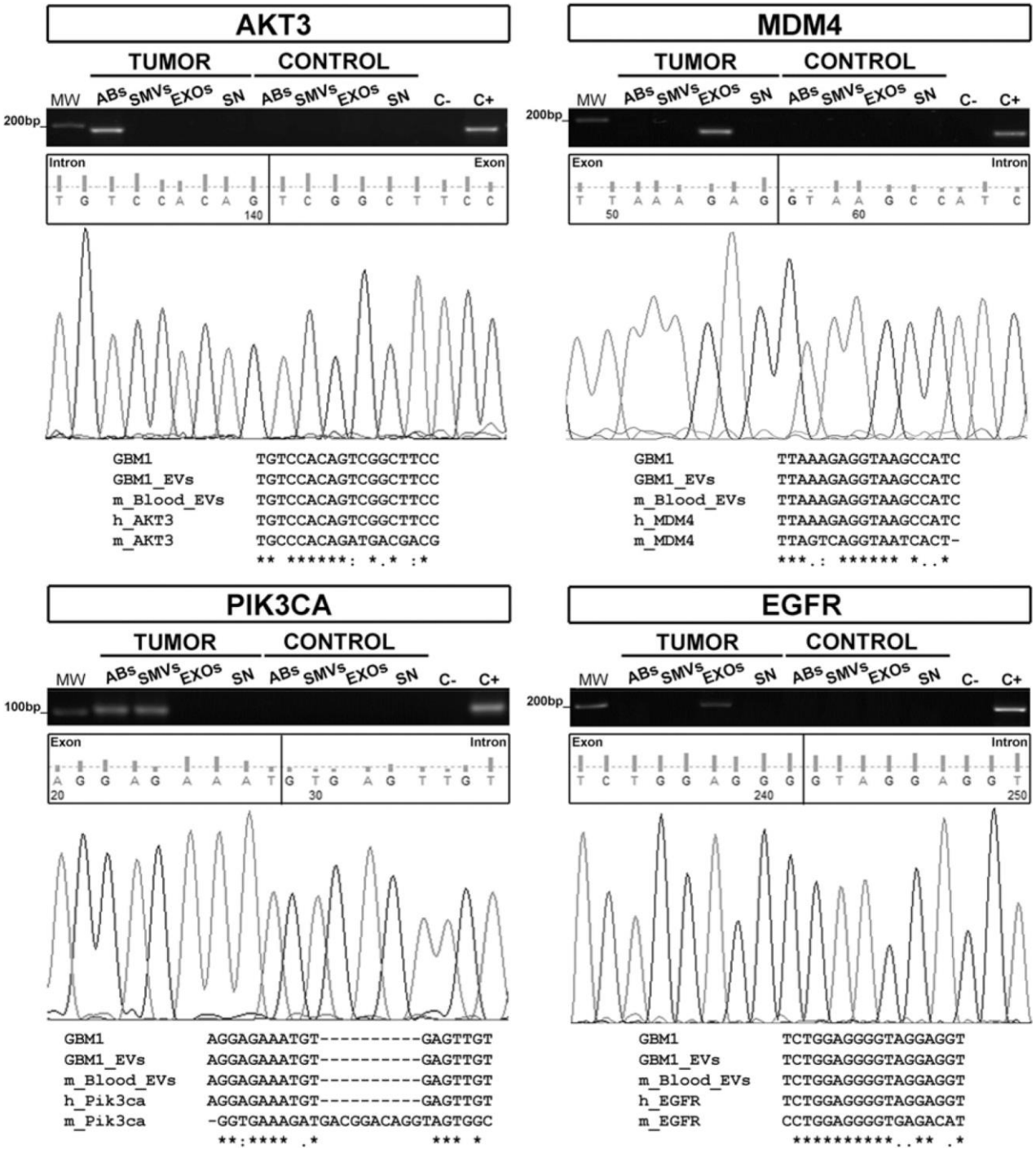

Figure 4: Human gDNA sequences are confined inside EVs isolated from xenografted mice. *AKT3*, *MDM4*, *PIK3CA*, and *EGFR* sequences were detected in EVs isolated from the peripheral blood of 10 xenografted mice. The multiple sequence alignment shows complete homology among gDNA sequences from GBM27 hCSCs, EVs isolated from hCSCs-enriched culture supernatants, and EVs found in mouse peripheral blood. These results confirm the human origin of the sequences. Keyword: GBM1= GBM27.

DISCUSSION

The BBB maintains the brain environment and protects it against external factors. In glioma-diagnosed patients and xenografted mice, the BBB dysfunction is partially due to the impairment of tight junctions, which explains the fluid leakage and cerebral oedema associated with these tumors [21, 22]. However, a completely functional BBB is occasionally found in orthotopic xenograft mouse models [23], in certain lowgrade human gliomas and a few high-grade gliomas [24]. In agreement with these reports, we demonstrated that the GBM27 orthotopic xenotransplant mouse model of hCSCs culture displays a functional BBB, using three approaches: Gd-DTPA MRI, external tracer Evans Blue, and evaluation of albumin extravasation by immunofluorescence. Thus, using the GBM27 model, we are able to assess the potential presence of brain tumor EVs in peripheral blood after crossing the intact

BBB.

We have shown that gDNA sequences are present inside all three types of EVs isolated from the hCSCs supernatant. Other groups have also demonstrated the presence of gDNA sequences within total and fractioned EVs [13, 25].

Interestingly, we noted a key variability in the detection of specific gDNA sequences in the EVs, and based also on previous reports [26], we hypothesised that this variability might be more related to the representation of such sequences within the cell of origin than to the isolation and pre-amplification procedures. Although analysing the gDNA sequences contained within all three types of EVs might be useful for obtaining clinically relevant information, our results raise at least two technical issues. Firstly, the amount of tumor-derived EVs within the total pool of circulating EVs is relatively low. Secondly, the relative presence of mutated gDNA versus wild type sequences within tumor-derived EVs cargo is questionable. Further investigation is therefore required to elucidate the mechanisms underlying nucleic acid uptake by EVs.

Another critical factor that must be addressed in order to assess the use of EVs as biomarkers is the ability to separate EVs secreted by tumor cells from the total EVs pool. Here, we have shown that orthotopic xenotransplant animal models of human tumor cells are suitable models for providing ‘proof of concepts’ related to the utility of specific molecular biomarkers present within EVs.

The presence of circulating EVs secreted from glioma cells has been strongly correlated with tumor size and the BBB status [27]. Here, we demonstrated for the first time that human gDNA sequences relevant for the GBM biology can be detected within all three types of EVs isolated from the bloodstream of tumor-bearing mice. In this context, some groups have recently postulated the use of CSF as a source of tumor-derived DNA sequences [19, 21]. However, the lumbar puncture is often unfeasible in glioma patients mostly due to the high intracranial pressure [28].

Notably, our findings confirm that not only tumorsecreted EXOs but also ABs and SMVs can cross the intact BBB into the bloodstream. This is essential to standardize the use of circulating EVs in serum as glioma biomarkers regardless of the BBB status, providing a minimally invasive method compared to CSF. However, the exact mechanism used by EVs to cross the BBB remains elusive and might differ depending on the EV type.

Finally, the new molecular pathology-based classification of gliomas expanded current molecular knowledge about prognostic and diagnostic implications of a variety of biomarkers used to characterize glioma patients. For example, IDH1-mutated patients are expected to have longer survival rates than their wildtype counterparts despite similar histopathologic features [29]. Moreover, immunotherapy is a field of growing interest in brain oncology and specific glioma hallmarks are considered as immuno-targets. In this regard, a few IDH1 peptide vaccines trials are currently going on [30]. Unfortunately, there are obvious limitations to obtain a representative glioma tissue sample. This restrains the access to new therapies and clinical trials and impairs monitoring of drug resistance and/or clonal dynamics during treatment. As a consequence, almost all clinical trials accept first biopsies as a tissue to assess $IDH1^{R132H}$ or any other target status. In this context, we addressed the potential use of tumor-derived EVs cargo in serum isolated from high or low grade brain tumor patients by looking for the presence of $IDH1^{G395A}$, currently the most valuable molecular marker for human glioma diagnostics and prognostics [3]. In our hands, conventional PCR was useful to detect the wild type form, but unable to reveal the mutated form of IDH1 in DNA sequences from peripheral blood EVs, which might explain why previous works also reported negative results [19, 21]. Here, we demonstrated for the first time, that fast Cold-PCR can be successfully used to enrich the mutated form of IDH1 in DNA sequences from peripheral blood EVs isolated from brain tumor patients.

In our cohort, the results obtained from liquid biopsies were consistent with those observed from solid samples of low-grade gliomas, but not with high-grade gliomas.

The higher number of positive $IDH1^{G395A}$ observed in high-grade gliomas, as compared with their corresponding solid samples, might be explained by the intra-tumor heterogeneity, for the small specimen analyzed by pathological anatomy barely represents the whole tumor. However, additional studies with larger cohorts are needed to consolidate and validate the use of DNA sequences isolated from the peripheral blood EVs of brain tumor patients.

In conclusion, we have demonstrated that all three types of EVs secreted by human glioma cells can cross the intact BBB. Furthermore, we prove that DNA sequences from peripheral blood EVs isolated from brain tumor patients can be successfully used to detect the presence or absence of specific molecular alterations such as $IDH1^{G395A}$. This finding supports, for the first time, the utility of tumor-derived DNA within all three types of circulating EVs as potential biomarkers to improve diagnostics, prognostics and follow-up for both low- and high-grade gliomas.

Table 1: IDH1^{G395A} gDNA sequence identification in liquid biopsies from human glioma patients with or without BBB disruption

Patient ID	Patient variables		Pathological anatomy		BBB integrity evaluation by MRI-based techniques			Surgical sample analysis			Liquid biopsy analysis	
	Sex	Age	Pathologic diagnosis	Grade	BBB integrity	Contrast acquisition	Ktrans (10-3/ min)	IHQ	FFPE Conventional PCR	FFPE Fast COLDPCR	EVs Conventional PCR	EVs Fast ColdPCR
HGUGM002	F	63	Oligodendro glioma	II	No disrupted	No	0	WT	G395A	G395A	N/D	G395A
HGUGM003	M	33	Oligodendro glioma	II	No disrupted	No	10	R132H	G395A	G395A	WT	G395A
HGUGM007	F	48	Oligoastro cytoma	II	No disrupted	No	N/D	R132H	G395A	G395A	N/D	G395A
HM001	M	31	Astrocytoma	II	Disrupted	Yes	N/D	R132H	G395A	G395A	WT	G395A
HM012	M	56	Astrocytoma	II	Disrupted	Yes	N/D	WT	WT	WT	N/D	WT
HM009	M	56	Astrocytoma	III	Disrupted	Yes	N/D	WT	WT	WT	WT	WT
HGUGM004	M	47	Grade III Astrocytoma with grade IV areas	IV	Disrupted	Yes	184427	WT	WT	WT	N/D	WT
HGUGM005	F	43	Giant-Cells GBM	IV	Disrupted	Yes	N/D	WT	WT	WT	G395A	G395A
HGUGM006	M	53	GBM	IV	Disrupted	Yes	N/D	WT	WT	WT	WT	G395A
HGUGM008	M	39	GBM, recurrence	IV	Disrupted	Yes	N/D	R132H	WT	WT	G395A	G395A
HGUGM009	F	64	GBM, recurrence	IV	Disrupted	Yes	N/D	WT	WT	WT	N/D	WT
HM002	M	42	GBM	IV	Disrupted	Yes	N/D	WT	WT	WT	WT	WT
HM003	F	61	GBM	IV	Disrupted	Yes	N/D	WT	WT	WT	G395A	G395A
HM004	M	65	GBM	IV	Disrupted	Yes	N/D	WT	WT	WT	WT	WT
HM005	F	36	GBM	IV	Disrupted	Yes	N/D	WT	WT	WT	WT	WT
HM006	M	48	GBM	IV	Disrupted	Yes	N/D	WT	WT	WT	G395A	G395A
HM007	F	66	GBM	IV	Disrupted	Yes	N/D	WT	WT	WT	N/D	G395A
HM008	F	65	GBM	IV	Disrupted	Yes	N/D	WT	WT	WT	N/D	WT
HM010	M	43	GBM	IV	Disrupted	Yes	N/D	WT	WT	WT	N/D	WT
HM011	F	61	GBM	IV	Disrupted	Yes	N/D	WT	WT	WT	WT	WT
HGUGM001	F	61	Adenocarcinoma Brain metastases	O	Disrupted	Yes	638	WT	WT	WT	WT	WT

Samples are organized by tumor grade. BBB integrity is evaluated mainly by contrast acquisition, but also by K^{trans} when possible. Surgical tumor tissues were analyzed by IHQ, conventional PCR and Fast Cold PCR. Liquid biopsies were analyzed mainly by Fast Cold PCR. Keywords: BBB, blood brain

MATERIALS AND METHODS

Human samples and derivation of glioblastomacancer stem cells-enriched cultures

Two tumor samples from GBM patients (GBM27 and GBM38) were processed within 12 h after extraction according to the protocol described previously [31]. Briefly, the samples were minced and washed in Ca^{2+}/ Mg^{2+}-free HBSS (Hanks balanced salt solution). Enzymatic digestion was sequentially performed with Solution I (papain (14 U ml^{-1}, Sigma-Aldrich) and DNase I (10 U ml^{-1}, Sigma) in PIPES solution) for 90 min at 37°C and Solution II (papain (7 U ml^{-1}) and DNase I (15 U ml^{-1}) in 1:1 PIPES: proliferation medium) for 30 min at 37°C. The cells were then dissociated using diametertapering polished Pasteur pipettes, filtered through a 70-μm mesh, and resuspended in defined proliferative media. These CSCs lines were previously described and characterized in detail by our laboratory [20].

Solid surgical tissue samples and peripheralblood were obtained from patients operated at HM Hospitales (HM), Madrid, Spain; Hospital Universitario la Fe (HUlaFe), Valencia Sapin and Hospital General Universitario Gregorio Marañón (HGUGM), Madrid, Spain. Peripheralblood samples from patients were collected prior to surgery. These blood samples were left to clot for 30 min at room temperature and serum was isolated and stored at -80°C until use.

Xenotransplants

Approximately 10^5 cells from 2 cancer-stem cell cultures (GBM27 and GBM38) were injected into the right striatum of 10 immunosuppressed athymic nude female mice by using a stereotactic device. As a negative control, PBS was injected into 2 mice following the same protocol. Twelve weeks post-injection, mice were anaesthetised and then transcardially perfused with saline and prefixed with 4% paraformaldehyde. The brains were post-fixed for 48 h after the infusion and embedded in paraffin, after which 3-μm coronal sections were obtained.

Magnetic resonance imaging (MRI) in mice

Magnetic resonance experiments were performed on a 7.0-T Bruker Pharmascan (Bruker Medical Gmbh, Ettlingen, Germany) superconducting magnet, with Paravision 5.1 software. T2-weighted MRI and T1weighted MRI after paramagnetic contrast-agent administration were used to assess tumor implantation and BBB integrity, at time 0 and at 90 days. Prior to scanning, mice were anaesthetised with isofluorane.

T2-weighted images were acquired by using the rapid acquisition with refocused echo (RARE) sequence with the following parameters: TR/TE (repetition time/ echo time) = 2500/44 ms, field of view = 2.3 cm, 6 averages, matrix size = 256 × 256, number of slices = 14, and slice thickness = 1 mm without a gap. The total scan time required to concurrently acquire T2-weighted images was 6 min.

Subsequently, we modified certain parameters for T1-weighted images; for example, we used the multislice multi-echo (MSME) sequence, TR/TE = 3500/10.6 ms, 3 averages, and total time of acquisition = 3 min 2 s. The contrast agent used, 0.3 M Gd-DTPA, was injected intraperitoneally.

Evans blue injection and brain extraction

A 2% Evans Blue dye solution (Sigma-Aldrich) was administered (2 ml kg^{-1}) through the tail vein and, 1 h later, the mice were transcardially perfused and the brains were extracted, weighed, and homogenised using a TissueLyser LT (Qiagen) in twice their volume of *N*,*N*-dimethylformamide (Sigma-Aldrich). The tissues were incubated overnight at 55°C and then centrifuged for 20 min at 9300 × *g*. The optical density (OD) of the supernatant was measured at 610–635 nm, and the amount of Evans Blue extravasation was quantified as nanograms per milligram of tissue.

Immunofluorescence staining

Immunofluorescence staining for mouse albumin was performed to determine the vascular integrity of the brain. Brain sections obtained from GBM27 and GBM38 hCSCs and PBS control xenotransplants were incubated with a 5% blocking solution of the specific serum, and then incubated (overnight, 4°C) in solutions containing the following primary antibodies: goat anti-mouse CD105 (R&D Systems), goat anti-mouse albumin (Santa Cruz Biotechnology), and mouse anti-human vimentin (Santa Cruz Biotechnology). Then, Alexa Fluor-conjugated secondary antibodies were used for 1 h (donkey anti-goat 568, rabbit anti-goat 488, and goat anti-mouse 660; Life Technologies, USA), and then nuclei were counterstained with DAPI and coverslips were mounted using FluorSave™ reagent (Millipore). Fluorescence was examined under a Leica TCS SP5 inverted confocal microscope.

Immunohistochemistry

Formalin-fixed paraffin-embedded sections were stained (as per the manufacturer's staining protocol) with the Bond Polymer Refine Detection Kit on a Bond-max™ fully automated staining system (Leica Microsystems GmbH, Germany), using a mouse monoclonal antibody against human $IDH1^{R132H}$ (Clon H09, Dianova) for the detection of mutant $IDH1^{R132H}$.

Mice plasma samples

Twelve weeks after the xenotransplantation, mouse peripheral blood was collected from the inferior vena cava, and centrifuged at 1500 × *g* for 10 min to obtain the plasma.

Extracellular vesicles isolation

EVs from plasma and serum samples and cell medium supernatants were isolated through differential ultracentrifugation as previously described [32], with certain modifications. Briefly, to remove cellular debris, samples were centrifuged at 1200 × *g* for 5 min. The supernatant was carefully aspirated off without disturbing the pellet and centrifuged at 8000 × *g* for 20 min to obtain ABs. Next, this supernatant was centrifuged at 25,000 × *g* for 20 min to obtain SMVs, and then the remaining supernatant was ultracentrifuged at 117,000 × *g* for 90 min to obtain EXOs (Optima-LE 80K ultracentrifuge, 50.2 Ti rotor; Beckman Coulter). All centrifugations were performed at 4°C. A sample of the EVs-free supernatant was collected after the ultracentrifugation and used as a negative control. In samples from human, total EVs were analyzed. Samples were immediately used or stored at -20°C.

Transmission electron microscopy

EVs samples were individually added onto glowdischarged 150-mesh formvar copper grids (EMS™), subjected to the glow-discharge procedure (2 min, 2.4 MA), and then incubated for 2 min at 4°C. The grids were washed, negatively stained with 2% aqueous uranyl acetate solution, dried, and analyzed by performing TEM (FEI Tecnai Spirit G2 and Tecnai 12) at 80 kV. EVs were classified based on their size, photographed, and counted using a Soft Image System Morada camera.

Tracking analysis

Mean droplet sizes of EVs were measured using the dynamic light scattering method and a Zetasizer Nano ZS (Malvern Instruments, UK).

Flow-cytometry analysis of CD63 expression

AB, SMV, or EXO samples were adsorbed onto 4-mm aldehyde/sulphate latex beads (Invitrogen, Paisley, UK) overnight at 4°C. The reaction was stopped by adding glycine 100 mM. Membrane-bound beads were washed in PBS/1% BSA, incubated with mouse anti-CD63 (Abcam, Cambridge, UK) or appropriate isotype control for 30 min at 4°C, stained with FITC-conjugated secondary antibody (R&D Systems) for 30 min at 4°C, and resuspended in 0.5 ml of PBS. Samples were analyzed using a FACS Calibur flow cytometer (BD Biosciences, San Jose, CA, USA).

DNA isolation and pre-amplification and PCR

Formalin-fixed paraffin-embedded (FFPE) samples were deparaffinized and extracted using the DNeasy Blood & Tissue Kit spin columns according to the manufacter´s protocol. (Qiagen, Germany). Before DNA isolation, supernatant and plasma samples were treated with 27 Kunitz U ml^{-1} of DNase I (Qiagen) for 30 min at 37°C

to remove potential free-DNA contaminants. Total DNA was extracted from EVs and cells by using a DNeasy Blood and Tissue Kit (Qiagen), as per manufacturer recommendations. Next, a working solution of the extracted DNA was pre-amplified using the GenomePlex Complete WGA2 Kit (Sigma-Aldrich), according to the manufacturer's instructions. All PCRs were performed following the protocol of the Paq5000 enzyme (Agilent Technologies) (Supplementary Figure S8B). The final PCR products were electrophoretically separated on 1.8% agarose gels.

Fast Cold-PCR

For the enrichment and detection of IDH1 mutated gDNA sequences within EVs isolated from peripheral blood of human patients, DNA was amplified using the reported primers: forward 5'- CGGTCTTCAGAGAAGCCATT-3' and reverse 5'-GCAAAATCACATTATTGCCAAC-3' [33] (Supplementary Figure S8A). Cycling conditions were as follows: a first denaturation step of 10 min at 96ºC, followed by a set of 20 cycles of 96ºC for 15 sec and 60ºC for 15 sec, and a second set of 30 cycles of 15 sec at T_c (critical temperature) and 60ºC for 15 sec (Supplementary Figure S8C).

Sequencing and assembly

DNA sequencing of the PCR-amplified products of *AKT3*, *EGFR*, *MDM4*, *PIK3CA* and *IDH1* was performed by the sequencing service at Spanish National Cancer Research Center (CNIO). Sequences were compared and aligned using the BLAST algorithm and CLUSTAL Omega, respectively.

Dynamic contrast enhanced (DCE)-MRI data acquisition and analysis

Preoperative MR images were obtained using a 1.5 T MRI scanner (Achieva of Intera, Philips Healthcar, Best, The Netherlands) and 8-channel SENSE head coil. For DCE-MRI, baseline 3D T1-weighted images were obtained with the following parameters: TR 76 ms, TE 3ms, slice thickness 5mm, Field of View (FOV) 230 mm, matrix size of 116 x128, 35 volumes, temporal resolution 5,4 s and flipangles of 5º and 15º to create two precontrast datasets. Then, a DCE perfusion imaging dynamic series was performed using T1-weigthed sequences with the same MR parameters except for an increased flip angle of 15º. At the end of the second volume acquisition, a bolus of 14 ml of gadobenate dimeglumine (Multihance, Bracco Imaging, Spain) was injected intravenously at a rate of 3-4 ml/s.

Structural contrast 3D T1 fast field echo (FFE) sequence was performed and the detail parameters were as follows: TR/TE= 4,6/9,4 ms, flip angle 8º, FOV 256 × 256 mm, matrix size 256x 256 and reconstructed voxel size of 1 × 1 × 1mm.

To observe BBB permeability, vascular constant transfer (K^{trans} min^{-1}) values were calculated using Philips IntelliSpace Portal v.6 Software by simultaneous observation of axial postcontrast T1-weigthed images and corresponding colour parametric K^{trans} maps. One region of interest was manually positioned on the solid tumoral area.

Statistics

Statistical analysis were performed using a 2-tailed Student *t* test. Data are presented as means ± standard deviation and were calculated using the software package GraphPad Prism v. 5.0. Statistical values of $p > 0.05$ were not considered significant.

Study approval

Procedures used on mice were approved by and performed according to the guidelines of the institutional animal-care committee of the Principe Felipe Research Center in agreement with the European Union and National directives. Permission to use human samples was obtained from the ethical review board in HM Hospitales, Hospital Universitario la Fe, Valencia, and Hospital General Universitario Gregorio Marañón, Madrid and written informed consent was obtained from patients

.

ACKNOWLEDGMENTS

We would like to thank Editage (www.editage.com) for English language editing. Additionally, we thank the confocal unit of ISCIII for technical assistance, the Biobank FiHM Hospitales, the Biobank la Fe, and the Biobank Hospital General Universitario Gregorio Marañón.

CONFLICTS OF INTEREST

N.G.R., J.C.N., C.B.I. and A.A.S. declare competing financial interest in this work related to a patent pending on the use of a method for the detection of gene mutations in DNA from extracellular vesicles. (Application number: 16382028.5 – 1403). The other authors have no conflict of interests to declare.

GRANT SUPPORT

We are grateful for the financial support from the 'Fondo de Investigaciones Sanitarias' (FIS) (PI10/01069 and PI14/00077) and the 'Miguel Servet Program' (CP11/00147) from the 'Instituto de Salud Carlos III' (AAS), RTC-2015-3846-1 from Ministerio de Economía y Competitividad and FEDER funds.

Author contributions

N.G.R., J.C.N., S.E.R. and A.A.S. conceived, designed and performed research with assistance from E.L.I., M.P.C. and C.B.I.. M.M.A. analyzed CD63 expression in EVs supernatants. A.O.M. and J.G.V. provided MRI assistance. All authors contributed to the general discussion and comment on the manuscript. N.G.R., J.C.N., S.E.R. and A.A.S. wrote the manuscript with inputs from C.E.L., C.F.C., S.G.C., R.P.A. and C.B.I.

REFERENCES

1. Siegel RL, Miller KD, Jemal A. Cancer statistics. 2016; 66: 7–30. doi: 10.3322/caac.21332.

2. Chinot OL, Wick W, Mason W, Henriksson R, Saran F, Nishikawa R, Carpentier AF, Hoang-Xuan K, Kavan P, Cernea D, Brandes AA, Hilton M, Abrey L, et al. Bevacizumab plus radiotherapy-temozolomide for newly diagnosed glioblastoma. N Engl J Med. 2014; 370: 709–22. doi: 10.1056/NEJMoa1308345.

3. Louis DN, Perry A, Reifenberger G, von Deimling A, Figarella-Branger D, Cavenee WK, Ohgaki H, Wiestler OD, Kleihues P, Ellison DW. The 2016 World Health Organization Classification of Tumors of the Central Nervous System: a summary. Acta Neuropathol. Springer Berlin Heidelberg; 2016; 131: 803–20. doi: 10.1007/s00401-016-1545-1.

4. Killock D. CNS cancer: Molecular classification of glioma. Nat Rev Clin Oncol. Nature Publishing Group; 2015; 12: 502–502. doi: 10.1038/nrclinonc.2015.111.

5. Redzic JS, Ung TH, Graner MW. Glioblastoma extracellular vesicles: Reservoirs of potential biomarkers. Pharmgenomics Pers Med. 2014; 7: 65–77. doi: 10.2147/PGPM.S39768.

6. Best MG, Sol N, Zijl S, Reijneveld JC, Wesseling P, Wurdinger T. Liquid biopsies in patients with diffuse glioma. Acta Neuropathol. Springer Berlin Heidelberg; 2015; 129: 849–65. doi: 10.1007/s00401-015-1399-y.

7. Dalton A J. Microvesicles and vesicles of multivesicular bodies versus "virus-like" particles. J Natl Cancer Inst. 1975; 54: 1137–48. doi: 10.1093/jnci/54.5.1137.

8. Ashcroft BA, De Sonneville J, Yuana Y, Osanto S, Bertina R, Kuil ME, Oosterkamp TH. Determination of the size distribution of blood microparticles directly in plasma using atomic force microscopy and microfluidics. Biomed Microdevices. 2012; 14: 641–9. doi: 10.1007/ s10544-012-9642-y.

9. Marzesco A-M, Janich P, Wilsch-Bräuninger M, Dubreuil V,

Langenfeld K, Corbeil D, Huttner WB. Release of extracellular membrane particles carrying the stem cell marker prominin-1 (CD133) from neural progenitors and other epithelial cells. J Cell Sci. 2005; 118: 2849–58. doi: 10.1242/jcs.02439.

10. Llorente A, Skotland T, Sylvanne T, Kauhanen D, Róg T, Orlowski A, Vattulainen I, Ekroos K, Sandvig K. Molecular lipidomics of exosomes released by PC-3 prostate cancer cells. Biochim Biophys Acta - Mol Cell Biol Lipids. 2013; 1831: 1302–9. doi: 10.1016/j.bbalip.2013.04.011.

11. Scanu A, Molnarfi N, Brandt KJ, Gruaz L, Dayer J-M, Burger D. Stimulated T cells generate microparticles, which mimic cellular contact activation of human monocytes: differential regulation of pro- and anti-inflammatory cytokine production by high-density lipoproteins. J Leukoc Biol. 2008; 83: 921–7. doi: 10.1189/jlb.0807551.

12. Deregibus MC, Cantaluppi V, Calogero R, Iacono M Lo, Tetta C, Bruno S, Bussolati B, Camussi G, Dc W, Biancone L. angiogenic program in endothelial cells by a horizontal transfer of mRNA Endothelial progenitor cell – derived microvesicles activate an angiogenic program in endothelial cells by a horizontal transfer of mRNA. 2012; 110: 2440–8. doi: 10.1182/blood-2007-03-078709.

13. Lázaro-Ibáñez E, Sanz-Garcia A, Visakorpi T, EscobedoLucea C, Siljander P, Ayuso-Sacido Á, Yliperttula M. Different gDNA content in the subpopulations of prostate cancer extracellular vesicles: Apoptotic bodies, microvesicles, and exosomes. Prostate. 2014; 74: 1379–90. doi: 10.1002/pros.22853.

14. Thakur BK, Zhang H, Becker A, Matei I, Huang Y, CostaSilva B, Zheng Y, Hoshino A, Brazier H, Xiang J, Williams C, Rodriguez-Barrueco R, Silva JM, et al. Double-stranded DNA in exosomes: a novel biomarker in cancer detection. Cell Res. 2014; 24: 766–9. doi: 10.1038/cr.2014.44.

15. Kalra H, Simpson RJ, Ji H, Aikawa E, Altevogt P, Askenase P, Bond VC, Borrás FE, Breakefield X, Budnik V, Buzas E, Camussi G, Clayton A, et al. Vesiclepedia: A Compendium for Extracellular Vesicles with Continuous Community Annotation. PLoS Biol. 2012; 10: 8–12. doi: 10.1371/ journal.pbio.1001450.

16. Zhuang X, Xiang X, Grizzle W, Sun D, Zhang S, Axtell RC, Ju S, Mu J, Zhang L, Steinman L, Miller D, Zhang H-G. Treatment of brain inflammatory diseases by delivering exosome encapsulated anti-inflammatory drugs from the nasal region to the brain. Mol Ther. Nature Publishing Group; 2011; 19: 1769–79. doi: 10.1038/mt.2011.164.

17. Alvarez-Erviti L, Seow Y, Yin H, Betts C, Lakhal S, Wood MJA. Delivery of siRNA to the mouse brain by systemic injection of targeted exosomes. Nat Biotechnol. Nature Publishing Group; 2011; 29: 341–5. doi: 10.1038/nbt.1807.

18. De Mattos-Arruda L, Mayor R, Ng CKY, Weigelt B, Martínez-Ricarte F, Torrejon D, Oliveira M, Arias A, Raventos C, Tang J, Guerini-Rocco E, Martínez-Sáez E, Lois S, et al. Cerebrospinal fluid-derived circulating tumour DNA better represents the genomic alterations of brain tumours than plasma. Nat Commun. 2015; 6: 8839. doi: 10.1038/ncomms9839.

19. Chen WW, Balaj L, Liau LM, Samuels ML, Kotsopoulos SK, Maguire CA, Loguidice L, Soto H, Garrett M, Zhu LD, Sivaraman S, Chen C, Wong ET, et al. BEAMing and Droplet Digital PCR Analysis of Mutant IDH1 mRNA in Glioma Patient Serum and Cerebrospinal Fluid Extracellular Vesicles. Mol Ther Nucleic Acids. 2013; 2: e109. doi: 10.1038/mtna.2013.28.

20. García-Romero N, González-Tejedo C, Carrión-Navarro. Cancer stem cells from human glioblastoma resemble but do not mimic original tumors after in vitro passaging in serum-free media. Oncotarget. 2016; doi: 10.18632/ oncotarget.11676.

21. Coomberl BL, Stewart PA, Hayakawa K, Farrell CL, Del Maestros RF. Quantitative morphology of human

glioblastoma multiforme microvessels: structural basis of blood-brain barrier defect. J Neurooncol. 1987; 5: 299–307. doi: 10.1007/BF00148386.

22. Wolburg H, Noell S, Fallier-Becker P, MacK AF, WolburgBuchholz K. The disturbed blood-brain barrier in human glioblastoma. Mol Aspects Med. Elsevier Ltd; 2012; 33: 579–89. doi: 10.1016/j.mam.2012.02.003.

23. Leten C, Struys T, Dresselaers T, Himmelreich U. In vivo and ex vivo assessment of the blood brain barrier integrity in different glioblastoma animal models. J Neurooncol. 2014; 119: 297–306. doi: 10.1007/s11060-014-1514-2.

24. Nduom EK, Yang C, Merrill MJ, Zhuang Z, Lonser RR. Characterization of the blood-brain barrier of metastatic and primary malignant neoplasms. J Neurosurg. 2013; 119: 427–33. doi: 10.3171/2013.3.JNS122226.

25. Kahlert C, Melo SA, Protopopov A, Tang J, Seth S, Koch O, Zhang J, Weitz J, Chin L, Futreal A, Kalluri R. Identification of doublestranded genomic dna spanning all chromosomes with mutated KRAS and P53 DNA in the serum exosomes of patients with pancreatic cancer. J Biol Chem. 2014; 289: 3869–75. doi: 10.1074/jbc.C113.532267.

26. Balaj L, Lessard R, Dai L, Cho Y, Pomeroy SL, Breakefield XO, Skog J. NIH Public Access. Nat Commun. 2011; 1: 180. doi: 10.1038/ncomms1180.Tumour.

27. Wood MJ, O'Loughlin AJ, Lakhal S. Exosomes and the blood-brain barrier: implications for neurological diseases. Ther Deliv. 2011; 2: 1095–9. doi: 10.4155/tde.11.83.

28. Kong X, Wang Y, Liu S, Chen K, Zhou Q, Yan C, He H, Gao J, Guan J, Yang Y, Li Y, Xing B, Wang R, et al. Brain Stem and Entire Spinal Leptomeningeal Dissemination of Supratentorial Glioblastoma Multiforme in a Patient during Postoperative Radiochemotherapy: Case Report and Review of the Literatures. Medicine (Baltimore). 2015; 94: e962. doi: 10.1097/MD.0000000000000962.

29. Sanson M, Marie Y, Paris S, Idbaih A, Laffaire J, Ducray F, Hallani S El, Boisselier B, Mokhtari K, HoangXuan K, Delattre JY. Isocitrate dehydrogenase 1 codon 132 mutation is an important prognostic biomarker in gliomas. J Clin Oncol. 2009; 27: 4150–4. doi: 10.1200/JCO.2009.21.9832.

30. Bunse L, Schumacher T, Sahm F, Pusch S, Oezen I, Rauschenbach K, Gonzalez M, Solecki G, Osswald M, Capper D, Wiestler B, Winkler F, Herold-Mende C, et al. Proximity ligation assay evaluates IDH1R132H presentation in gliomas. J Clin Invest. 2015; 125: 593–606. doi: 10.1172/JCI77780.

31. Ayuso-Sacido A, Roy NS, Schwartz TH, Greenfield JP, Boockvar JA. Long-term expansion of adult human brain subventricular zone precursors. Neurosurgery. United States; 2008; 62: 223–31.doi:10.1227/01.NEU.0000311081.50648.4C.

32. Skog J, Würdinger T, van Rijn S, Meijer DH, Gainche L, Sena-Esteves M, Curry WT, Carter BS, Krichevsky AM, Breakefield XO. Glioblastoma microvesicles transport RNA and proteins that promote tumour growth and provide diagnostic biomarkers. Nat Cell Biol [Internet]. 2008; 10: 1470–6. doi: 10.1038/ncb1800.

33. Balss J, Meyer J, Mueller W, Korshunov A, Hartmann C, von Deimling A. Analysis of the IDH1 codon 132 mutation in brain tumors. Acta Neuropathol. 2008; 116: 597–602. doi: 10.1007/s00401-008-0455-2.

SUPPLEMENTARY MATERIAL

Human samples and derivation of glioblastomacancer stem cells-enriched cultures

Two tumor samples from GBM patients (GBM27 and GBM38) were processed within 12 h after extraction as per the protocol described previously [31]. Briefly, the samples were minced and washed in Ca^{2+}/Mg^{2+}-free HBSS (Hanks balanced salt solution). Enzymatic digestion was sequentially performed with Solution I (papain (14 U ml^{-1}, Sigma-Aldrich) and DNase I (10 U ml^{-1}, Sigma) in PIPES solution) for 90 min at 37°C and Solution II (papain (7 U ml^{-1}) and DNase I (15 U ml^{-1}) in 1:1 PIPES: proliferation medium) for 30 min at 37°C. The cells were then dissociated using diameter-tapering polished Pasteur pipettes, filtered through a 70-µm mesh, and resuspended in defined proliferative media.

Magnetic resonance imaging (MRI) in mice: T1- and T2- weighted images

T2-weighted images were acquired by using the rapid acquisition with refocused echo (RARE) sequence with the following parameters: TR/TE (repetition time/ echo time) = 2500/44 ms, field of view = 2.3 cm, 6 averages, matrix size = 256 × 256, number of slices = 14, and slice thickness = 1 mm without a gap. The total scan time required to concurrently acquire T2-weighted images was 6 min. Next, we modified certain parameters for T1weighted images; for example, we used the multi-slice multi-echo (MSME) sequence, TR/TE = 3500/10.6 ms, 3 averages, and total time of acquisition = 3 min 2 s. The contrast agent used, 0.3 M Gd-DTPA, was injected intraperitoneally.

Dynamic contrast enhanced (DCE)-MRI data acquisition and analysis: T1-weighted images

For DCE-MRI, baseline 3D T1-weighted images were obtained with the following parameters: TR 76 ms, TE 3ms, slice thickness 5mm, Field of View (FOV) 230 mm, matrix size of 116 × 128, 35 volumes, temporal resolution 5,4 s and flip-angles of 5º and 15º to create two precontrast datasets. Then, a DCE perfusion imaging dynamic series was performed using T1-weigthed sequences with the same MR parameters except for an increased flip angle of 15º. At the end of the second volume adquisition, a bolus of 14 ml of gadobenate dimeglumine (Multihance, Bracco Imaging, Spain) was injected intravenously at a rate of 3-4 ml/s. Structural contrast 3D T1 fast field echo (FFE) sequence was performed and the detail parameters were as follows: TR/TE= 4,6/9,4 ms, flip angle 8º, FOV 256 × 256 mm, matrix size 256x 256 and reconstructed voxel size of 1 × 1 × 1mm.

Immunohistochemistry

Formalin-fixed paraffin-embedded sections were stained (as per the manufacturer's staining protocol) with the Bond Polymer Refine Detection Kit on a Bond-max™ fully automated staining system (Leica Microsystems GmbH, Germany), using a mouse monoclonal antibody against human vimentin (V9) (Santa Cruz Biotechnology).

Primers design and PCR assays

Genomic sequences of known genes relevant for the GBM biology were obtained from the UCSC Genome Browser database and primers were designed covering intron/exon boundaries by using Primer 3 software. All primers were tested in PCR with human gDNA (positive control) and mouse gDNA (negative control). All PCRs were performed following the protocol of the Paq5000 enzyme (Agilent Technologies), and final PCR products were electrophoretically separated on 1.8% agarose gels.

Evaluation of DNA pre-amplification variability

To rule out the possibility that DNA preamplification procedures might be responsible for the variability observed in the PCR-amplification assays, we analysed the PCR-amplification results of 4 representative DNA sequences from hCSCs (*AKT3*, *MDM4*, *PIK3CA*, and *EGFR*) with or without the WGA kit. A representative gDNA sample from hCSCs was diluted to obtain a 1 ng $µl^{-1}$ working solution and was pre-amplified using the GenomePlex Complete WGA2 Kit (Sigma-Aldrich). The same sample was also used without the pre-amplification step. *AKT3*, *MDM4*, *PIK3CA*, and *EGFR* were amplified using conventional PCR. Cycling conditions included an initial denaturation step of 2 min at 95°C, followed by

34 cycles of 20 s at 95°C, 20 s at the primer hybridisation temperature, and 30 s at 72°C, and a final extension step at 72°C for 5 min. The experiment was performed twice to ensure reproducibility of the result. We observed a 15.6% variability when the pre-amplification step was included; *AKT3* and *MDM4* showed 100% reproducibility, whereas certain amount of bias was observed for *PIK3CA* and *EGFR*. However, the absence of this step resulted in 100% reproducibility. Unexpectedly, we observed 70.4% variability when we used the gDNA isolated from EVs as a template. These results suggest that the high variability observed does not depend on the pre-amplification procedure, and instead depends mainly on the EVs cargo (Supplementary Figure S6).

SUPPLEMENTARY FIGURES

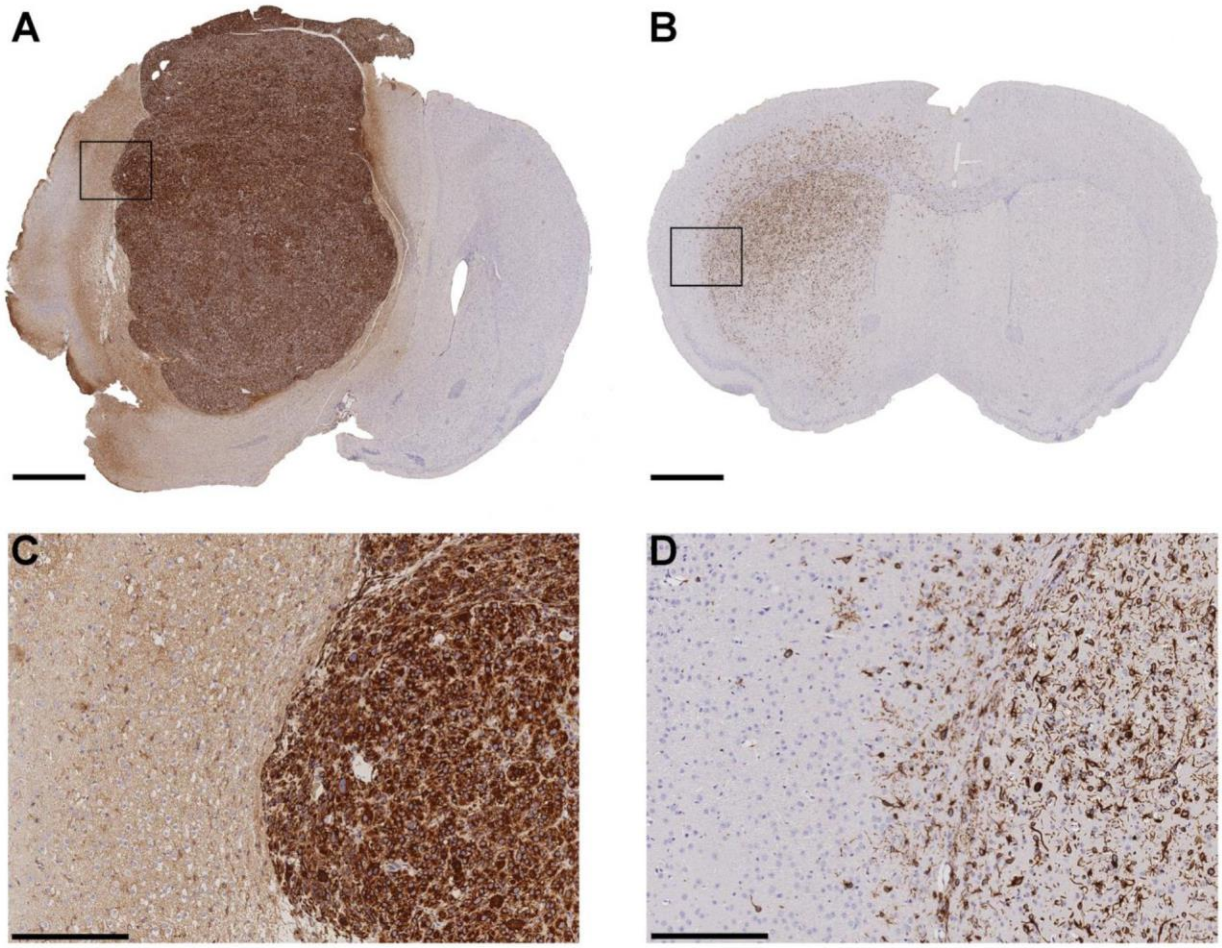

Supplementary Figure S1: Representative images of human vimentin staining. Histological analysis of paraffin-embedded tissue sections of formalin-fixed mouse brains. 3,3' Diaminobenzidine was used as the chromogen, and sections were counterstained with haematoxylin. **A.** GBM38 section showing a nodular growth pattern, with regular borders and no sign of invasiveness. **B.** GBM27 exibits diffuse growth, invading the tissue and migrating through the myelin tracts to the contralateral brain. Areas in the square are magnified in **C** and **D.** Scale bars: 1 mm (A, B), 200 μm (C, D).

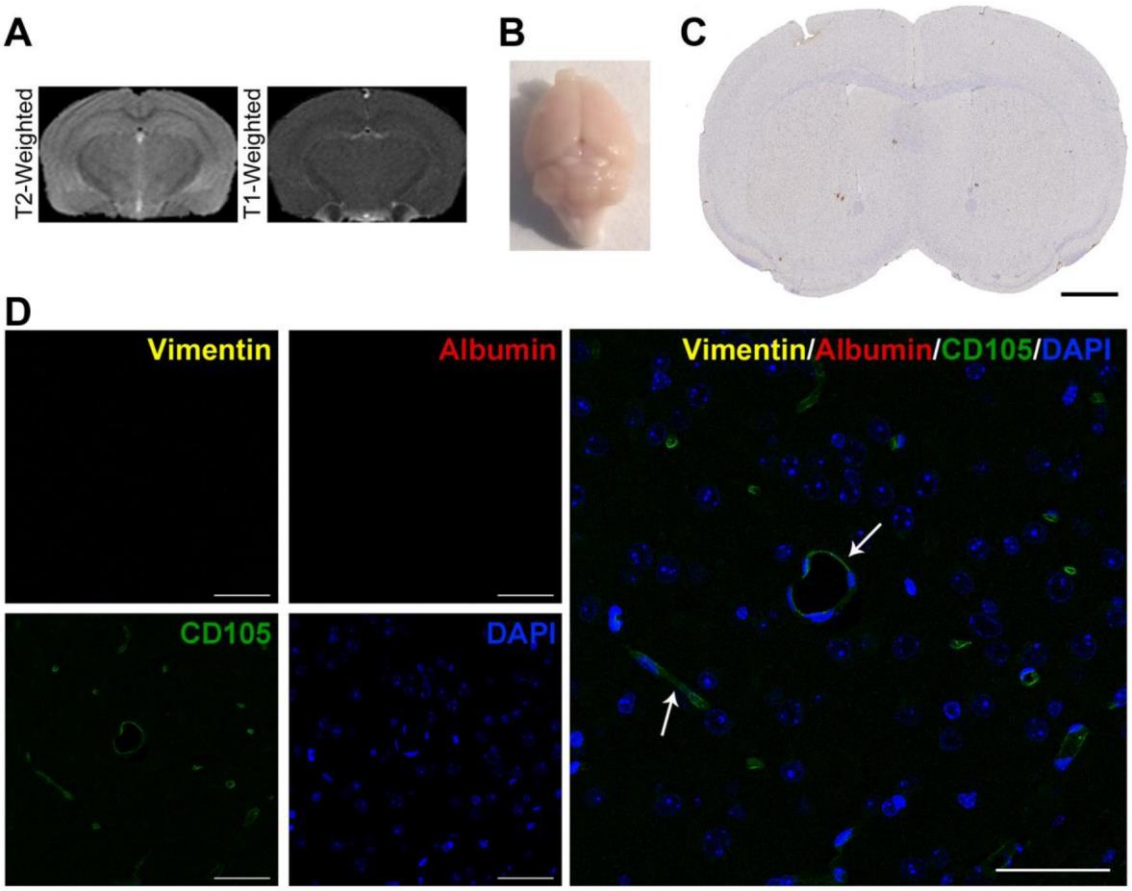

Supplementary Figure S2: Immunodeficient mice treated with control buffer (PBS) show an intact BBB. A. T2- and T1-weighted images of normal mouse brain injected with PBS. No abnormalities are shown. **B.** No Evans Blue dye extravasation. **C.** No human vimentin (V9) staining is detected, showing that no human cells were injected. **D.** Immunofluorescence staining, positive for mouse CD105 (white arrows) and negative for human vimentin (yellow) and mouse albumin (red). Nuclei were stained with DAPI (blue). Scale bars: 1 mm (C), 50 μm (D).

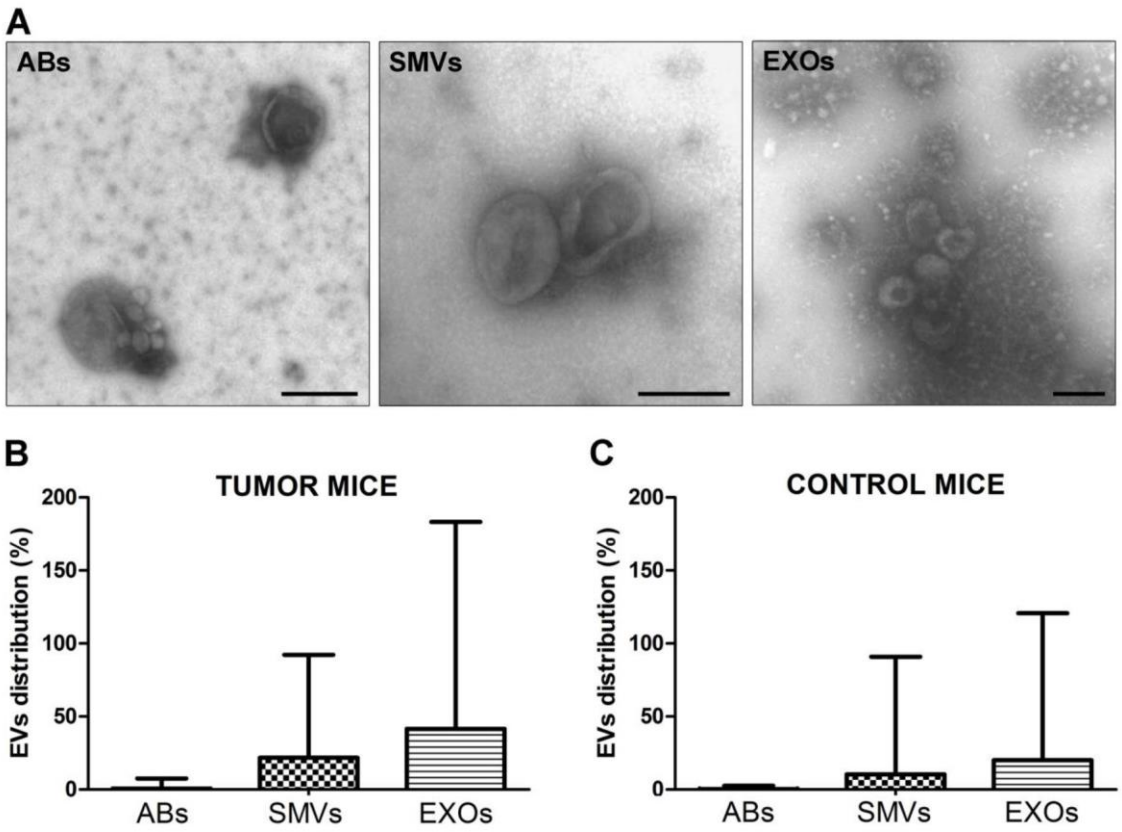

Supplementary Figure S3: Morphological characterisation and distribution of ABs, SMVs, ad EXOs in mouse plasma.

A. Transmission electron microscopy images. Relative distribution of EVs in tumor **(B)** and control **(C)** mice. Scale bars: 0.5 μm (ABs), 0.2 μm (SMVs and EXOs).

GENE	PRIMER NAME	SEQUENCE	AMPLICON SIZE
TP53 NM_000546	TP53e7_F	CTTTGAGGTGCGTGTTTGTG	423
	TP53i8_R	caaccaggagccattgtctt	
PTEN NM_000314	PTENe2_F	GCAGAAAGACTTGAAGGCGTA	232
	PTENi2_R	aaatgaactgtatccccctgaa	
MDM2 NM_002392	MDM2i1_F	ctcagAATCATCGGACTCAGG	330
	MDM2i3_R	gctgtgtgaatgcgtcaaat	
MDM4 NM_002393	MDM4i2_F	atcagGTACGACCAAAACTGC	154
	MDM4i3_R	ctgggcaaaagagggagact	
AKT1 NM_001014431	AKT1i12_F	gagggtgtgctgggagtg	163
	AKT1e13_R	CTTGGTCAGGTGGTGTGATG	
AKT3 NM_005465	AKT3i13_F	gccgtggaaacactgaagtaa	183
	AKT3e14_R	GTAGGAAGCCGActgtggac	
CDK4 NM_000075	CDK4i2_F	gggttggtaggcattgagag	211
	CDK4e3_R	TCCACCACTTGTCACCAGAA	
CDKN2A NM_000077	CDKN2Ae2_F	GCACCAGAGGCAGTAACCAT	208
	CDKN2Ai2_R	agggcgatagggagactcag	
ERBB2 NM_004448	erbb2e25_F	CCCTTGGACAGCACCTTCTA	205
	erbb2i25_R	ggtaagcagacagccacaca	
EGFR NM_005228	EGFRi12_F	tgctgtgacccactctgtct	192
	EGFRi13_R	caacgcaaggggattaaaga	
ASCL1 NM_004316	ASCL1i1_F	cctccatctccctctaccac	320
	ASCL1e2_R	GACTCAGGTCCCAGTTGCTC	
MGMT NM_002412	MGMTi3_F	tgtgtagatgcgtttcctgttt	226
	MGMTe4_R	ATTGCTCCTCCCACTGCTC	
RB1 NM_000321	RB1e25_F	GGAAGCAACCCTCCTAAACC	111
	RB1i25_R	ccatctcggctactggaaaa	
PIK3CA NM_006218	PIK3CAe19_F	GGCTCAAAGACAAGAACAAAGG	103
	PIK3CAi19_R	ggaatacacaaacaccgacaga	
IDH1 NM_005896	Idh1i3_F	aggggaatgtctggacctct	245
	Idh1e4_R	TCCGTCACTTGGTGTGTAGG	
IDH2 NM_002168	IDH2e10_F	GAGAAGGTGTGCGTGGAGA	266
	IDH2i10_R	tcagggatggggaggaac	
G3PDH	hmG3PDH_F	ACACACAGTCCATGCCATCAC	450
	hmG3PDH_R	TCCACCACCCTGTTGCTGTA	

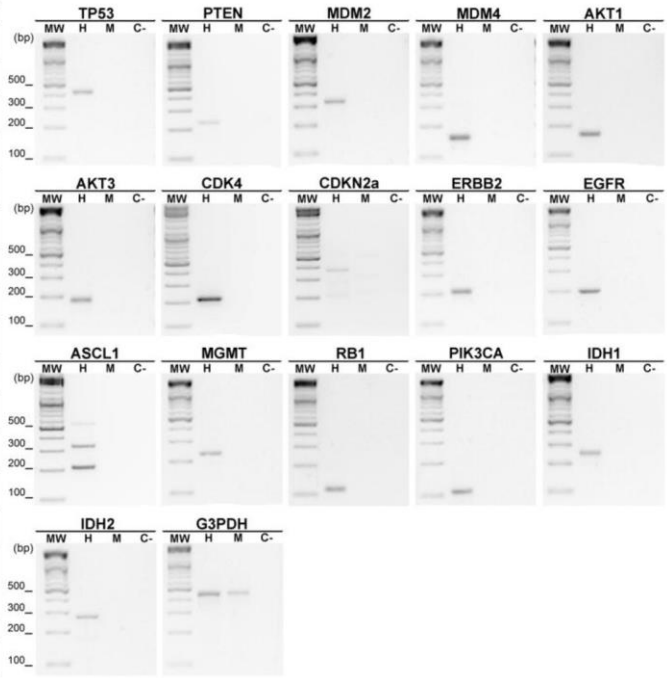

Supplementary Figure S4: Primer set designed using Primer 3 software and band size. Representative PCR products separated on a 1.8% agarose gel; the results show that all specific primers designed yielded amplified sequences of the expected size from human samples (H) but not mouse samples (M). *G3PDH* was the housekeeping gene used as reference in the human and mouse samples.

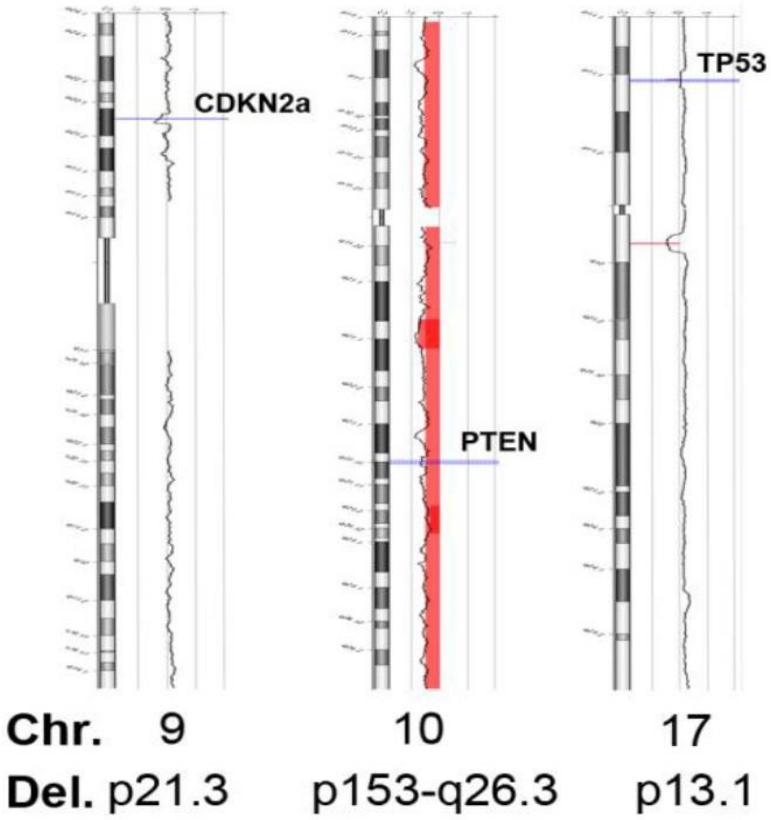

Supplementary Figure S5: Graphical representation of the Chromosomes 9, 10 and 17 of hCSCs culture (GBM27) by Comparative Genomic Hybridisation at passage 1. The figure shows loss of heterozygosity of chromosome 9 at p21.3, chromosome 10 at q23.1, and chromosome 17 at position p13.1, which respectively affect the *CDKN2a*, *PTEN*, and *TP53* locations.

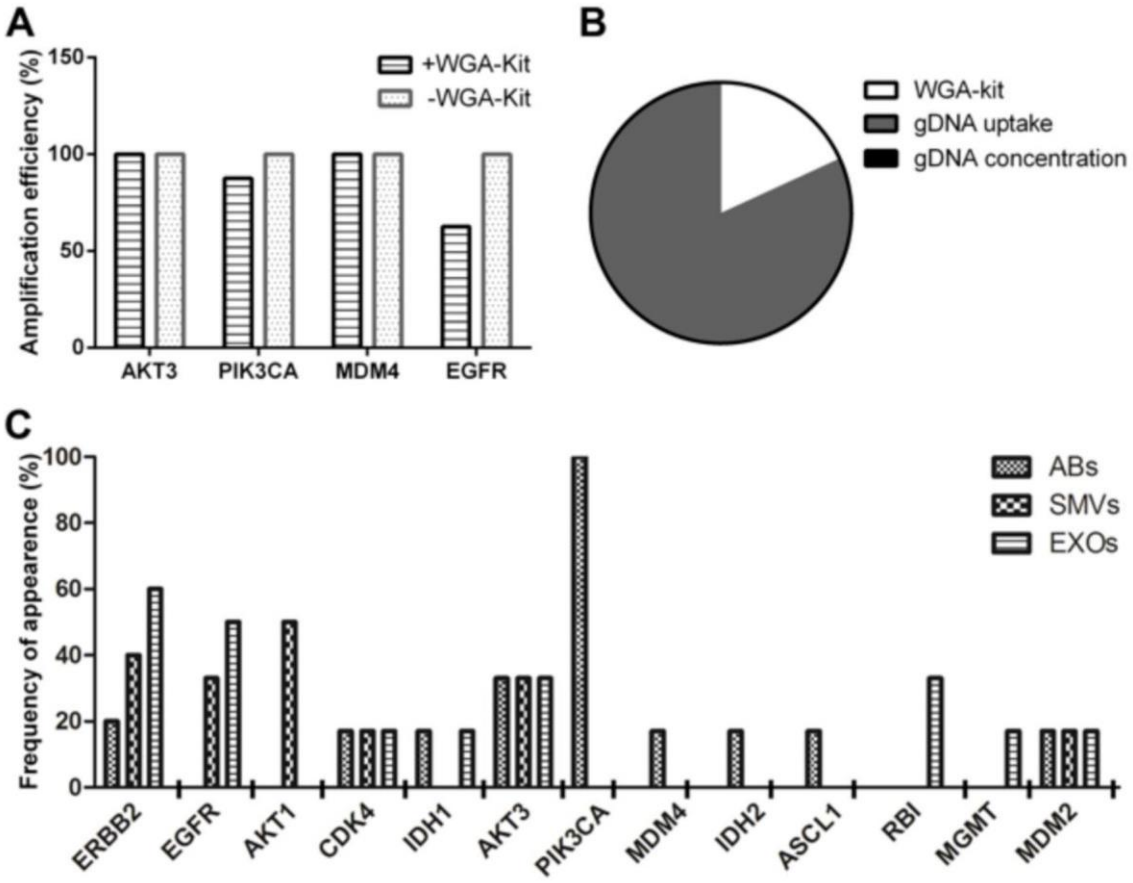

Supplementary Figure S6: Evaluation of DNA pre-amplification variability. A. Comparison of the variability induced with or without pre-amplification of 1 ng μl^{-1} of gDNA from hCSCs, based on PCR analysis of *EGFR*, *AKT3*, *PIK3CA*, and *MDM4* transcripts. **B.** Most of the bias observed appeared to be caused by gDNA uptake (70.4%), followed by the use of the WGA kit (15.6%). **C.** Detection frequency of analyzed sequences in each EVs fraction.

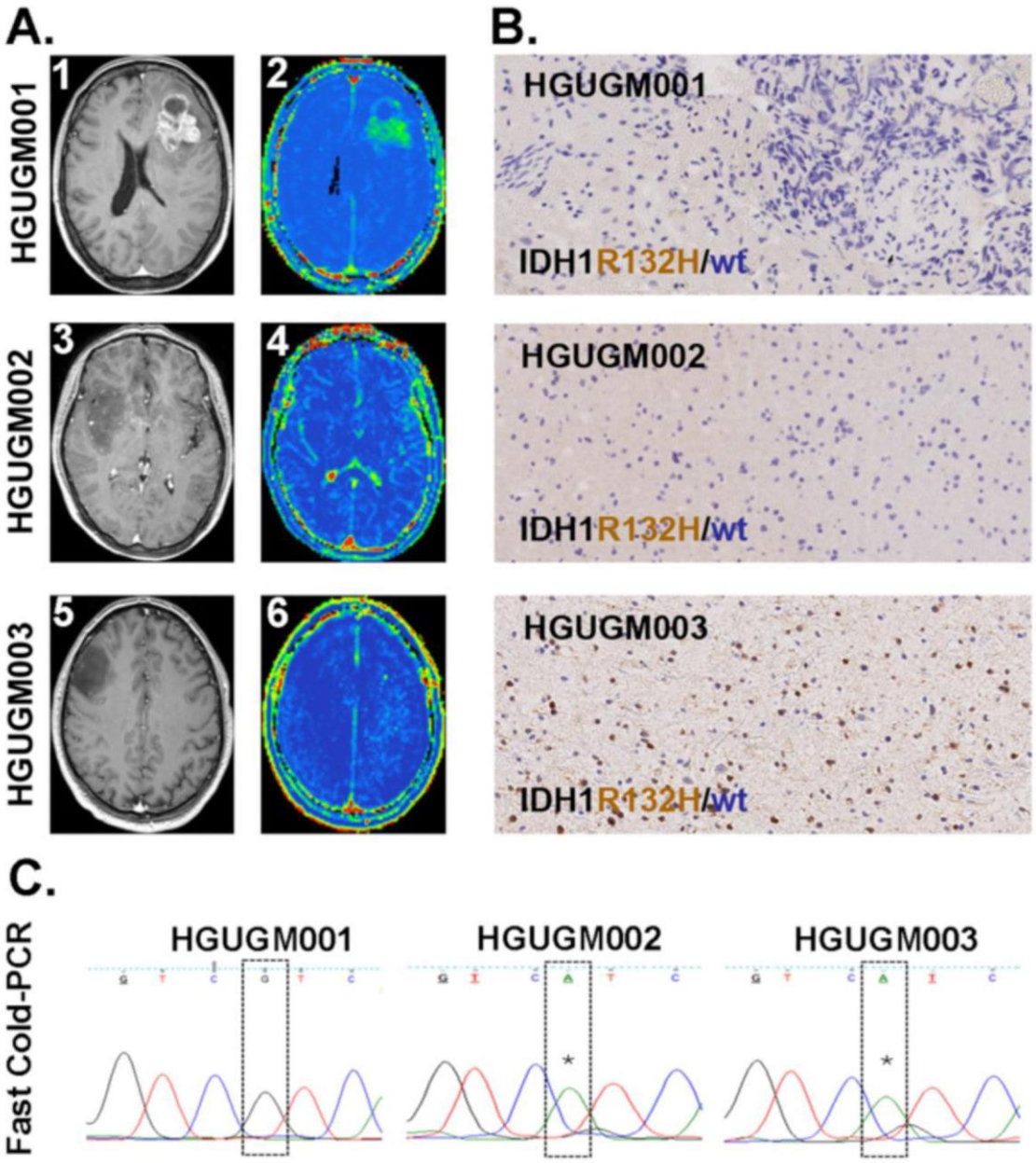

Supplementary Figure S7: Representative results showing the techniques used for the analysis of BBB state as well as the identification of IDH1^{G395A} on human glioma samples by immunohistochemistry and PCR. A. Post-contrast axial T1 weighted MRI of HGUGM001, HGUGM002 and HGUGM003 showing an adenocarcinoma brain metastasis (1) and non-enhancing low-grade gliomas (3 and 5) respectively. Representative K^{trans} maps from HGUGM001 (2), and HGUGM002 and HGUGM003 (4 and 6). Note that vasculature does not appear in these maps, and K^{trans} values in normal brain are insignificant. The K^{trans} values in the grade II tumor (4 and 6) are insignificant corresponding to the lack of enhancement with contrast. K^{trans} values are clearly elevated in peripheral brain metastasis. **B.** Representative IHC results (negative for HGUGM001 and HGUGM002 and positive for HGUGM003) on FFPE samples using a monoclonal antibody against human IDH1^{R132H}. **C.** DNA isolated from tumor-derived EVs extracted from peripheral blood and subjected to Fast ColdPCR. Fast ColdPCR rendered results consistent with those obtained on solid samples. * indicates the mutation G395A.

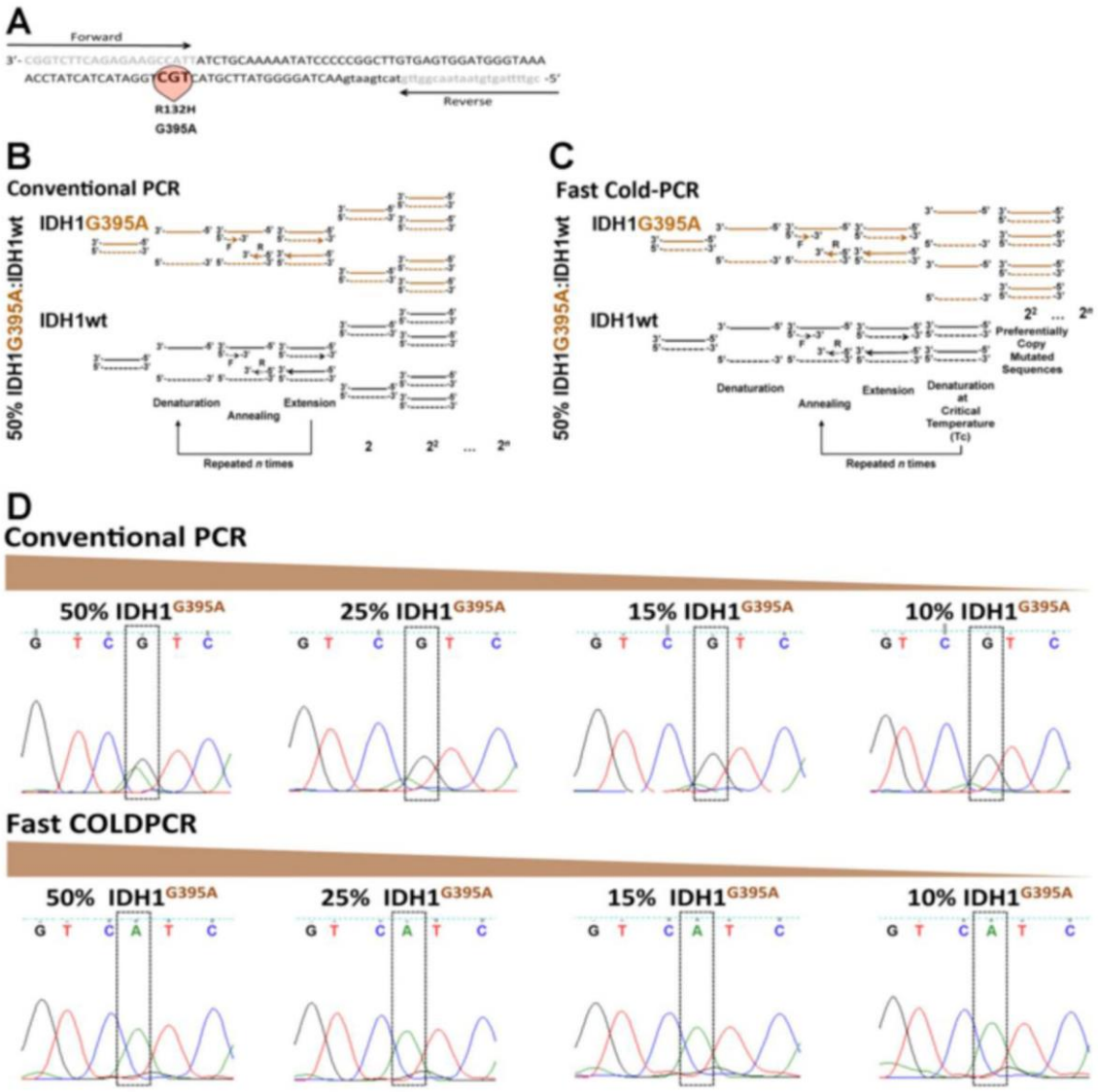

Supplementary Figure S8: Schematic representation of PCR procedures for the detection of IDH1^{G395A} and its identification on human glioma tumor samples. A. Specific primers designed to amplify out a 129 base pair amplicon flanking the 395 position within the human IDH1 genomic DNA sequence were used. For this aim two PCR amplification approaches were performed. **B.** Conventional PCR and **C.** Fast ColdPCR, which preferentially amplifies the mutated sequence. **D.** Conventional PCR was unable to detect and amplify IDH1^{G395A} when the presence of such a gDNA sequence appeared bellow a 50% of total IDH1 sequences. However, fast ColdPCR allowed for the selective enrichment and amplification of IDH1^{G395A} when its relative representation was at least as low as 10% of total IDH1 sequences.


5
Discusión

El glioblastoma es el tumor glial más frecuente y agresivo del SNC. Desafortunadamente, y a pesar del aumento en el número de ensayos clínicos y las mejoras introducidas en los procedimientos de cirugía, como la utilización del ácido aminolevulínico (5-ALA) y la craneotomía del paciente despierto, que han demostrado un aumento en la tasa de resección de hasta el 65% (Young *et al.,* 2015; Díez *et al.,* 2013) no se ha conseguido el aumento de la esperanza de vida de los pacientes, y la resección completa del tumor en muchas ocasiones no se consigue. Este hecho es debido en parte a la capacidad infiltrativa del GBM que provoca una gran diseminación por el parénquima cerebral, por lo que el abordaje clínico sigue en la misma situación de 2005 (protocolo de Stupp), tras el cual el 95% de los pacientes presenta progresión o recurrencia de la enfermedad. Se cree que las principales causas de esta resistencia al tratamiento y de la recidiva vienen dadas por la presencia de CIT residuales en el cerebro (Singh *et al.,* 2004) y por el microambiente tumoral (Borovski *et al.,* 2013).

A su vez, otro factor a tener en cuenta que puede estar influyendo en el poco éxito del abordaje de esta enfermedad es el planteamiento actual de los ensayos *in vitro*. Ya que la mayoría de estudios se llevan a cabo con líneas establecidas, debido a su fácil y rápido crecimiento. Sin embargo, estas líneas rara vez se parecen al tumor de origen, necesitan la presencia de suero en el medio de cultivo para crecer y, además, se caracterizan por presentar un alto número de alteraciones cromosómicas, algunas muy diferentes a las que se encuentran en los tumores gliales (Lee *et al.,* 2006). Por el contrario, las CIT se caracterizan por tener un genotipo y fenotipo bastante similar al del tumor de origen, manteniendo las alteraciones genómicas y las propiedades histopatológicas del tumor de origen e incluso responden de una manera similar al tratamiento (Joo *et al.,* 2013).

Por todos estos motivos, parece que el mejor modelo experimental para estudiar tanto la biología del tumor, como la sensibilidad a determinados fármacos y los posibles mecanismos de resistencia, son las CIT aisladas a partir del tejido tumoral. Sin embargo, estos cultivos primarios también son susceptibles de evolucionar *in vitro*, de igual forma que lo hacen *in vivo*, como han puesto de manifiesto Wakimoto *et al*.,

en los ensayos realizados en siete líneas de CIT derivadas de pacientes con GBM, donde se encontraron una serie de alteraciones que no corresponden con las encontradas en el tejido de origen (Wakimoto *et al.,* 2012). Esta evolución puede suponer un sesgo importante en los resultados obtenidos en ensayos funcionales como la sensibilidad a fármacos, por lo que es fundamental, analizar en profundidad las limitaciones de dicho sistema. En este sentido, partiendo de 20 muestras de tejido, obtuvimos 11 cultivos primarios crecidos en ausencia de suero y suplementando el medio con EGF y bFGF (Lee *et al.,* 2006), esta eficiencia de aislamiento es ligeramente superior a los datos publicados anteriormente en el que lograban aproximadamente un 31-47 % de cultivos primarios procedentes de GBM (Galli *et al.,* 2004). En este contexto, Günther *et al.,* describen 3 grupos de cultivos primarios en función de su patrón de crecimiento (Günther *et al.,* 2008), por esta razón, seleccionamos un representante de cada grupo para los posteriores estudios.

Con el objetivo de cerciorarnos de que la población aislada presentaba características compatibles con CIT, y descartar que fueran células pertenecientes a la población de NSC, realizamos varias aproximaciones. Por un lado, mediante un ensayo de Hibridación Genómica Comparativa (CGH) detectamos aberraciones cromosómicas compatibles con CIT de GBM, como por ejemplo la pérdida de heterocigosidad (LOH) en el cromosoma 10, donde se encuentra PTEN o la duplicación del cromosoma 7, ambas alteraciones con una elevada frecuencia en GBM (Fujisawa et al., 2000). También, observamos la expresión de marcadores de troncalidad, como *Nestin* o *SOX2*, entre otros. Y por último, confirmamos la capacidad de CIT de formar tumores *in vivo* que detallaremos más adelante. En este contexto, también se realizó una caracterización molecular, realizando un análisis de expresión proteogenómica de ciertos marcadores característicos de células madre, de CIT y de marcadores de los tres linajes de células neurales. Todos estos métodos nos permitieron demostrar que la población aislada presentaba características compatibles con CIT. Sorprendentemente, en la línea GBM38 no detectamos expresión de CD133, ni de SSEA-1, que aunque frecuentemente son hallados en CIT de GBM existen evidencias que demuestran que estos marcadores de superficie no son marcadores universales de CIT (Brescia *et al.,*

2012), como indica uno de los trabajos publicados anteriormente, en los que no detectan CD133 en muchos tejidos frescos de GBM (Son et al., 2009). Sin embargo, en la línea GBM38, esta ausencia fue más tarde justificada debido a la LOH encontrada en las posiciones de estos genes. De este modo, podemos indicar que la utilización de marcadores de superficie *per sé*, no constituyen un método suficientemente robusto para la caracterización de CIT, por lo que es conveniente la utilización de otros métodos complementarios como los utilizados en el presente trabajo que aumenten la capacidad de aislar la heterogeneidad de CIT dentro de cada tumor. Tras estas aproximaciones, demostramos que efectivamente las tres líneas seleccionadas para el primer artículo de esta Tesis doctoral tienen características de células iniciadoras de tumor, por lo que decidimos profundizar en la evolución de estas líneas a lo largo de los 20 primeros pases en cultivo.

Consistente con otros trabajos descritos en la bibliografía (Tang *et al.,* 2012), observamos una alta heterogeneidad entre los tres cultivos primarios, sobre todo respecto a inclusiones celulares. Sin embargo, y apoyando al modelo de evolución clonal (Bradshaw *et al.,* 2016), o también conocido como estocástico, la morfología estructural parece mantenerse en todos los pases estudiados dentro de cada neuroesfera, mostrando una gran homogeneidad intra-tumoral. Cabe resaltar que al comparar pases tempranos con tardíos, distinguimos algunos cambios morfológicos comunes a los tres. En este contexto, observamos un aumento en el espacio intercelular de las neuroesferas, así como en la superficie de membrana, a medida que aumentaba el tiempo en cultivo. Suceso que puede estar relacionado con el transporte de oxígeno, nutrientes, y sustancias de desecho, ya que de esta manera, se facilita el acceso de estas moléculas a las células más internas de la esfera. En este contexto, también observamos un mayor número de proyecciones citoplasmáticas en los pases tardíos, así como alteraciones en las crestas de las mitocondrias, algunas de las cuales habían desaparecido o tenían una estructura inusual. Estos cambios estructurales detectados a lo largo de los pases, pueden ser debido al tipo de metabolismo que desarrollan estos cultivos, ya que las mitocondrias de las CIT de glioma producen mayores niveles de ATP y consumen menos glucosa que las células gliales (Vlashi *et al.,*

2011). En base a estos hallazgos, sería interesante realizar un ensayo más profundo para determinar las causas que generan estos cambios y sus consecuencias en la biología de las células tumorales.

Por otro lado, los resultados obtenidos en cuanto a los cambios de expresión génica a lo largo del tiempo, sugieren que al menos durante los 20 primeros pases, los marcadores de diferenciación se mantienen constantes sin ningún cambio destacable. Y de forma general, los genes de células madre y CIT aumentan su expresión significativamente a medida que transcurre el tiempo en cultivo, sugiriendo una preferencia por un estado de indiferenciación. Hasta donde alcanza nuestro conocimiento, éste es el primer trabajo donde se estudia los cambios de expresión de estos marcadores entre distintos pases en cultivo de CIT de GBM. De esta manera, quizás se pudiera favorecer la erradicación del nicho de CIT residuales en el tejido mediante fármacos dirigidos que fuerzen su diferenciación hacia linajes neurales (Vicente-Dueñas *et al.,* 2013).

La existencia de inestabilidad cromosómica en células tumorales, tanto *in vivo* como *in vitro*, como consecuencia tanto de causas intrínsecas como extrínsecas, está ampliamente documentada en la bibliografía (Liang *et al.,* 2010, Lengauger *et al.,* 1998). En este escenario, nosotros demostramos que nuestras condiciones de cultivo no son las responsables de la inestabilidad cromosómica observada en CIT, como se puede observar en las líneas aisladas de NSC y GBM18, que permanecen constantes a lo largo de los pases. Sin embargo, observamos una ligera inestabilidad cromosómica en la línea GBM27 y, en mayor medida, en la línea GBM38, la cual presenta alteraciones en todos los cromosomas. En general, el patrón de alteraciones cromosómicas en estas células, como resultado de eventos frecuentes de inestabilidad cromosómica, está formada por un gran número de deleciones, la mayoría en heterocigosis, que aumenta a medida que se incrementa el tiempo en cultivo. Además, es importante resaltar, que la mayoría de las alteraciones observadas afectan al total de la población, hecho que junto a lo observado a nivel morfológico reafirma el origen clonal. En esta misma línea, Meyer *et al.*, aíslan una variedad de clones distintos procedentes de cuatro pacientes con los que realizan un análisis filogenético, que les permite afirmar que los clones aislados de un mismo tumor son genéticamente más

similares entre ellos que los derivados de otros pacientes (Meyer *et al.,* 2015). Con una aproximación parecida, Piccirillo *et al.,* aislaron dos líneas distintas de CIT procedentes del mismo tumor, y observaron que compartían el mismo patrón cromosómico, a excepción de algunas alteraciones genómicas, lo que de nuevo apuntaba a un origen común (Piccirillo *et al.,* 2009). En este sentido, es interesante resaltar que el estudio individualizado de los clones de CIT derivados de pacientes pueden ayudar a identificar clones con perfiles más agresivos o resistentes, que pueden contribuir a la búsqueda de nuevas terapias o incluso a predecir la respuesta al tratamiento.

En los primeros pases de GBM27 y GBM38 observamos ganancias de ADN que afectaban a menos del 50% de la población, y que se fueron perdiendo a lo largo de los pases en cultivo, lo que apunta a que dentro de una misma población existen varios clones con distinta capacidad para sobrevivir en cultivo o con diferente tasa de proliferación. Todo esto apoya la idea de que las poblaciones de CIT evolucionan tanto *in vivo* como *in vitro*, por lo que nos planteamos si estos cambios se podían traducir en alteraciones funcionales como la viabilidad en cultivo. Inesperadamente, sólo detectamos cambios en la línea GBM18, en la que se observaba un aumento de la viabilidad celular en paralelo con los pases en cultivo. Este hecho, junto con el incremento significativo de la expresión de marcadores de CIT y de indiferenciación en pases tardíos, puede sugerir que, en los primeros pases habría una mayor proporción de células tumorales más diferenciadas y posiblemente, muchas en estado quiescente, mientras que en pases tardíos aumenta la población de células indiferenciadas con mayor tasa de proliferación. Aunque necesitaríamos realizar más estudios para confirmar dicha hipótesis, el modelo jerárquico, en el que sólo las CIT son capaces de replicarse indefinidamente (La Porta *et al.,* 2012), explica en parte nuestras observaciones. Por otro lado, es importante destacar que estudios anteriores han observado patrones de crecimiento muy similares al comparar entre pase 3, 20 y 35 de células aisladas a partir de tejido obtenido de pacientes con GBM (Lee *et al.,* 2006), consistente con lo observado en la línea GBM27 y GBM38 en los que no hay cambios significativos en los tiempos de duplicación. Estas diferencias observadas en el perfil de viabilidad entre distintos pases de un mismo cultivo, deben ser tenidas en cuenta en el diseño experimental de ensayos *in vitro*, donde sería conveniente fijar unas ventanas

de trabajo para disminuir su influencia, dado que utilizar pases muy alejados entre sí, puede afectar de forma notable en el resultado final.

En consonancia con trabajos previos en células de GBM de origen astrocítico (Le Calvé *et al.,* 2010) nosotros observamos una correlación entre los tiempos de duplicación *in vitro* y la tasa de supervivencia al observar el comportamiento de las tres líneas de CIT en cebrero de animales inmunodeprimidos. Este hecho parece indicar que al menos en estas líneas de CIT, el microambiente tumoral no juega un papel decisivo en el perfil de proliferación. Además, al estudiar los patrones de diseminación en el parénquima cerebral, observamos que las tres líneas presentaban patrones diferentes, que sin embargo, eran reproducibles dentro de cada línea, al margen del pase utilizado. En este sentido, en los últimos años se han descrito dos patrones de diseminación de las CIT *in vivo.* El primero, presenta un patrón infiltrativo y diseminado por el parénquima cerebral, con una gran cantidad de células $CD133^{+}$, consistente con el subtipo proneural. Mientras que el segundo, presenta un patrón nodular, con bordes bien definidos y células $CD133^{-}$, mas consistente con el subtipo mesenquimal (Phillips *et al.,* 2006, Günther *et al.,* 2007). Así pues, las líneas analizadas en el presente trabajo encajan perfectamente en estos dos grupos, perteneciendo las GBM38 y GBM18 al subtipo mesenquimal. Y la línea GBM27 al fenotipo proneural. Esta asignación de fenotipos viene dada no solo por sus patrones de diseminación *in vivo*, sino también por la expresión del marcador de linaje *OLIG2* y del marcador CD133. Sin embargo, coincidiendo con la publicación de este artículo, se demostró la presencia de tres fenotipos histopatológicos distintos, en cerebros de ratón xenotrasplantados con CIT de GBM (Bougnaud *et al.,* 2016a). Uno de ellos corresponde al fenotipo denominado *invasivo* en el que las células tumorales invaden tejidos vecinos llegando al hemisferio contralateral, este fenotipo es consistente con lo observado en la línea GBM27. Además, este fenotipo se caracteriza por tener mejor pronóstico, lo que explica nuestros resultados en la gráfica de supervivencia. Otro de los subgrupos ha sido descrito como *angiogénico* en el cual predomina una alta densidad de células en el hemisferio ipsilateral con bordes bien definidos, características coincidentes con las mostradas en la línea GBM38. Y, por último, el fenotipo *intermedio* al que parece pertenecer la línea GBM18.

Al observar más en detalle la línea GBM18 *in vivo*, observamos que las CIT se presentan localizadas junto a las células endoteliales, consistente con trabajos publicados anteriormente en el que observan una asociación entre células $Nestin^{+}/CD133^{+}$ y el endotelio vascular (Calabrese *et al.,* 2007). Dicha asociación puede ser explicada al menos por dos mecanismos. Por un lado, las CIT contribuyen a la estructura vascular diferenciándose a pericitos y favoreciendo así el crecimiento del tumor (Cheng *et al.,* 2013). Por otro lado, la unión entre los ligandos Notch de las células endoteliales y los receptores de las CIT median la activación de la vía de señalización Notch, la cual es necesaria para la auto-renovación de las CIT del tumor (Zhu *et al.,* 2011). Aunque cabe resaltar que en las otras dos líneas estudiadas no se encontró esta asociación, ambas teorías pueden ser las responsables de la aparición de las CIT en el endotelio vascular, lo cual pudiera estar relacionado con el fenotipo característico de cada línea de CIT.

Cabe mencionar que las CIT se han postulado como uno de los mejores modelos para su utilización en programas de búsqueda de nuevos fármacos, así como para estudiar los mecanismos de respuesta a fármacos actualmente en el mercado frente a diferentes tumores (Romaguera-Ros *et al.,* 2012). En este sentido, nuestros resultados muestran importantes fluctuaciones en la respuesta a determinados fármacos, en cada una de las líneas, a lo largo de los pases en cultivo. Cambios que afectan tanto a líneas estables a nivel de alteraciones cromosómicas, como es el caso de GBM18; como líneas con elevada tasa de inestabilidad cromosómica. Estos resultados sugieren que, no solamente alteraciones cromosómicas adquiridas a lo largo de los pases, sino también alteraciones genéticas o epigenéticas, no reflejadas en los anásisis de CGHs, pueden ser responsables de dichas variaciones. Además, estos resultados destacan una importante limitación de los modelos de cultivos primarios de CIT, como es la posibilidad de que alteraciones adquiridas entre pases muy distantes tengan una influencia importante en los resultados de ensayos funcionales.

En resumen, los resultados presentados en el primer artículo de esta memoria muestran que las CIT son el modelo *in vitro* que más se asemeja al tumor de origen. Sin embargo, dicho modelo presenta algunas limitaciones, como la inestabilidad cromosómica a lo largo de los pases en cultivo, que se deben de tener en cuenta a la

hora de utilizarlos como modelos pre-clínicos. Estableciendo siempre unos límites, en cuanto al número de pases celulares, en los diseños experimentales de ensayos funcionales de toxicidad o viabilidad, e incluso al realizar cribado masivo para identificar nuevas dianas terapéuticas.

La mayoría de las determinaciones moleculares en tumores sólidos, se realizan a partir de muestras de tejido fresco, congelado o, más frecuentemente, incluido en bloques de parafina. Estos tejidos son, en muchas ocasiones, las únicas muestras del tumor disponible. Sin embargo, estas muestras presentan dos limitaciones importantes: no representan la totalidad del tumor, y no permiten dar información sobre la evolución del tumor a lo largo del curso de la enfermedad. En este escenario, las biopsias líquidas, principalmente a partir de sangre periférica, van a permitir en un futuro próximo cubrir dichas limitaciones. En sangre periférica encontramos tres compartimentos, que pueden ser utilizados para identificar biomarcadores moleculares de las células tumorales, como son: las CCT, el ADNct y las VEs. En el caso de pacientes con GBM, sólo se han logrado encontrar CCT en porcentajes cercanos al 20% (Müller *et al.,* 2014), y aunque se ha encontrado ADNct de células tumorales en líquido cefalorraquídeo (LCF) (De Mattos *et al.,* 2015), los resultados han sido negativos cuando se ha buscado en sangre periférica (Böhm *et al.,* 2003; De Mattos *et al.,* 2015). Por lo que no hay en la bibliografía evidencias suficientes para determinar que los análisis de ADNct o de CCT sean unas buenas aproximaciones para identificar biomarcadores moleculares en sangre periférica en pacientes diagnosticados con glioma. Por el contrario, con respecto al compartimento de VEs, varios grupos han demostrado la presencia de ácidos nucleicos en los EXOs del sobrenadante de cultivos celulares de líneas de GBM (Balaj *et al.,* 2011) o de sangre periférica de pacientes con glioma (Nilsson *et al.,* 2011; Skog *et al.,* 2008). En consonancia con estos resultados, nosotros hemos demostrado que no solamente en EXOs, sino también en vesículas de Shedding y cuerpos apoptóticos es posible encontrar ADN procedente de las células tumorales productoras *in vitro*, en sobrenadante de CITs. Cabe resaltar la alta variabilidad encontrada al analizar una serie de secuencias de gran relevancia para la biología del GBM, la cual pudiera estar relacionada por el mecanismo, aún desconocido, de entrada de los ácidos nucleicos en el interior de las VEs, o incluso en

algunos casos, por la representación de tales secuencias en las células de origen (Balaj *et al.,* 2011).

En este sentido, hay varios ensayos realizados en animales que demuestran que los EXOs son capaces de alcanzar el cerebro. En uno de ellos, han observado que EXOs cargados con un ARN interferente provocan un silenciamiento en distintas áreas del cerebro de ratones (Álvarez-Erviti *et al.,* 2011). En un modelo animal de pez cebra, en el que vieron que sólo los EXOs derivados de células endoteliales de cerebro eran capaces de atravesar la BHE, sugiriendo que la composición de la membrana vesicular juega un papel importante a la hora de alcanzar el parénquima cerebral (Yang *et al.,* 2015). En la misma línea, detectaron que sólo los EXOs alcanzan el cerebro al ser administrados por vía intranasal, pero no las partículas de mayor tamaño (Zhuang *et al.,* 2011).

Ahora bien, si queremos utilizar el contenido de todas las VEs, aisladas desde sangre periférica, para identificar biomarcadores moleculares de gliomas, una de las cuestiones importantes es verificar que todos los tipos de VEs son capaces de atravesar la BHE, tanto si esta se encuentra intacta, como ocurre en la mayoría de los tumores gliales de bajo grado, como si aparece deteriorada, hecho que se observa en la mayoría de los gliomas de alto grado. En el presente trabajo, hemos descrito dos modelos murinos de gliomas, basados en trasplante ortotópico de CITs humanas, en los que hemos demostrado, mediante la utilización de tres aproximaciones diferentes, que la BHE puede estar intacta (GBM27) o defenestrada (GBM38). Es cierto que, aunque la integridad de la BHE ha sido validada por varios métodos, al cuantificar la concentración de *Evans Blue* presente en los cerebros xenotrasplantados con las CIT del GBM27, detectamos una ligera cantidad de dicho colorante, la cual puede ser debida a trazas del colorante libre o incluso a su presencia en los capilares del cerebro, hechos ya descritos en otros modelos con BHE intacta (Saunder *et al.,* 2015). En este contexto, y como hemos comentado anteriormente, la línea GBM27 puede pertenecer al fenotipo invasivo, el cual se caracteriza por presentar una vasculatura intacta (Bougnaud *et al.,* 2016).

En este sentido, y debido a la dificultad para generar modelos animales de gliomas de bajo grado y a su escasa tasa de éxito de proliferar y reproducir sus características *in vivo* (Huszthy *et al.,* 2012), creemos que la línea GBM27 a pesar de ser aislada de un

glioma de grado IV, posee una de las principales características propias de gliomas de bajo grado, como es la presencia de una BHE intacta.

Así pues, en base a los resultados obtenidos, concluimos que el modelo animal basado en el trasplante ortotópico de GBM27 presentaba las características adecuadas para estudiar la posibilidad de que todos los subtipos de VEs producidas por células del tumor sean capaces de atravesar la BHE intacta y llegar al torrente sanguíneo.

Una de las ventajas que presenta este modelo, es que mediante la amplificación de secuencias de ADNg humano en el interior de las VEs, podemos obtener información de las VEs procedentes del tumor, diferenciándolas, de una manera indirecta, de las secretadas por las células sanas del propio ratón. A este respecto, son muchos los intentos de búsqueda de un marcador específico tumoral presente en la membrana vesicular que permita el aislamiento selectivo de las VEs tumorales (Shao *et al.,* 2012; Hosseini-Beheshti et al., 2012). Sin embargo, todos ellos se basan en la detección de proteínas que, aunque frecuentemente aparecen mutadas o sobre expresadas en el tumor de origen, no necesariamente se encuentran en la membrana de las VEs ni en la totalidad de pacientes diagnosticados con la enfermedad en estudio. Por lo que el modelo animal que presentamos en este trabajo puede ser de gran utilidad para profundizar en todos los aspectos biológicos de las VEs no elucidados hasta el momento. Como son los mecanismos exactos de biogénesis y de secreción de estos tres tipos de VEs o las vías de internalización de los ácidos nucleicos, entre otros.

Con el fin de validar si el aislamiento de las VEs nos puede servir para detectar marcadores en pacientes con glioma, decidimos analizar la secuencia del gen *IDH1*, así como la presencia de la mutación puntual $IDH1^{G395A}$ con alto valor pronóstico. Nuestros resultados muestran que independientemente del estado de la BHE somos capaces de aislar ADNg dentro de las VEs totales procedentes del suero de pacientes con gliomas de bajo y alto grado.

Sin embargo, uno de los grandes inconvenientes que se nos presentó fue la cantidad relativa del alelo minoritario dentro de las VEs. Ya que utilizando el método tradicional de amplificación por reacción en cadena de la polimerasa (PCR), en muchos

de los casos, no éramos capaces de observar dentro de estas VEs la mutación puntual, lo que explicaría los resultados negativos que obtuvieron en anteriores estudios (Chen *et al.,* 2013, De Mattos *et al.,* 2015).

Llegados a este término, existen varias aproximaciones en la literatura para aumentar la sensibilidad de la técnica de amplificación, así como para el enriquecimiento del alelo mutado. Algunas de ellas son: del inglés *BEAMing PCR, Droplet PCR,* o *Cold-PCR* (Wang *et al.,* 2015, Chen *et al.,* 2013, Boisselier *et al.,* 2010). Nosotros, decidimos poner a punto una variante de estas técnicas, del inglés *"Fast Cold-PCR"*, con la que hemos conseguido aumentar la sensibilidad de la amplificación de $IDH1^{G395A}$, obteniendo una concordancia del 100% en las muestras procedentes de pacientes de bajo grado al compararlas con el análisis del tejido, e incluso hemos observado un aumento de dicha mutación en el suero de los pacientes con GBM de la cohorte analizada. Aunque se necesita aumentar el número de pacientes analizados, según nuestros resultados, esta técnica se podría utilizar para detectar otras mutaciones puntuales tanto en muestra sólida como en biopsia líquida.

Otra de las limitaciones existentes respecto al uso de las VEs para la búsqueda de biomarcadores es la cantidad relativa de VEs de interés, es decir; en un paciente oncológico podemos encontrar VEs procedentes de las células del tumor, de las células sanas, y de las células que conforman el microambiente tumoral, por lo que la representación de las tumorales puede variar enormemente. En este sentido, se está ampliando la búsqueda de marcadores que permita diferenciar la procedencia de estas VEs. Un factor a favor, es que la línea somática secreta aproximadamente un número constante de VEs, mientras que si aparecen números elevados de éstas pueden sugerir algún tipo de anomalía.

En base a nuestros resultados, podemos concluir que el análisis de las VEs procedentes de suero refleja mejor la alta heterogeneidad intra-tumoral que presentan estos gliomas y que, sin embargo, no es detectable en la gran mayoría de los casos por los métodos tradicionales en la biopsia sólida. Además, nuestros resultados revelan que el análisis del contenido genómico de las VEs puede ayudar a la hora del diagnóstico del paciente pudiendo detectar la mutación $IDH1^{G395A}$ mediante un método minimamente

invasivo. Lo que supone una gran diferencia respecto a lo publicado anteriormente en el que analizan secuencias procedentes del LCF (Akers *et al.,* 2013, De Mattos *et al.,* 2015) con los riesgos que ello conlleva debido a la alta presión intracraneal que sufren estos pacientes y al potencial riesgo de herniación cerebral (Kong *et al.,* 2015). En este contexto, sería interesante realizar análisis comparativos de las dos técnicas en paralelo para demostrar su sensibilidad y efectividad.

Así mismo, en la práctica clínica el análisis de VEs procedentes de suero puede también ser útil durante el transcurso de la enfermedad para observar las posibles variaciones del patrón genético del tumor y ver marcadores afectados por el tratamiento que han seguido estos pacientes. Además, pueden apoyar a las técnicas de imagen en las que en ocasiones no se clarifica la progresión del tumor tras el tratamiento con RT al confundirlo con radionecrosis.

En definitiva, a lo largo de la presente Tesis doctoral, hemos demostrado que, aunque las CIT aisladas de pacientes diagnosticados con GBM, son el mejor modelo *in vitro* para el estudio de estos tumores. Dichas células son susceptibles de evolucionar en cultivo y pueden presentar eventos de inestabilidad cromosómica, así como cambios en la respuesta a distintos fármacos. Por lo que sería conveniente establecer un número limitado de pases en cultivo a la hora de utilizarlos como modelos pre-clínicos.

Además, hemos comprobado que las VEs son capaces de atravesar la BHE intacta y llegar al torrente sanguíneo en nuestro modelo de CIT xenotrasplantadas en ratones inmunodeprimidos. El ADNg que contienen estas VEs permite distinguir las VEs procedentes del tumor de las del propio ratón, por lo que esta metodología indirecta se presenta como una buena aproximación para profundizar en el conocimiento de estas VEs. En este sentido, también hemos demostrado, en una cohorte de pacientes con gliomas de bajo y alto grado, que la búsqueda de biomarcadores en estas VEs se presenta como un método minimamente invasivo que puede ser de gran utilidad para el diagnóstico, pronóstico y el seguimiento de los pacientes.


6
Conclusiones

CONCLUSIONES

1. Los cultivos primarios de CIT aisladas de pacientes diagnosticados con GBM son susceptibles de sufrir eventos de intestabilidad cromosómica a lo largo de los pases en cultivo.
2. Los cultivos primarios de CIT aisladas de pacientes diagnosticados con GBM presentan fluctuaciones importantes en el perfil de viabilidad *in vitro* y en su patrón de respuesta a fármacos, por lo que es necesario establecer un número limitado de pases en cultivo para su estudio.
3. Los cultivos primarios de CIT xenotrasplantados en un modelo animal inmunodeprimido mantienen el mismo fenotipo y patrón de diseminación que el observado en el tumor de origen, por lo que se presentan como el mejor modelo pre-clínico para el estudio de la biología del GBM.
4. El modelo animal generado por las CIT del GBM27 presenta una BHE intacta, característica de los gliomas de bajo grado, por lo que se presenta como un buen modelo para estudiar la posibilidad de las VEs de atravesar la BHE y aparecer en el torrente sanguíneo.
5. Los tres tipos de VEs: ABs, SMVs y EXOs atraviesan la BHE independentemente de su integridad y llegan al torrente sanguíneo, transportando en su interior ADNg del tumor, lo que supone un método no invasivo para la búsqueda de biomarcadores.
6. La utilización de la técnica de amplificación *Fast Cold-PCR* aumentó la sensibilidad de detección de la mutación puntual con alto valor clínico *IDH1*^{G395A} en el ADNg aislado de las VEs en una cohorte de pacientes con gliomas de alto y bajo grado.
7. La detección de la secuencia *IDH1*^{G395A} en el interior de las VEs aisladas de sangre periférica de pacientes se presenta como uno de los mejores métodos no invasivos de biopsia líquida.

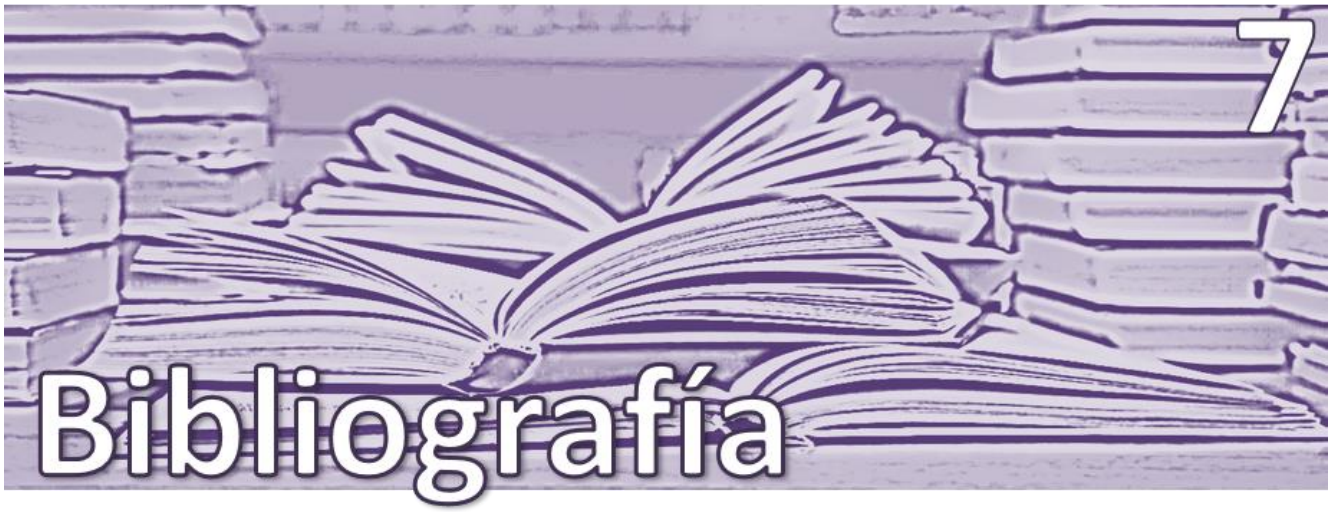
7
Bibliografía

1. Akers JC, Ramakrishnan V, Kim R, et al. miR-21 in the Extracellular Vesicles (EVs) of Cerebrospinal Fluid (CSF): A Platform for Glioblastoma Biomarker Development. PLoS One. 2013; 8: 1–13.
2. Alamgeer M, Peacock CD, Matsui W, et al. Cancer stem cells in lung cancer: Evidence and controversies. Respirology. 2013; 18: 757–64.
3. Andreola G, Rivoltini L, Castelli C, et al. Induction of lymphocyte apoptosis by tumor cell secretion of FasL-bearing microvesicles. J Exp Med 2002; 195:1303-1316.
4. Antunes L, Angioi-Duprez KS, Bracard SR, et al. Analysis of tissue chimerism in nude mouse brain and abdominal xenograft models of human glioblastoma multiforme: what does it tell us about the models and about glioblastoma biology and therapy? J Histochem Cytochem. 2000; 48: 847–58.
5. Arienti G, Carlini E, Saccardi C, et al. Role of human prostasomes in the activation of spermatozoa. J Cell Mol Med. 2004; 8: 77–84.
6. Asea A, Jean-Pierre C, Kaur P, et al. Heat shock protein-containing exosomes in mid-trimester amniotic fluids. J Reprod Immunol. 2008; 79: 12–7.
7. Ashcroft BA, De Sonneville J, Yuana Y, et al. Determination of the size distribution of blood microparticles directly in plasma using atomic force microscopy and microfluidics. Biomed Microdevices. 2012; 14: 641–9.
8. Balaj L, Lessard R, Dai L, et al. Tumour microvesicles contain retrotransposon elements and amplified oncogene sequences. Nat. Comm; 2011; 2: 180.
9. Barteneva, Fasler-Kan E, Bernimoulin M, et al. Circulating microparticles: square the circle. BMC Cell Biology. 2013; 14:23.
10. Bhatnagar S, Shinagawa K, Castellino FJ, et al. Exosomes released from macrophages infected with intracellular pathogens stimulate a proinflammatory response in vitro and in vivo. Blood. 2007;110(9):3234-3244.
11. Böhm C, Wassmann H, Paulus W. No evidence of tumour cells in blood of patients with glioma. Mol Pathol. 2003; 56: 187–9.
12. Boisselier B, Marie Y, Labussière M. COLD PCR HRM: a highly sensitive detection method for IDH1 mutations. Hum Mutat. 2010;31(12):1360-5.
13. Bolukbasi M, Mizrak A, Ozdener G, et al. miR-1289 and “Zipcode”-like Sequence Enrich mRNAs in Microvesicles. Molecular Therapy–Nucleic Acids. 2012; 1, e10.
14. Borovski T, Verhoeff J, ten Cate R, et al. Tumor microvasculature supports proliferation and expansion of glioma-propagating cells. Int. J. Cancer. 2009; 125(5):1222–1230.

15. Bougnaud S, Golebiewska A, Oudin A, et al. Molecular crosstalk between tumour and brain parenchyma instructs histopathological features in glioblastoma. Oncotarget. 2016; 7 (22):31955-31971.
16. Bradshaw A, Wickremsekera A, Tan ST, et al. Cancer Stem Cell Hierarchy in Glioblastoma Multiforme. Front Surg. 2016; 3: 21.
17. Bray, F. et al., 2012. Global cancer transitions according to the Human Development Index (2008-2030): A population-based study. The Lancet Oncology. 2012; 13(8), pp.790–801.
18. Brescia P, Richichi C, Pelicci G. Current strategies for identification of glioma stem cells: Adequate or unsatisfactory? J Oncol. 2012; 2012.
19. Buschow S, Nolte-'t Hoen E, van Niel G, et al. MHC II in dendritic cells is targeted to lysosomes or T cell-induced exosomes via distinct multivesicular body pathways. Traffic. 2009; 10, 1528– 1542.
20. Calabrese C, Poppleton H, Kocak M et al. A perivascular niche for brain tumor stem cells. Cancer Cell. 2007; 11(1):69-82.
21. Chargaff E, West R. The biological significance of the thromboplastic protein of blood. J Biol Chem. 1946; 166:189–97.
22. Chen WW, Balaj L, Liau LM, et al. BEAMing and Droplet Digital PCR Analysis of Mutant IDH1 mRNA in Glioma Patient Serum and Cerebrospinal Fluid Extracellular Vesicles. Mol Ther Nucleic Acids. 2013; 2: e109.
23. Cheng L, Huang Z, Zhou W, et al. Glioblastoma stem cells generate vascular pericytes to support vessel function and tumor growth. Cell. 2013; 153: 139–152.
24. Chiasserini D, Van Weering JRT, Piersma SR, Pham T V., Malekzadeh A, Teunissen CE, De Wit H, Jiménez CR. Proteomic analysis of cerebrospinal fluid extracellular vesicles: A comprehensive dataset. J Proteomics. 2014; 106: 191–204.
25. Christensen BC, Smith AA, Zheng S, et al. DNA methylation, isocitrate dehydrogenase mutation, and survival in glioma. J Natl Cancer Inst. 2011; 103: 143–53.
26. Clayton A, Mitchell JP, Court J, et al. Human tumor-derived exosomes down-modulate NKG2D expression. J Immunol. 2008; 180:7249-58
27. Cohen A, Holmen S, Colman H. IDH1 and IDH2 Mutations in Gliomas. Curr Neurol Neurosci Rep. 2013; 13(5): 345.
28. Collins J, Schandi C, Young K, et al. Major DNA fragmentation is a late event in apoptosis. J Histochem Cytochem. 1997; 45 (7): 923-34.
29. Crea F, Danesi R, Farrar WL. Cancer stem cell epigenetics and chemoresistance. Epigenomics. 2009; 1: 63–79.
30. Crocetti E, Trama A, Stiller C, et al. Epidemiology of glial and non-glial brain tumours in Europe. Eur J Cancer. 2012; 48: 1532–42.

31. Cvjetkovic A, Chul Jang S, Konečná B, et al. Detailed Analysis of Protein Topology of Extracellular Vesicles–Evidence of Unconventional Membrane Protein Orientation. Scientific Reports. 2016; 36338.
32. Dalton AJ. Microvesicles and vesicles of multivesicular bodies versus "virus-like" particles. J Natl Cancer Inst. 1975; 54: 1137–48.
33. De Mattos-Arruda L, Mayor R, Ng CKY, et al. Cerebrospinal fluid-derived circulating tumour DNA better represents the genomic alterations of brain tumours than plasma. Nat Commun. 2015; 6: 8839.
34. Deregibus MC, Cantaluppi V, Calogero R, et al. Angiogenic program in endothelial cells by a horizontal transfer of mRNA Endothelial progenitor cell – derived microvesicles activate an angiogenic program in endothelial cells by a horizontal transfer of mRNA. 2012; 110: 2440–8.
35. Di Trapani M, Bassi G, Midolo M, et al. Differential and transferable modulatory effects of mesenchymal stromal cell-derived extracellular vesicles on T, B and NK cell functions. Sci Rep. 2016; 6: 24120.
36. Dick JE. Looking ahead in cancer stem cell research. Nat Biotechnol. 2009; 27:44–6.
37. Díez R, Slof J, Galván J. Estudio observacional retrospectivo sobre la efectividad del ácido 5-aminolevulínico en la cirugía de los gliomas malignos en España (Estudio VISIONA). 2013; Neurología – 506.
38. Do J, Foster D, Renier C, et al. Ex vivo Evans blue assessment of the blood brain barrier in three breast cancer brain metastasis models. Breast Cancer Res Treat. 2014; 144: 93–101.
39. EL Andaloussi S, Mäger I, Breakefield XO, et al. Extracellular vesicles: biology and emerging therapeutic opportunities. Nat Rev Drug Discov. 2013; 12: 347–57.
40. Fendl B, Weiss R, Fischer MB, et al. Characterization of extracellular vesicles in whole blood: Influence of pre-analytical parameters and visualization of vesicle-cell interactions using imaging flow cytometry. Biochem Biophys Res Commun. 2016; 478: 168–73.
41. Fujisawa H, et al. Loss of heterozygosity on chromosome 10 is more extensive in primary (de novo) than in secondary glioblastomas. Lab Invest. 2000; 80(1):65–72.
42. Galli R, Binda E, Orfanelli U, et al. Isolation and Characterization of Tumorigenic, Stem-like Neural Precursors from Human Glioblastoma. Cancer Res. 2004; 64: 7011–21.
43. Gan HK, Cvrljevic AN, Johns TG. The epidermal growth factor receptor variant III (EGFRvIII): Where wild things are altered. FEBS J. 2013; 280: 5350–70.
44. Graner M, Alzate O, Dechkovskaia A. et al. Proteomic and immuno- logic analyses of brain tumor exo- somes. FASEB J. 2009; 23, 1541–1557.

45. Gudinaviciene I, Pranys D, Juozaityte E, et al. Impact of morphology and biology on the prognosis of patients with gliomas Medicina (Kaunas). 2004; 40:112-20.
46. Guescini M, Genedani S, Stocchi V, et al. Astrocytes and Glioblastoma cells release exosomes carrying mtDNA. J Neural Transm. 2010; 117: 1–4.
47. Günther HS, Schmidt NO, Phillips HS, et al. Glioblastoma-derived stem cell-enriched cultures form distinct subgroups according to molecular and phenotypic criteria. Oncogene. 2008; 27: 2897–909.
48. Halicka HD, Bedner E, Darzynkiewicz Z. Segregation of RNA and Separate Packaging of DNA and RNA in Apoptotic Bodies during Apoptosis. Exp Cell Res. 2000; 260: 248–56.
49. Hamilton J, Rapp M, Schneiderhan M, et al. Glioblastoma Multiforme Metastasis Outside the CNS: Three Case Reports and Possible Mechanisms of Escape. Journal of Clinical Oncology. 2014; pp e80-e84.
50. Hannafon B, Ding WQ. Intercellular Communication by Exosome-Derived microRNAs in Cancer. *Int. J. Mol. Sci.* 2013, *14*(7), 14240-14269.
51. Hasselmann D, Rappl G, et al. Extracellular tyrosinase mRNA within apoptotic bodies is protected from degradation in human serum. Clinical Chemistry. 2001; 47 (8): 1488.
52. Hawkins BT, Davis TP. The Blood-Brain Barrier / Neurovascular Unit in Health and Disease. Pharmacol Rev. 2005; 57: 173–85.
53. Hosseini-Beheshti E, Pham S, Adomat H, et al. Exosomes as biomarker enriched microvesicles: Characterization of exosomal proteins derived from a panel of prostate cell lines with distinct AR phenotypes. Mol Cell Proteomics. 2012;11: 863-85.
54. Hong C-S, Muller L, Whiteside TL, Boyiadzis M. Plasma exosomes as markers of therapeutic response in patients with acute myeloid leukemia. Front Immunol. 2014; 5: 160.
55. Huber V, Filipazzi P, Iero M, et al. More insights into the immunosuppressive potential of tumor exosomes. J Transl Med. 2008; 6: 63.
56. Huszthy P, Daphu I, Niclou S, et al. In vivo models of primary brain tumors: pitfalls and perspectives. Neuro Oncol. 2012; 14(8): 979–993.
57. Jagtap P, Szabo C. Poly(ADP-ribose) polymerase and the therapeutic effects of its inhibitors. Nat Rev Drug Discov. 2005; 4:421–40.
58. Jayachandran M, Miller VM, Heit JA, et al. Methodology for isolation, identification and characterization of microvesicles in peripheral blood. J Immunol. 2012; 375: 207–14.
59. Joo KM, Kim J, Jin J, et al. Patient-Specific Orthotopic Glioblastoma Xenograft Models Recapitulate the Histopathology and Biology of Human Glioblastomas In Situ. Cell Rep. The Authors; 2013; 3: 260–73.

60. Kahlert C, Melo SA, Protopopov A, et al. Identification of doublestranded genomic dna spanning all chromosomes with mutated KRAS and P53 DNA in the serum exosomes of patients with pancreatic cancer. J Biol Chem. 2014; 289: 3869–75.
61. Kalra H, Drummen GPC, Mathivanan S. Focus on extracellular vesicles: Introducing the next small big thing. Int J Mol Sci. 2016; 17.
62. Kalra H, Simpson RJ, Ji H, et al. Vesiclepedia: A Compendium for Extracellular Vesicles with Continuous Community Annotation. PLoS Biol. 2012; 10: 8–12.
63. Koliha N, Wiencek Y, Heider U, et al. A novel multiplex bead-based platform highlights the diversity of extracellular vesicles. *Journal. Extracellular Vesicles. 2016; (*5) 29975.
64. Kong X, Wang Y, Liu S, et al. Stem and Entire Spinal Leptomeningeal Dissemination of Supratentorial Glioblastoma Multiforme in a Patient during Postoperative Radiochemotherapy: Case Report and Review of the Literatures. Medicine (Baltimore). 2015; 94: e962.
65. La Porta CAM, Zapperi S, Sethna JP. Senescent cells in growing tumors: Population dynamics and cancer stem cells. PLoS Comput Biol. 2012; 8.
66. Lakhal S, Wood MJA. Exosome nanotechnology: An emerging paradigm shift in drug delivery: Exploitation of exosome nanovesicles for systemic in vivo delivery of RNAi heralds new horizons for drug delivery across biological barriers. BioEssays. 2011; 33: 737–41.
67. Laks DR, Visnyei K, Kornblum HI. Brain tumor stem cells as therapeutic targets in models of glioma. Yonsei Med J. 2010; 51: 633–40.
68. Lázaro-Ibáñez E, Sanz-Garcia A, Visakorpi T, et al. Different gDNA content in the subpopulations of prostate cancer extracellular vesicles: Apoptotic bodies, microvesicles, and exosomes. Prostate. 2014; 74: 1379–90.
69. Le Calvé B, Rynkowski M, Le Mercier M, et al. Long-term In Vitro Treatment of Human Glioblastoma Cells with Temozolomide Increases Resistance In Vivo through Up-regulation of GLUT Transporter and Aldo-Keto Reductase Enzyme AKR1C Expression. Neoplasia. 2010; 12(9): 727-739.
70. Le Pecq JB. Dexosomes as a therapeutic cancer vaccine: from bench to bedside. Blood Cells Mol Dis. 2005; 35(2):129-35.
71. Lee HM, Choi EJ, Kim JH, et al. A membranous form of ICAM-1 on exosomes efficiently blocks leukocyte adhesion to activated endothelial cells. Biochem Biophys Res Commun. 2010; 397:251–256.
72. Lee J, Kotliarova S, Kotliarov Y, et al. Tumor stem cells derived from glioblastomas cultured in bFGF and EGF more closely mirror the phenotype and genotype of primary tumors than do serum-cultured cell lines. Cancer Cell. 2006; 9: 391–403.

73. Lee JK, Young Jang J, Kyung Jeon Y, et al., Extracellular Vesicles as an Emerging Paradigm of Cell-to-Cell Communication in Stem Cell Biology. J Stem Cell Res Ther. 2014, 4:5.
74. Lee TH, D'Asti E, Magnus N, et al. Microvesicles as mediators of intercellular communication in cancer-the emerging science of cellular "debris." Semin Immunopathol. 2011; 1–13.
75. Lengauer C, Kinzler KW, Vogelstein B. Genetic instabilities in human cancers. Nature. 1998; 396: 643–9.
76. Leonardi R, Subramanian C, Jackowski S, et al. Cancer-associated isocitrate dehydrogenase mutations inactivate NADPH-dependent reductive carboxylation. J Biol Chem. 2012; 287: 14615–20.
77. Leten C, Struys T, Dresselaers T, et al. In vivo and ex vivo assessment of the blood brain barrier integrity in different glioblastoma animal models. J Neurooncol. 2014; 119: 297–306.
78. Liang Y, Zhong Z, Huang Y, et al. Stem-like cancer cells are inducible by increasing genomic instability in cancer cells. J Biol Chem. 2010; 285: 4931–40.
79. Losman JA, Kaelin WG. What a difference a hydroxyl makes: Mutant IDH, (R)-2-hydroxyglutarate, and cancer. Genes Dev. 2013; 27: 836–52.
80. Louis DN, Perry A, Reifenberger G et al. The 2016 World Health Organization Classification of Tumors of the Central Nervous System: a summary. Acta Neuropathol. 2016; 131:803–20.
81. Luissint AC, Artus C, Glacial F, et al. Tight junctions at the blood brain barrier: physiological architecture and disease-associated dysregulation. Fluids Barriers CNS. 2012; 9: 23.
82. Manterola L, Guruceaga E, Pérez-Larraya JG, et al. A small noncoding RNA signature found in exosomes of GBM patient serum as a diagnostic tool. Neuro Oncol. 2014; 16: 520–7.
83. Martin-Villalba A, Okuducu AF, von Deimling A, et al. The evolution of our understanding on glioma. Brain Pathol. 2008; 18:455–63.
84. Marzesco A-M, Janich P, Wilsch-Bräuninger M, et al. Release of extracellular membrane particles carrying the stem cell marker prominin-1 (CD133) from neural progenitors and other epithelial cells. J Cell Sci. 2005; 118: 2849–58.
85. Mathivanan S, Ji H, Simpson RJ. Exosomes: Extracellular organelles important in intercellular communication. J Proteomics. 2010; 73: 1907–20.
86. Melo S., Luecke LB, Kahlert C, et al. Glypican-1 identifies cancer exosomes and detects early pancreatic cancer. Nature. 2015; 523: 177–82.
87. Meyer M, Reimand J, Lan X, et al. Single cell-derived clonal analysis of human glioblastoma links functional and genomic heterogeneity. Proc Natl Acad Sci. 2015; 112: 851–6.

88. Milasan A, Tessandier N, Tan S, Brisson A, Boilard E, Martel C. their level differs in atherosclerosis. 2016; 1: 1–9.
89. Minciacchi V, Sungyong You1, Cristiana Spinelli C, et al. Large oncosomes contain distinct protein cargo and represent a separate functional class of tumor-derived extracellular vesicles. Oncotarget; 2015; (6):13.
90. Momen-Heravi F, Balaj L, Alian S, et al. Current methods for the isolation of extracellular vesicles. Biol Chem. 2013; 394: 1253–62.
91. Müller C, Holtschmidt J, Auer M, et al. Hematogenous dissemination of glioblastoma multiforme. 2014; 6: 1–10.
92. Muralidharan-Chari V, Clancy J, Sedgwick A, et al. Microvesicles: mediators of extracellular communication during cancer progression. Journal of Cell Science. 2010; 123 (10): 1603-1611.
93. Nilsson RJA, Balaj L, Hulleman E, et al. Blood platelets contain tumor-derived RNA biomarkers. Blood. 2011; 118: 3680–3.
94. Noerholm M, Balaj L, Limperg T, et al. RNA expression patterns in serum microvesicles from patients with glioblastoma multiforme and controls. BMC Cancer. BioMed Central Ltd; 2012; 12: 22.
95. Ohgaki H, Peraud A, Nakazato Y, et al. Giant cell glioblastoma. In: Kleihues P, Cavenee WK, editors. World Health Organization Classification of Tumours: Pathology and Genetics of Tumours of the Nervous System. Lyon, France: IARC Press; 2000. pp. 40–41.
96. Ostrom QT, Bauchet L, Davis FG et al. The epidemiology of glioma in adults: A state of the science review. Neuro Oncol. 2014; 16:896–913.
97. Ostrom QT, Gittleman H, De Blank PM, et al. American Brain Tumor Association Adolescent and Young Adult Primary Brain and Central Nervous System Tumors Diagnosed in the United States in 2008-2012. Neuro Oncol. 2015; 18: i1–50.
98. Ostrom QT, Gittleman H, Farah P et al. NEURO-ONCOLOGY CBTRUS Statistical Report : Primary Brain and Central Nervous System Tumors Diagnosed in the United States in 2006-2010. 2013.
99. Patel AP, Tirosh I, Trombetta JJ, et al. Single-cell RNA-seq highlights intratumoral heterogeneity in primary glioblastoma. Science. 2014; 344: 1396–401.
100. Petty MA, Lo EH. Junctional complexes of the blood-brain barrier: Permeability changes in neuroinflammation. Prog Neurobiol. 2002; 68: 311–23.
101. Phillips HS, Kharbanda S, Chen R, et al. Molecular subclasses of high-grade glioma predict prognosis, delineate a pattern of disease progression, and resemble stages in neurogenesis. Cancer Cell. 2006; 9: 157–73.
102. Piccin A, Murphy WG, Smith OP. Circulating microparticles: pathophysiology and clinical implications. Blood Rev. 2007. 21:157–171.

103. Piccirillo SGM, Combi R, Cajola L, et al. Distinct pools of cancer stem-like cells coexist within human glioblastomas and display different tumorigenicity and independent genomic evolution. Oncogene. 2009; 28: 1807–11.
104. Pietras, A. Cancer stem cells in tumor heterogeneity. Advances in cancer research. 2011; 112, 256.
105. Pointer K, Clark P, Zorniak M, et al. 2014. Glioblastoma Cancer Stem Cells: Biomarker and Therapeutic Advances. Neurochem Int. 2014; 71: 1–7.
106. Pollard SM, Yoshikawa K, Clarke ID, et al. Glioma Stem Cell Lines Expanded in Adherent Culture Have Tumor-Specific Phenotypes and Are Suitable for Chemical and Genetic Screens. Cell Stem Cell. 2009; 4: 568–80.
107. Reitman ZJ, Yan H. Isocitrate dehydrogenase 1 and 2 mutations in cancer: Alterations at a crossroads of cellular metabolism. J Natl Cancer Inst. 2010; 102: 932–941.
108. Revenfeld ALS, Bæk R, Nielsen MH, et al. Diagnostic and prognostic potential of extracellular vesicles in peripheral blood. Clin Ther. Elsevier; 2014; 36: 830–46.
109. Romaguera-Ros M, Peris-Celda M, Oliver-De La Cruz J, et al. Cancer-initiating enriched cell lines from human glioblastoma: preparing for drug discover assays. Stem Cell Rev. 2012; 8(1):288-98
110. Ronquist G, Brody I. The prostasome: its secretion and function in man. Biochim Biophys Acta. 1985; 822:203–218.
111. Rupp A, Rupp C, Keller S et al. Loss of EpCAM expression in breast cancer derived serum exosomes: role of proteolytic cleavage. Gynecologic Oncology. 2011; (2). 437–446, 2.
112. Ryan R, Booth S, Price S. Corticosteroid-use in primary and secondary brain tumour patients: a review. J Neurooncol. 2012; 106(3):449-59.
113. Sanson M, Marie Y, Paris S, et al., Isocitratedehydrogenase 1 codon 132 mutation is an important prognostic biomarker in gliomas. Journal of Clinical Oncology. 2009; (25):4150– 4154.
114. Saunders N, Dziegielewska K, Møllgård K, et al. Markers for blood-brain barrier integrity: How appropriate is Evans blue in the twenty-first century and what are the alternatives? Front Neurosci. 2015; 9: 1–16.
115. Shao H, Chung J, Balaj L, et al. Protein typing of circulating microvesicles allows real-time monitoring of glioblastoma therapy. Nat.Medicine. 2012; 10: 1470–6.
116. Shelke GV, Lässer C, Gho YS, et al. Importance of exosome depletion protocols to eliminate functional and RNA-containing extracellular vesicles from fetal bovine serum. J Extracell vesicles. 2014; 3: 1–8.

117. Shet AS, Aras O, Gupta K et al. Sickle blood contains tissue factor-positive microparticles derived from endothelial cells and monocytes. Blood.2003 102:2678–2683.
118. Singh SK, Hawkins C, Clarke ID, et al. Identification of human brain tumour initiating cells. Nature. 2004; 432: 396–401.
119. Skog J, Würdinger T, van Rijn S, et al. Glioblastoma microvesicles transport RNA and proteins that promote tumour growth and provide diagnostic biomarkers. Nat Cell Biol. 2008; 10: 1470–6.
120. Smith JS, Perry A, Borell TJ. Alterations of chromosome arms 1p and 19q as predictors of survival in oligodendrogliomas, astrocytomas, and mixed oligoastrocytomas. J Clin Oncol. 2000; 18(3):636-45.
121. Son MJ, Woolard K, Nam D, et al. SSEA-1 is an enrichment marker for tumor-initiating cells in human glioblastoma. Cell StemCell. 2009; 4, (5): 440– 452.
122. Sottoriva A, Spiteri I, Piccirillo SGM, et al. Intratumor heterogeneity in human glioblastoma reflects cancer evolutionary dynamics. Proc Natl Acad Sci. 2013; 110: 4009–14.
123. Stancheva G, Goranova T, Laleva M, et al. IDH1/IDH2 but not TP53 mutations predict prognosis in Bulgarian glioblastoma patients. Biomed Res Int. 2014; 9.
124. Stancheva G, Goranova T,Laleva M, et al. IDH1/IDH2 but Not TP53 Mutations Predict Prognosis in Bulgarian Glioblastoma Patients. Biomed Res.Int. 2014; 654727.
125. Stegmayr B, Ronquist G. Promotive effect on human sperm progressive motility by prostasomes. Urol Res. 1982; 10(5):253-7.
126. Strotman L, Millner L, Valdes R, et al. Liquid Biopsies in Oncology and the Current Regulatory Landscape. Mol Diagn Ther. 2016; (5):429-36.
127. Stuffers S, Wegner C, Stenmark H, et al. Multivesicular endosome biogenesis in the absence of ESCRTs. Traffic. 2009; 10: 925–937.
128. Stupp R, Hegi ME, Gilbert MR, et al. Chemoradiotherapy in malignant glioma: Standard of care and future directions. J Clin Oncol. 2007; 25: 4127–36.
129. Stupp R, Mason WP, van den Bent MJ, et al. Radiotherapy plus concomitant and adjuvant temozolomide for glioblastoma. N Engl J Med. 2005; 352:987–996.
130. Szajnik M, Derbis M, Lach M. Exosomes in Plasma of Patients with Ovarian Carcinoma: Potential Biomarkers of Tumor Progression and Response to Therapy. Gynecol. 2013; 1–11.
131. Tang DG. Understanding cancer stem cell heterogeneity and plasticity. Cell Res. 2012; 22: 457–72.

132. Taraboletti G, D'Ascenzo S, Giusti I, et al. Bioavailability of VEGF in tumor-shed vesicles depends on vesicle burst induced by acidic pH. Neoplasia. 2006; 8: 96–103.
133. Taylor DD, Gercel-Taylor C. Exosomes/microvesicles: mediators of cancer-associated immunosuppressive microenvironments. Semin Immunopathol. 2011; 1–14.
134. Tetta C, Ghigo E, Silengo L, et al. Extracellular vesicles as an emerging mechanism of cell-to-cell communication. Endocrine. 2013; 44(1): 11–19.
135. The Cancer Genome Atlas Research Network. Comprehensive genomic characterization defines human glioblastoma genes and core pathways. Nature. 2008. 455, 1061–1068.
136. Trams EG, Lauter CJ, Norman Salem J, et al. Exfoliation of membrane ecto-enzymes in the form of micro-vesicles. BBA - Biomembr. 1981; 645: 63–70.
137. Turcan S, Rohle D, Goenka A, et al. IDH1 mutation is sufficient to establish the glioma hypermethylator phenotype. Nature. 2012; (7390):479-83.
138. Valadi H, Ekstrom K, Bossios A, Sjostrand M, et al. Exosome-mediated transfer of mRNAs and microRNAs is a novelmechanism of genetic exchange between cells. Nat. Cell Biol.2007. 9, 654– 659.
139. Verhaak RGW, Hoadley KA, Purdom E, et al. Integrated Genomic Analysis Identifies Clinically Relevant Subtypes of Glioblastoma Characterized by Abnormalities in PDGFRA, IDH1, EGFR, and NF1. Cancer Cell. 2010; 17: 98–110.
140. Vicente-Dueñas C, Romero-Camarero I, Cobaleda C, et al. Function of oncogenes in cancer development: A changing paradigm. EMBO J. 2013; 32, 1502-1513.
141. Villà S, Balañà C, Comas S. Radiation and concomitant chemotherapy for patients with glioblastoma multiforme. Chin J Cancer. 2014; 33: 25–31.
142. Vlashi E, Lagadec C, Vergnes L, et al. Metabolic state of glioma stem cells and nontumorigenic cells. Proc Natl Acad Sci U S A. 2011; 108: 16062–7.
143. Wang J, Zhao Y, Li J. et al. IDH1 mutation detection by droplet digital PCR in glioma. Oncotarget. 2015; 6:37.
144. Wakimoto H, Mohapatra G, Kanai R, et al. Maintenance of primary tumor phenotype and genotype in glioblastoma stem cells. Neuro Oncol. 2012; 14: 132–44.
145. Wiestler B, Capper D, Holland-Letz T, et al. ATRX loss refines the classification of anaplastic gliomas and identifies a subgroup of IDH mutant astrocytic tumors with better prognosis. Acta Neuropathol. 2013; 126: 443–51.
146. Wunder A, Schoknecht K, Stanimirovic DB, et al. Imaging blood-brain barrier dysfunction in animal disease models. Epilepsia. 2012; 53 Suppl 6: 14–21.
147. Yan H, Parsons W, Genglin J, et al. IDH1 and IDH2 Mutations in Gliomas. N Engl J Med. 2009; 19; 360(8): 765–773.

148. Yang T, Martin P, Fogarty B, et al. Exosome delivered anticancer drugs across the blood-brain barrier for brain cancer therapy in Danio rerio. Pharm Res. 2015; 32: 2003–14.
149. Yuana Y, Sturk A, Nieuwland R. Extracellular vesicles in physiological and pathological conditions. Blood Rev. 2013; 27: 31-39.
150. Young R, Jamshidi A, Davis G, et al. Current trends in the surgical management and treatment of adult glioblastoma. Ann Transl Med. 2015; 3(9):121.
151. Zhang W, Fulci G, Buhrman JS, et al. Bevacizumab With Angiostatin-armed oHSV Increases Antiangiogenesis and Decreases Bevacizumab-induced Invasion in U87 Glioma. Mol Ther. Nature Publishing Group; 2012; 20: 37–45.
152. Zhu T, Costello M, Talsma C, et al. Endothelial cells create a stem cell niche in glioblasto- ma by providing NOTCH ligands that nurture self-renewal of cancer stem-like cells. Cancer Res. 2011; 71: 6061–6072.
153. Zhuang X, Xiang X, Grizzle W, et al. Treatment of brain inflammatory diseases by delivering exosome encapsulated anti-inflammatory drugs from the nasal region to the brain. Mol Ther. 2011; 19: 1769–79.
154. Zonneveld MI, Brisson AR, Herwijnen MJC Van, et al. ENMN-. Isolation procedures. 2014; 1: 1–12.

ANEXOS

ANEXO I

ANEXO II

ANEXO III